

An investigation of series hybrid-electric vehicle operation

by

Christopher John Merriman

A thesis submitted to the graduate faculty
in partial fulfillment of the requirements for the degree of
MASTER OF SCIENCE

Department: Mechanical Engineering

Major: Mechanical Engineering

Major Professors: Jon Van Gerpen and Greg Luecke

Iowa State University

Ames, Iowa

1996

**Graduate College
Iowa State University**

**This is to certify that the Master's thesis of
Christopher John Merriman
has met the thesis requirements of Iowa State University**

Signatures have been redacted for privacy

TABLE OF CONTENTS

1. INTRODUCTION.....	1
1.1. Series Hybrid Description.....	2
1.2. Parallel Hybrid Description.....	3
1.3. Thesis Outline and Objectives.....	4
2. BACKGROUND INFORMATION.....	6
2.1. Electric Vehicles.....	6
2.1.1. Electric Vehicle Performance.....	6
2.1.2. Electric Vehicle Charging.....	9
2.2. Environmental Aspects of Hybrid-Electric Vehicles.....	10
2.2.1. Types of Emissions.....	10
2.2.2. Effects of Emissions.....	11
2.2.3. Hybrid-Electric Vehicle Emissions.....	12
2.3. Engine Control Strategies for Series HEVs.....	12
2.3.1. Engine Performance.....	13
2.3.2. Number of Engine Starts.....	16
2.4. Auxiliary Power Unit Selection.....	16
2.4.1. Basic Requirements.....	16
2.4.2. Four-Stroke Engine Designs.....	21
2.4.3. Two-Stroke Engine Designs.....	22
2.4.4. A Gas Turbine Design.....	23
2.4.5. Rotary Engines.....	24
2.5. Battery Information.....	24
2.5.1. Battery Operating Characteristics.....	24
2.5.2. Battery Charging.....	31
2.5.3. Summary of Battery Information.....	36
3. VEHICLE SIMULATION DESCRIPTION.....	37
3.1. Model Description.....	38
3.1.1. Force Balance on the Simulated Vehicle.....	38
3.1.2. Battery Energy Flow Calculation.....	40
3.2. Simulation Test Descriptions.....	42
3.2.1. Steady State Simulation Test.....	42
3.2.2. Transient Simulation Tests.....	42
3.3. Simulation Results.....	44
3.3.1. Simulation Tests for Prescribed Battery Energy Cases.....	45
3.3.2. Program Modifications for Prescribed Vehicle Range Cases.....	46
3.3.3. Effect of Distance Traveled.....	50
3.3.4. Effect of APU Power Output.....	52
3.4. Simulation Summary.....	57

4. EXPERIMENTAL EQUIPMENT AND PROCEDURE	59
4.1. Measured Parameters.....	59
4.2. OPTO-22 Data Acquisition System.....	61
4.3. Fuel Mass Flow Rate Measurement	63
4.4. Emissions Measurements	65
4.5. Test Matrix Generation	68
4.5.1. Test Information	68
4.5.2. Matrix Determination.....	68
4.6. Test Procedure.....	72
4.6.1. Procedure to Regulate the Timing of the Engine Events.....	72
4.6.2. Procedure to Maintain a Constant Torque Output.....	73
4.6.3. Procedure to Start and Stop the Engine	74
4.6.4. Test Procedure Summary	74
5. RESULTS AND DISCUSSION	76
5.1. Data Analysis Procedure.....	76
5.1.1. Analysis Methods for the Steady State Tests.....	77
5.1.2. Analysis Methods for On/Off Testing	80
5.2. Test Accuracy.....	82
5.2.1. Engine Power Stability and Accuracy	82
5.2.2. Engine On/Off Timing Accuracy.....	85
5.3. Normalized Results	86
5.3.1. Trends of the Air/Fuel Ratio Variation	87
5.3.2. Brake Specific Fuel Consumption	87
5.3.3. Specific Carbon Monoxide Emissions	90
5.3.4. Specific Hydrocarbon Emissions	92
5.4. Variation of Engine Temperature in the On/Off Testing	93
5.5. Application of Engine Test Results to the Operation of a HEV	94
5.5.1. Calculation of Fuel Economy and Emissions for a Simulated HEV	95
5.5.2. Engine Modifications Needed for Hybrid Vehicle Use	96
5.6. On/Off Test Results Summary.....	98
6. CONCLUSIONS.....	100
REFERENCES	102

1. INTRODUCTION

In an effort to decrease pollution levels and dependence on non-renewable energy sources, much research has been conducted in the area of alternative fuels for vehicles. One type of alternative fueled vehicle is the electric vehicle (EV). EVs have the potential to significantly reduce urban smog levels in cities like Los Angeles. Pure electric vehicles have many shortcomings, however. The greatest inconvenience associated with EVs is their limited range. With existing technology, an electric vehicle can only travel about 80 miles on a single charge. Hybrid-electric vehicles (HEVs) address the range problem associated with electric vehicles. HEVs combine the range capabilities of a gasoline powered vehicle with the low emissions of an electric vehicle. The objective of the project described in this thesis was to determine if hybrid vehicles actually would reduce emission levels, and if so, by how much. A more complete outline of the thesis will be given in section 1.3. Sections 1.1 and 1.2 are devoted to a general description of different hybrid vehicle designs.

By definition, a hybrid vehicle is a vehicle with two separate and distinct power generating units on board. The most common combination of power sources is a gasoline-powered engine combined with an electric motor. This combination merges the range capabilities of a conventional vehicle with the low emissions of an electric vehicle. There are three ways of implementing the electric/gasoline powered HEV: the parallel, series, and split configurations. In the parallel hybrid design, the gasoline engine is used in tandem with the electric motor to directly power the drive shaft. The series hybrid uses the engine to run a generator that charges the battery, while the electric motor is used to drive the wheels. The third design is a variation of the parallel hybrid and is called the split hybrid vehicle. In it, the electric motor is connected to one axle, while the engine is connected to the other axle. Two examples of split shaft hybrids are given in references [2] and [3]. All three HEV designs are shown schematically in Figure 1 [4].

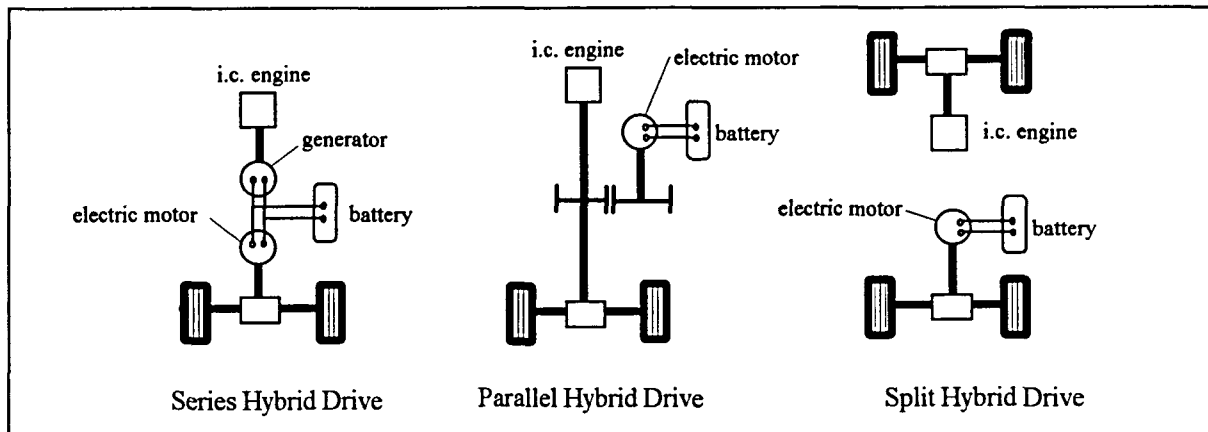


Figure 1. Structures of series and parallel hybrid drives.

1.1. Series Hybrid Description

A series configuration is simpler to design and operate than the parallel HEV. The series design is a direct extension of an electric vehicle, so the vehicle drive train is modified very little. Because of this simplicity, this design tends to be more reliable than the other two.

The main advantage of the series configuration is the control that can be maintained over the engine. The engine can be decoupled from the operation of the vehicle itself, so the engine operating condition can be set for either best fuel economy or least emissions. Also, since the engine can be set at relatively constant conditions, alternate sources of power can be used. For example, gas turbines, two-stroke engines, and stirling cycle engines have been proposed for use in series configurations [5,6,7,8].

The main disadvantage of the series design is size. The drive train tends to be larger and heavier than in a parallel hybrid. A series hybrid drive train includes an electric motor, a generator, and an engine. The motor is the sole power source to the wheels, so it must be sized to give all the power needed to drive the vehicle. Motors ranging from 30 kW to 100 kW have been used in electric vehicle prototypes [9]. The generator must be large enough to charge the batteries, which requires a 20-25 kW unit. The engine must have sufficient power to run the generator, meaning that it should be 5 to 10 kW larger than the generator. An engine rated at around 30 kW

will be able to drive a series HEV generator [9]. In general, the engine size will vary between 15 and 40 kW depending on the size and weight of the vehicle [10].

1.2. Parallel Hybrid Description

The parallel design is lighter and more compact than the series configuration. Since both the engine and the motor provide power to the drive shaft, each power source can be downsized from the series hybrid. A typical motor size for a parallel hybrid passenger vehicle is 15 kW, and the engine produces around 25 kW of power. Also, the motor can be used as a generator to charge the battery, which means no separate generator is needed. So, the parallel drive line is much smaller than in the series hybrid. Because the system is lighter and more compact, this design costs less and is more efficient.

The primary disadvantage of the parallel HEV is the sporadic nature of the engine operation. During periods of sudden acceleration and deceleration, say in urban driving, the vehicle may exceed the maximum power capability of the electric motor often and for short time intervals, which would cause the engine to turn on and off frequently. This affects the vehicle design in four ways. First, more complex control strategies are required to operate a parallel HEV and necessitate more highly developed computer software and hardware. Second, the transient operation of the engine will cause higher emissions and worse fuel economy. Third, the torque of the engine must be applied smoothly. Abrupt changes in torque would be undesirable and should be avoided. Finally, the durability of the engine may be affected by unsteady operation [10].

A split hybrid vehicle is a variation of the parallel HEV. The split design resembles the parallel design, except that the drive trains are not physically connected in the split HEV. Because of the similarity between the two designs, control strategies for split HEVs would be similar to those used for parallel hybrids. The main advantage of a split hybrid is that relatively few modifications need to be made to the vehicle. For example, if the vehicle has front-wheel-drive, only the rear axle must be modified [4].

1.3. Thesis Outline and Objectives

The project described in this thesis focused on research pertaining to series hybrid-vehicle applications. The primary objective of the project was to determine if hybrid vehicles would reduce emissions and improve fuel economy relative to conventional vehicles. The underlying issue in making this comparison was the performance of the engine used in HEV applications. As mentioned in section 1.1, engines rated at 30 kW would be used in the typical series HEV. Engines of this size are unregulated and not designed for passenger use. They have high fuel consumption rates and give off large amounts of pollution.

This project investigated the trade-off between running a small engine in a HEV for less time at its optimal setting and running a larger engine in a conventional vehicle for a longer period of time at a less than optimal setting. The project sought to answer the following questions:

- What methodology should be used to predict the performance of a hybrid vehicle?
- For a given driving cycle, how much fuel and battery energy will a HEV consume, and what levels of emissions will a HEV produce? Will the fuel consumption and emissions be higher or lower than for a conventional vehicle?
- What size engine is appropriate for hybrid vehicle use?
- At what power level should the engine operate, and how many times will it start over the course of a trip? How do the engine power level and number of engine starts affect fuel economy and emissions?
- What should the start frequency be? How long should the engine remain on after starting, and how long should the engine remain off in between starts?

These questions were addressed in this thesis through a numerical vehicle simulation and through engine dynamometer tests. The numerical simulation determined the energy consumption of a hybrid-electric vehicle over a defined driving cycle. The vehicle used in the simulation was an electric G-van that utilized a 24 hp 2-cylinder engine for range extension. Dynamometer tests were performed on a 2-cylinder spark-ignition engine like the one placed in the G-van. The

dynamometer tests varied the engine power output and number of engine starts, while fixing the total engine running time as specified by the simulation. Fuel economy and emissions were measured during the test. Combining the energy information from the simulation with the fuel consumption information from the dynamometer tests, an estimated gas mileage and emission output rate were calculated for the G-van. In the process of estimating the vehicle gas mileage and fuel economy, all of the above questions were addressed.

The following chapters of this thesis discuss in greater detail the process used in answering the questions listed above. Chapter 2 gives background information on basic HEV concepts. Chapter 3 describes the numerical simulation and what was learned from it. Chapter 4 provides information on how the 2-cylinder engine was tested, and Chapter 5 discusses the results of the tests. Finally, Chapter 6 discusses how the information acquired in the first five chapters addresses the underlying questions of the thesis.

2. BACKGROUND INFORMATION

This chapter gives background information applicable to hybrid-electric vehicles. As their name implies, hybrid-electric vehicles (HEVs) are extensions of their electric counterparts, and share many of the same characteristics, so section 2.1 will describe general attributes of electric vehicles. Section 2.2 will deal with the environmental aspects of HEVs. After that, control strategies for the series hybrid vehicle will be discussed in section 2.3. The last two sections (2.4 and 2.5) deal with specific aspects of hybrid vehicles, namely the selection of an auxiliary power unit (APU) and the operation of vehicle batteries.

2.1. Electric Vehicles

Since hybrid vehicles share many of the same characteristics of electric vehicles (EVs), general aspects of EVs should be addressed before an investigation of HEVs can begin. In recent years, there has been a move on the part of law makers to reduce pollution in urban areas. Electric vehicles could play an important role in cutting down on urban smog problems. In California, legislation has been passed that requires major car manufacturers to produce a specified number of electric vehicles per year. Ten percent of new vehicles sold must be electric by the year 2003 [11]. Since EV technology is relatively new, many issues could be addressed relating to electric vehicles. The following sections will address the issues most related to hybrid-electric vehicles. Specifically, EV performance and battery charging will be covered.

2.1.1. Electric Vehicle Performance

Performance of an electric vehicle can be measured by range, top speed, and acceleration. In general, electric vehicles have a very short range. Most of the vehicles cannot travel more than 80 miles on one charge. In comparison, a typical gasoline fueled car can travel 300 to 400 miles on a full tank of gas [1]. EV range is limited by the energy stored in a battery. To compete with

conventional automobiles, batteries are being developed that give off more energy per unit weight and volume.

The vehicle's top speed is limited by the power of the electric motor. Some newer electric vehicles can reach speeds up to and exceeding 80 mph, but acceleration tends to be very slow. Like top speed, the acceleration times are limited by the motor's power output. Improvements in acceleration come with decreased frictional effects and lighter vehicle weights. Newer vehicles use light-weight composite frames and high pressure tires to reduce friction.

The performance characteristics of currently operating electric vehicles are shown in Table 1. This table is broken down into vehicles that are available in production and those that are still in the experimental stages of operation. Range is the most important characteristic of an EV, so the designs are organized by how far they are able to travel. Also included in this chart are the vehicle range, acceleration, and top speed. In general, the experimental vehicles have longer ranges, quicker accelerations, and higher top speeds than the currently available models.

The U.S. Department of Transportation (DOT) National Highway Traffic Safety Administration has set minimum performance standards for electric vehicles. These requirements are shown in Table 2 [5] and include acceleration, gradeability, and top speed. A description of each criteria is also given in Table 2. Acceleration is the time it takes for a vehicle to reach a specified speed. Gradeability has two subcategories. These are the speed that a vehicle can maintain on a given grade and the maximum grade capability of a vehicle. The final criteria for electric vehicles is top speed, which is defined as the maximum speed that a vehicle can reach on level ground. As can be seen from Table 1, most current vehicles and all experimental designs meet the 45 mph (72 km/h) top speed requirement for private vehicles. In addition, most vehicles meet the 12 second 0-30 mph (0-48 km/h) acceleration time. Comparisons between the accelerations of different vehicles are difficult to make because a different reference speed was used for each vehicle. For example, the General Motors Impact was timed to 96 km/h and the

Table 1. Performance parameters of various electric vehicles [14].

Model	Manufacturer	Battery	Battery Weight kg	Motor	Range km (conditions)	Acceleration seconds (speed reached)	Top Speed km/h	Price
Currently Available Designs								
Mini-el City	Citycom	Pb-Acid	90	DC	30-35 (city) 40-50 (hwy.) 60-70 (city)	----- 13 (0-50 km/h)	35	Dkr 40,000
Eicat	Eicat	Pb-Acid	440	DC	100 (50 km/h)	-----	72	-----
Panda	Fiat	Pb-Acid	350	DC	70 (city)	10 (0-50 km/h)	70	L 30,000,000
J5/C25	Peugeot/Citroean	Pb-Acid	868	DC	75 (city)	12 (0-50 km/h)	90	-----
Volta	SEER	Pb-Acid	480	DC	80 (city)	-----	73	FF 125,000
G-Van	Conceptor	Pb-Acid	1,270	DC	100 (city)	12 (0-50 km/h)	83	US\$50,000
Hi-Jet	Daihatsu	Pb-Acid	344	DC	90 (40 km/h)	8 (0-40 km/h)	75	Y 2,170,000
Town-Ace	Toyota Motor Co.	Pb-Acid	688	AC	166 (40 km/h)	6.5 (0-40 km/h)	110	Y 8,000,000
Libero	Mitaubiatu	Ni-Cd or Pb-Acid	---	AC	166 (40 km/h, Pb-acid) 250 (40 km/h, Ni-Cd)	4.1 (0-40 km/h)	130	Y 10,000,000
Experimental Designs								
Clean Air LA301	CAT	Pb-Acid	470	DC	65 (city)	9 (0-50 km/h)	83	US\$25,000
106E	Peugeot	Ni-Cd	260	DC Induction	90-160 (city)	9 (0-50 km/h)	90	-----
CITELA	PSA	Ni-Cd	---	DC	110 (city)	8.5 (0-50 km/h)	110	-----
TE Van	Chrysler	Ni-Fe	700	DC	210 (40 km/h)	7.5 (0-48 km/h)	105	-----
ETX-II	US DOE	Na-S	575	AC Synchronous	193 (city)	<20 (0-80 km/h)	105	-----
EcoStar	Ford	Na-S	360	AC Induction	240 (city)	<14 (0-88 km/h)	115	-----
Impact	General Motors	Pb-Acid	395	AC Induction	>160 (hwy.)	8 (0-96 km/h)	120	-----
FEV	Nissan	Ni-Cd	200	AC Induction	192 (hwy.)	3.6 (0-40 km/h)	130	-----
IZA	Tokyo Elec. Power	Ni-Cd	531	DC Brushless	250 (40 km/h)	20 (0-400m)	176	-----
190-Electric	Mercedes Benz	Na-NiCl2	---	DC	160 (72 km/h)	10 (0-400m)	120	-----
E-1	BMW	Na-S	200	DC Brushless	548 (40 km/h) 174 (48 km/h) 215 (50 km/h) 155 (80 km/h)	13 (0-48 km/h) 6 (0-50 km/h)	120	-----

Table 2. Safety performance standards for baseline electric vehicles [5].

Standard	Description	Vehicle Class	
		Private	Commercial
Acceleration	Time to reach given speed	12 sec. (0-30 mph)	15 sec. (0-30 mph)
Gradeability	Speed that can be maintained on a given grade	20 mph on 10% grade 25 mph on 7% grade	15 mph on 10% grade 22 mph on 7% grade
	Maximum grade capability	20%	20%
Top Speed	Minimum top speed capability	45 mph	35 mph

Original Source: Federal Motor Vehicle Standards (DOT HS 802 611)

Nissan FEV was timed to 40 km/h. Before private or commercial use in the United States, these vehicles would most likely be tested under standard conditions set by the U.S. DOT.

2.1.2. Electric Vehicle Charging

An electric vehicle designed for residential use would typically serve as a means of transportation to and from work. Charging would be done over-night from electrical outlets in the owner's home. If the car is driven only on short trips, over-night charging would be enough. Problems arise, however, if longer trips are needed. Additional problems occur if the home charging system operates improperly. If a power failure occurs during the night, the car may remain half charged [1]. For these reasons, alternate sources of charging should be put in place, such as portable on-board charging units and public charging stations.

Electric vehicles are usually purchased with portable on-board chargers. These chargers can be plugged into conventional outlets, but tend to be slow. For example, a 110 volt unit designed for the GM Impact EV takes eight hours to completely charge the battery [12]. In response to this lack of speed, Nissan designed a quick-charge unit that can charge their nickel-cadmium powered FEV to 40% capacity in six minutes and to the fully charged state in 15 minutes [13]. Portable charging devices allow a driver to charge the car while away from home or in an emergency, provided a source of electric power is available.

Public charging stations have also been proposed. Located at a shopping mall, restaurant, or office building, public stations would allow for "opportunity charging" of a vehicle. While a person is doing other things, the vehicle could be charged. To accommodate longer trips, a charging infrastructure should be constructed. Like gas stations, charging stations would be needed at various points along the roadway. Roadside charging stations would only be effective if a quick-charge method was used, so as not to delay travelers.

2.2. Environmental Aspects of Hybrid-Electric Vehicles

The main reason for changing from gasoline-powered vehicles to electric vehicles is pollution. In cities such as Los Angeles, the pollutants formed by automobiles have caused high urban smog levels. Other cities, including Tokyo, Beijing, Mexico City, and Moscow also have smog problems [15]. Through the use of electric vehicles, pollutants would be produced only by electric power plants, removing the pollutants from urban centers.

There is a pollution tradeoff between using gasoline power and electric energy in a HEV. Some pollution will occur regardless of how the energy is produced. When the vehicle runs on electric power, emissions will be produced from a power plant. If gasoline is used, emissions will come directly from the vehicle. The types of emissions produced by each source, the effect of those emissions, and the trade-off provided by HEVs are discussed below.

2.2.1. Types of Emissions

Coal burning power plants are the most common source of electric power. The emissions produced by a coal plant include oxides of sulfur and nitrogen, particulates, volatile organic compounds, carbon monoxide, lead, and toxics. Toxics include 189 different species listed in the Clean Air Act. The major air toxics given off by coal-fueled plants are mercury, hydrochloric acid, and hydrofluoric acid [16]. Of the pollutants produced by a coal burning plant, the major polluting agents are sulfur dioxide (SO₂) and oxides of nitrogen (NO_x).

Vehicles produce other pollutants. The emissions coming from an automobile tailpipe include carbon monoxide (CO), hydrocarbons (HC), and oxides of nitrogen (NO_x). In 1990,

transportation contributed 40% of the NO_x emissions in the United States [17]. More detailed pollution information for twenty world cities is contained in reference [15], including two U.S. cities: New York City (NYC) and Los Angeles (LA). Los Angeles exceeds World Health Organization (WHO) standards in four categories: Suspended Particulate Matter (SPM), CO, NO_x , and Ozone (O_3). The ozone levels in LA are double the WHO standards, while the other three are moderately higher than the WHO guidelines. NYC complies with the WHO standards in all categories except CO and O_3 . In these two categories NYC is only slightly above the WHO guidelines.

2.2.2. Effects of Emissions

The effects of SO_2 and NO_x emissions from coal burning power plants have been highly studied and are well known. These two pollutants are lofted into the upper atmosphere by tall stacks. While there, they oxidize to form SO_3 and NO_2 . The compounds return to earth in the form of wet and dry deposition. Dry deposition occurs when NO_x and SO_2 form acidic particles. The particles then settle to the ground. Wet deposition, known as acid rain, results from the formation of nitric acid and sulfuric acid in the atmosphere. These acids fall as rain and lower the pH levels of lakes and rivers. Many plants and animals have adapted to a narrow range of pH levels. With an abrupt change in pH, large numbers of trees and fish have been known to die off. The effects of acid rain have been seen in European mountain ranges, as well as in the lakes of the Adirondack mountains in the United States. Acid rain has also been known to corrode buildings.

The emissions from vehicles (HC, CO, and NO_x) have different effects. Unburned hydrocarbons turn into photochemical smog when exposed to sunlight. Unburned hydrocarbons also produce undesirable odors and are possibly carcinogenic [18]. Carbon monoxide combines with hemoglobin in the blood stream. By replacing oxygen in the blood, CO causes headaches, dizziness, vision impairment, and slowed reaction time [19]. Oxides of nitrogen also combine with hemoglobin, giving the same results. In addition, NO_x forms nitric acid in the lungs. Like

unburned hydrocarbons, NO_x is a major contributor to photochemical smog. When exposed to sunlight, NO_2 gives an oxygen atom to an oxygen molecule, forming O_3 , one element of smog.

2.2.3. Hybrid-Electric Vehicle Emissions

Since hybrids utilize both electric and gasoline power, hybrid vehicles provide a compromise between the two sources of energy. HEV emissions will come from both the power plant and the vehicle exhaust. The amount of energy used from each source will depend on the vehicle driving cycle. In urban driving, a hybrid vehicle operates mainly on electric vehicle power, so hybrids driven in the city use about the same amount of electrical energy per mile as an electric vehicle. This means that the vehicle emissions over an urban cycle would be primarily attributed to a power plant. For longer commutes, the engine turns on more often to charge the batteries. The vehicle will then produce some pollutants directly. Not much emissions testing has been done on HEVs, but the tailpipe emissions per mile for the hybrid designs that have been tested are lower than for a conventional vehicle. This is primarily because the engine is operated less frequently. The magnitude of typical HEV exhaust emissions can be seen in a diesel-powered vehicle that was converted into a prototype parallel hybrid [4]. The hybrid vehicle gave off less CO and NO_x and showed improved fuel economy in comparison to its diesel counterpart. By converting the diesel vehicle into a hybrid, the researchers reduced CO emissions from 0.91 g/km to 0.40 g/km and NO_x emissions from 0.96 g/km to 0.24 g/km. At the same time, fuel consumption went down from 6.4 L/100km to 2.4 L/100km [4].

2.3. Engine Control Strategies for Series HEVs

With this background in electric vehicles and in hybrid vehicle emissions, the series HEV will now be considered in more detail. A series HEV is sometimes called a range-extender electric vehicle. This is because it simply gives the EV a longer driving range. The main advantage of the series hybrid configuration is the ability to decouple the engine from the vehicle operation. In a series hybrid-electric vehicle, the engine drives a generator that supplies power to the battery. The engine can operate independently from the vehicle drive train. This means that the engine could

run close to its optimal point of operation without affecting the vehicle drivability, while still providing the power needed for proper use of the vehicle.

Over the course of a driving cycle, the vehicle will consume a certain amount of energy. If the energy consumption were known exactly, the engine could turn on at an optimal time dictated by the battery charging characteristics, and operate continuously until either the battery was fully charged or the prescribed amount of energy for the journey had been generated. Unfortunately, the exact amount of energy consumed will not be known until the vehicle has completed the set course. A reasonable guess of the energy use can be made from previous trips, but variations in day-to-day factors such as weather and traffic can cause the energy consumption to change. Since the amount of energy used is not known beforehand, the starting and stopping of the engine should be dictated by some other means. A common method of timing the engine events is by the battery energy level. When the battery reaches a certain state of charge (say 20%), the engine will turn on. When the battery charges up to a higher state of charge (say 30%) the engine will turn off again. This results in an on/off pattern of engine operation, which has been implemented for a number of series hybrid vehicles [6,20,21].

The total length of time the engine must remain on depends on the energy required by the vehicle and on the engine power output. A low-power engine must remain on for a longer time than a higher-powered engine to provide the same amount of energy. Two factors must be considered in determining the power level: engine performance and the number of starts. The performance of an engine will depend on its operating point, and the number of starts should be minimized.

2.3.1. Engine Performance

Engine performance is determined by fuel economy and emissions, which both vary with engine speed and load. Engine fuel economy characteristics are usually shown on a performance map. A typical performance map is shown in Figure 2 [22]. The map plots the variation of fuel consumption with speed and load. Fuel consumption is measured relative to the brake power

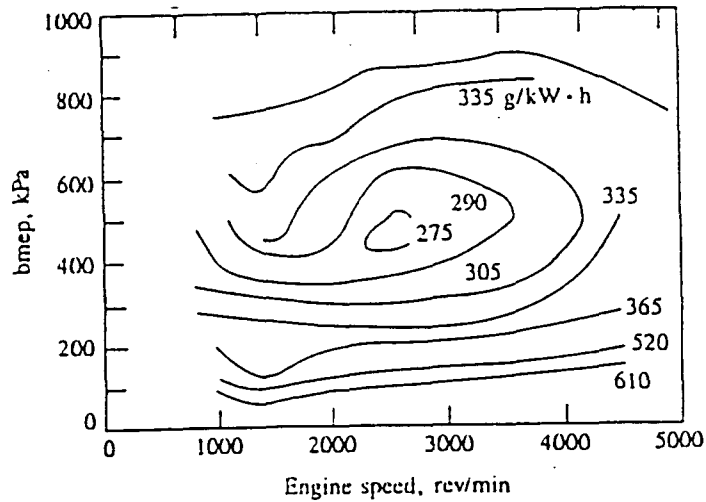


Figure 2. Typical performance map for a spark-ignition engine. Contours of constant brake specific fuel consumption (bsfc) are in grams per kilowatt-hour. [22]

output. This is known as the brake specific fuel consumption (bsfc). Load is indicated by a quantity called the brake mean effective pressure (bmep), which is equal to the engine torque divided by the displacement volume. The bmep allows for comparisons between engines of different sizes. The speed and load settings of an engine usually depend on external factors such as gear ratio and power demand. In a series hybrid vehicle, the engine speed is determined by the generator because the engine speed is controlled to match the optimal generator speed. This assumes that the generator efficiency changes more than the bsfc when the speed is varied from the optimal point. The engine load setting will determine the amount of power put into charging the battery. From a fuel efficiency standpoint, there will be an optimal load setting for a given speed. For example, when the engine with a performance map shown in Figure 2 is running at 2500 rpm, it will have an optimal load setting of around 450 kPa. When the engine runs at a lower load, say 15-20% full power, it will operate at a less efficient point on the engine map.

For a given energy demand, a high-powered engine will operate for a shorter period of time than a low-powered engine. At a lower load, the engine runs almost continuously and at a

less efficient setting. A higher power output operates in an on/off manner with greater efficiency. So, the continuous mode could be expected to perform more poorly than the on/off mode. In a simulation done by A.F. Burke, the on/off hybrid increased fuel economy by 50% compared with continuous operation at a lighter load [10].

Like fuel consumption, exhaust emissions vary with engine operating conditions. Figure 3 [22] shows the variation of nitric oxide (NO) and hydrocarbon (HC) emissions with load for a typical spark-ignition engine. The engine parameters associated with this figure are given in the figure caption. The engine ran at an equivalence ratio of 0.9, meaning that the actual fuel/air (F/A) ratio was 0.9 times the stoichiometric F/A ratio, which is by definition a lean mixture composition. The spark timing was set at maximum brake torque (MBT) timing. MBT timing is the spark timing that gives the maximum torque output for a given F/A ratio. Also, the engine had a compression ratio (r_c) of 7. Compression ratio is the ratio between the maximum cylinder

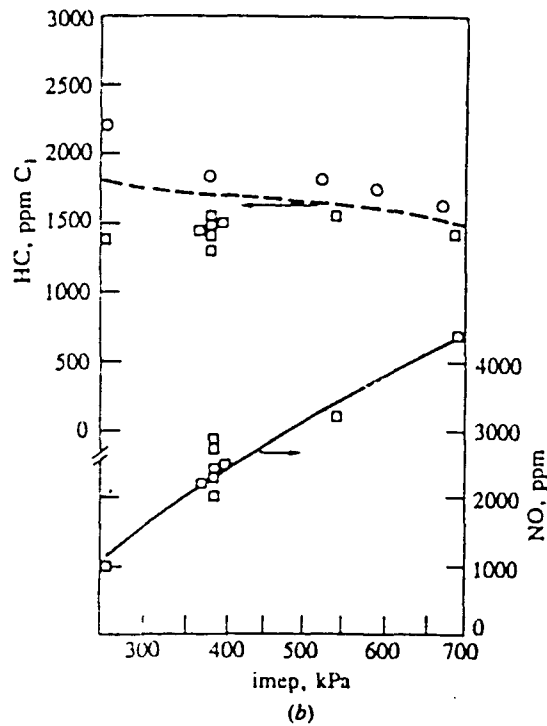


Figure 3. Variation in spark-ignition engine HC and NO emissions with load (or imep) at 1250 rev/min. Equivalence ratio = 0.9, MBT spark timing, $r_c=7$. [22]

volume and the minimum cylinder volume [22]. For this engine, Figure 3 shows that as load increases, oxides of nitrogen increase and hydrocarbon emissions decrease. The effect of load on HC emissions is relatively weak. As shown in Figure 3, HC emissions decrease only slightly with increased load. The trends for both NO_x and HC emissions that apply for the engine in Figure 3 are typical and apply to most spark ignition engines.

2.3.2. Number of Engine Starts

In addition to engine performance, the number of times that the engine starts will affect the engine setting used for a given application. During startup, an engine typically produces more emissions and consumes more fuel. When the engine starts, it will be at a low temperature. Colder engine temperatures require more fuel to be put into the engine so enough vaporizes to form a combustible mixture [22]. This means that the engine must run fuel rich. Running an engine rich will cause more HC and CO emissions to be produced. These increased emissions will pass through the catalyst unconverted because it, too, will be cold. A cold catalytic converter is ineffective at oxidizing HC and CO emissions. When a converter becomes 50% effective it is said to have reached its "light-off temperature." The light-off temperature of an oxidizing catalytic converter is around 250 to 300 degrees Celsius. The effectiveness of a typical oxidizing catalyst is shown in Figure 4 [22].

2.4. Auxiliary Power Unit Selection

So far, general aspects of EVs and series hybrid-electric vehicles have been discussed. The next two sections move from general to more specific topics. The section 2.4 deals with the selection of an auxiliary power unit (APU), and section 2.5 discusses battery information.

2.4.1. Basic Requirements

The engine is a central component to the hybrid-electric vehicle drive train and is referred to as the auxiliary power unit. When choosing an APU, a few specifications must be taken into account. The most important parameters to look at are engine size, weight, power, emissions, and durability. To compare the performance of different APUs, the power output can be normalized

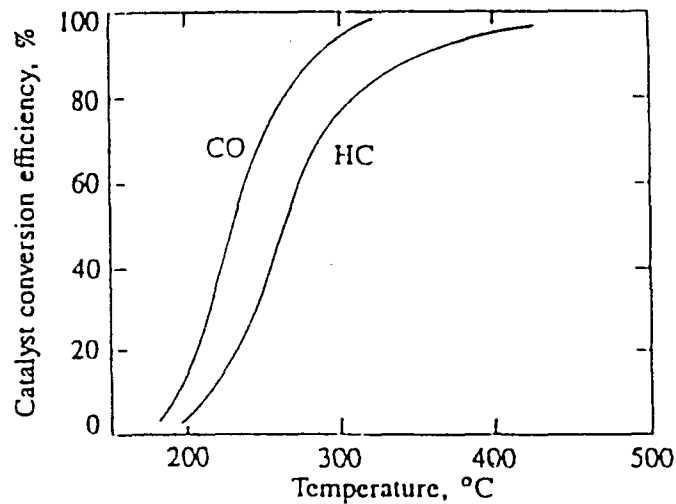


Figure 4. Conversion efficiency for CO and HC as a function of temperature for typical oxidizing catalytic converter. [22]

against size and weight, where the power per unit weight is called the specific power. An engine designer seeks to have a high power to volume ratio, as well as a high specific power. The absolute power that an engine puts out is also important. Many passenger car 4-stroke spark-ignition (SI) engines are rated above 100 kW [5,10], and a hybrid vehicle does not need this much power. The typical power requirement for a HEV engine is between 15 and 40 kW. Downsizing an engine requires adjusting the number of cylinders, the displacement, and the air and fuel flows. Much work has yet to be done in the area of efficient small engine design [10].

The following sections address the advantages and disadvantages of four types of engines. The main candidates for hybrid vehicle engines are the 4-stroke, 2-stroke, gas turbine, and rotary engine designs. Other engines that have been considered are the Stirling and Brayton cycle engines. The power per unit weight and per unit volume for all of these engines are shown in Figure 5. Figure 6 shows the minimum brake specific fuel consumption (bsfc) for each engine. The same information that is contained in both the figures is listed in Table 3 [5,8,9,10]. The figures convey the information in graphical form, so that relative comparisons can be made

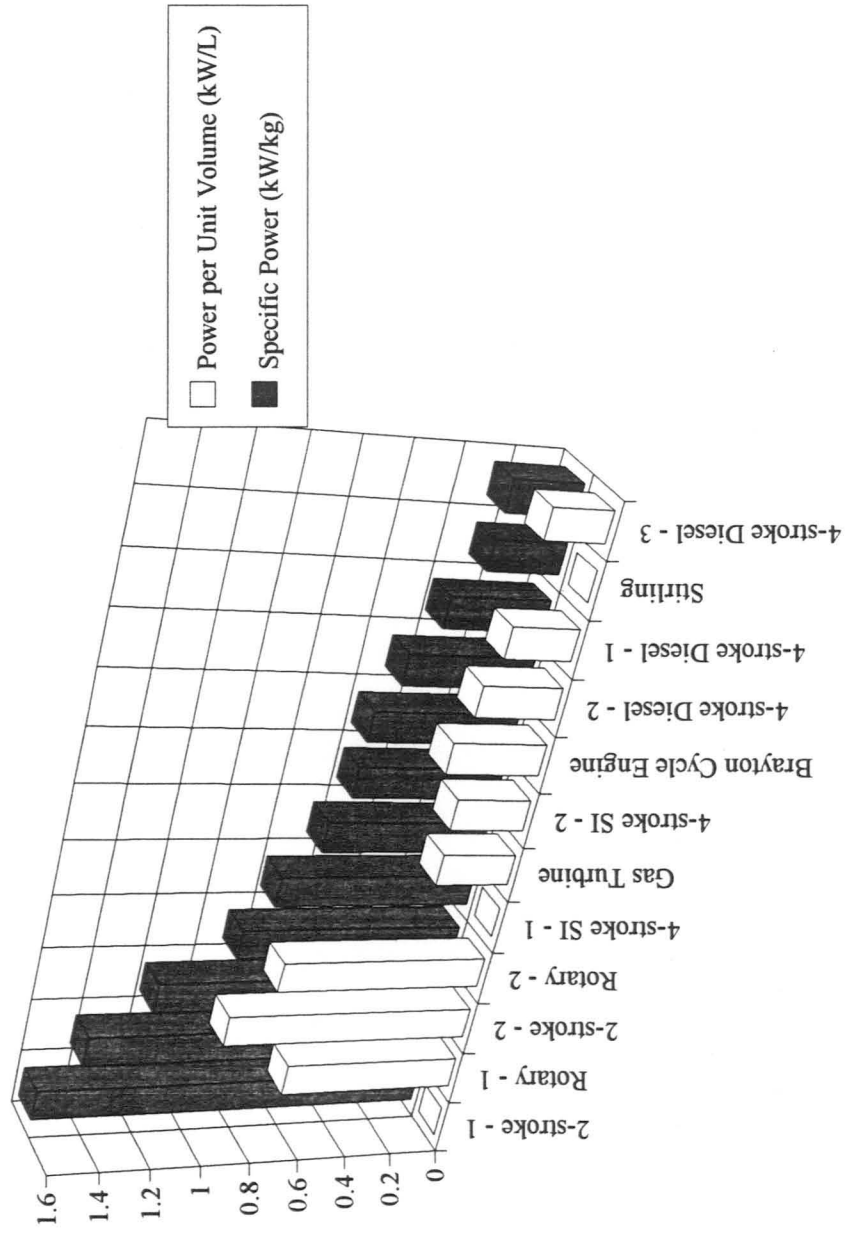


Figure 5. Power per unit weight and volume of potential hybrid/electric vehicle engines.

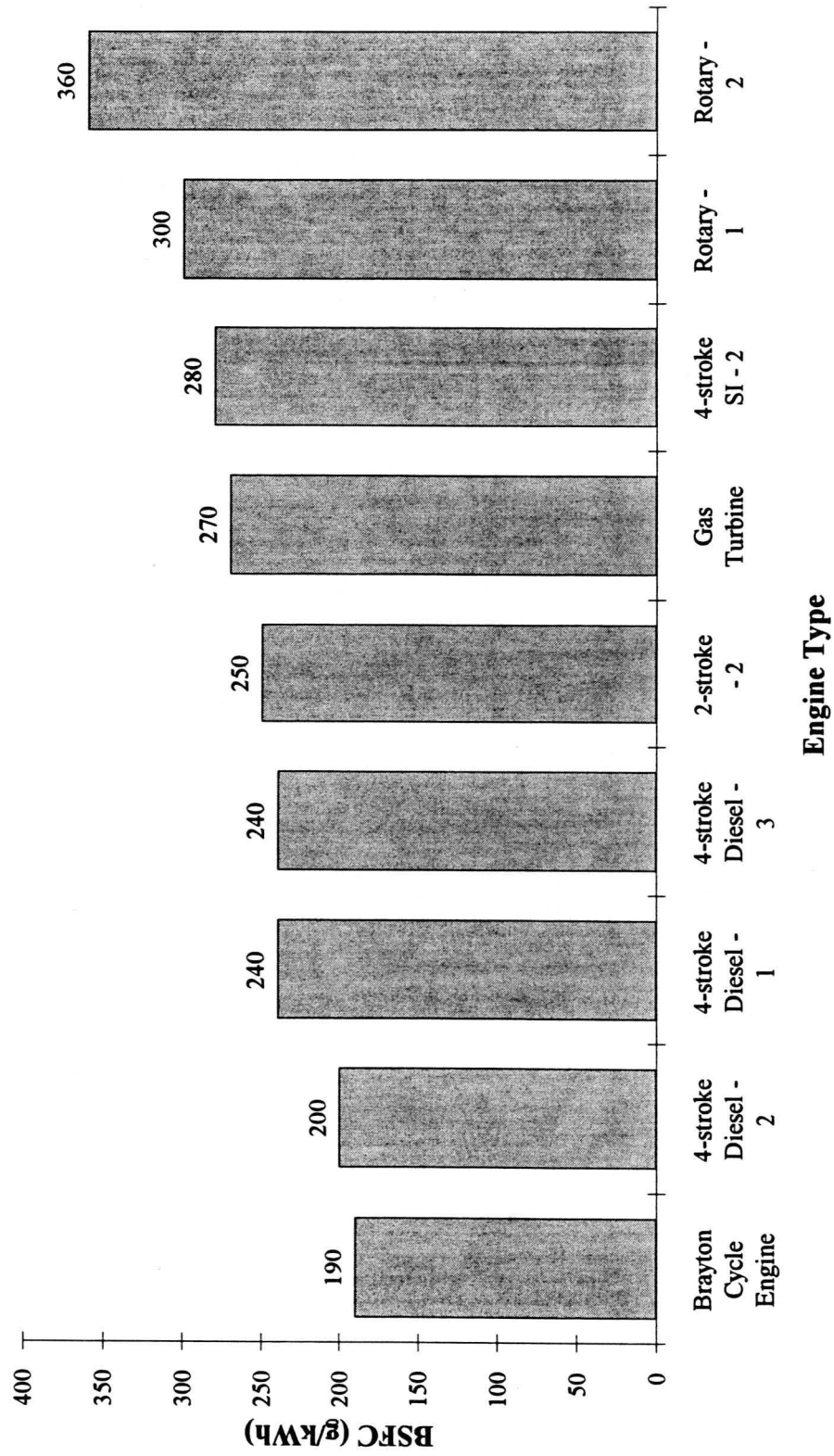


Figure 6. Minimum brake specific fuel consumption of potential hybrid-electric vehicle engines.

Table 3. A comparison of performance parameters for potential hybrid-electric vehicle engines.

Engine Type	Model/Manufacturer	Power per Unit Volume kW/L	BSFC	Specific Power kW/kg	Power kW	Weight kg	Volume Liters	Reference
2-stroke - 1	Orbital OCP X-series	-----	7 gal/hr	1.59	65	40.8	-----	5
2-stroke - 2	typical 30 kW	1.000	250 g/kWh	1.20	30	25.0	30.0	9
Rotary - 1	Norton	0.714	300 g/kWh	1.43	30	21.0	42.0	9
Rotary - 2	Rotec	0.833	360 g/kWh	0.91	26	28.6	31.2	9
Rotary - 3	NASA series 70	-----	4.4 gal/hr	-----	35	-----	-----	5
4-stroke SI - 1	GM Quad-4	-----	10.9 gal/hr	0.81	110	136.5	-----	5
4-stroke SI - 2	predicted future 2 cyl, 4-valve	0.300	280 g/kWh	0.60	30	50.0	100.0	9
Gas Turbine	NoMac	0.296	270 g/kWh	0.67	24	36.0	81.2	8,9
Brayton Cycle Engine		0.379	190 g/kWh	0.60	---	---	---	10
4-stroke Diesel - 1	typical IDI	0.272	240 g/kWh	0.41	---	---	---	10
4-stroke Diesel - 2	predicted DI	0.324	200 g/kWh	0.51	---	---	---	10
4-stroke Diesel - 3	Supercharged VW DI	0.244	240 g/kWh	0.29	29	101.5	118.9	9
Stirling		-----	5.5 gal/hr	0.30	60	202.8	-----	5

between the engine types. The table provides a list of the information for each engine, and gives the engine manufacturer. In the figures and the table the engines are labeled according to type. If more than one engine is listed for a certain type, the engine is indexed after its name. For example, since there is data available for three 4-stroke diesel engines, they are labeled 1 through 3.

The two figures show how the engines compare with respect to power per unit volume, specific power, and brake specific fuel consumption. An engine should have a high specific power output and low fuel consumption rate. In both cases, the engines positioned closer to the left on the x-axis would be more desirable for a HEV application. Figure 5 shows that 2-stroke and rotary engines could be used in a hybrid vehicle where specific power and power per unit volume are important. If the fuel consumption rate is used for criteria, Figure 6 shows that the Brayton cycle engine and the 4-stroke diesel engine should be chosen. Once again, the tabular form of this information is contained in Table 3, which also gives the references where the information can be found.

2.4.2. Four-Stroke Engine Designs

The four-stroke is the standard engine used in many applications. There are two types of four-stroke reciprocating engines: gasoline and diesel powered. Diesel engines are used in applications where high fuel economy is required, such as in semi-trailer trucks. Diesels have not been popular in United States passenger car applications because of noise, smell, and starting factors. The general bias against diesel fueled engines for passenger car use may have affected one researcher, who claims that diesel engines are not the preferred choice for hybrid applications [5]. Ford Motor Company and General Motors Corporation, however, both have installed diesel engines in their prototype hybrid vehicles. This is in response to a mandate by the Partnership for a New Generation of Vehicles (PNGV) to achieve a production prototype of a conventionally fueled, mid-sized, 80 mpg vehicle by 2004. The PNGV is a coalition of the big three auto makers and government agencies led by the Department of Commerce, which was founded in 1993 to

develop new vehicle technologies [23]. So, if fuel consumption reduction is the primary goal, diesel engines are well suited for HEV applications. When HEVs are used as passenger vehicles for the average consumer, however, diesel driven vehicles may not be marketable.

Spark ignition engines are the second type of four-stroke engine, and have recently improved in a number of ways. Air flow through the engine has improved by using 3 or 4 valves per cylinder and through variable valve timing. Engines have also been made more structurally stable, decreasing vibrations and noise levels. Higher compression ratios have led to increased power and efficiency, and more compact designs and lighter weight materials have increased the specific power of newer engines. Some examples of new engine designs are shown in References [24], [25], and [26].

Most SI engines have a good power to weight ratio. The engines are larger than needed for HEV applications, however. In recent years, the major developments in SI engines have come in 4 to 6 cylinder designs. Only 2 to 3 cylinders are needed for hybrid applications [10].

2.4.3. Two-Stroke Engine Designs

Two-stroke engines are most commonly used in applications where a high power density and simple construction are required, such as motorcycles, small hand-held lawn and garden equipment, and outboard motors. The traditional two-stroke uses a scavenging system to bring air into the combustion chamber. The types of two-stroke scavenging are not relevant to this discussion, but all allow air into the combustion chamber by ports toward the bottom of the cylinder [22]. The exhaust gases leave the chamber either through ports opposite the intake ports, or through valves in the cylinder head. The absence of a valve train in the first configuration reduces friction losses, pumping losses, and engine size. The shorter cycle than the 4-stroke cycle has two negative effects, however. First, the valve overlap in a two-stroke is greater than in a four-stroke. This causes fresh charge to leave the chamber with the exhaust gas, directly wasting fuel, and producing higher HC emission levels. Second, the exhaust port must open earlier than in

a four-stroke engine, so less work is produced by the combusting gases, which leads to a lower bmep and lower efficiency.

Attempts have been made to improve the two-stroke engine by adding intake poppet valves or by using direct injection in a spark-ignition design. Engines with poppet valves have limited speed because the valve train rotates twice as fast as in a four-stroke engine. Inertial effects in the valves limit the rotational speed of the engine [27]. Direct injection spark-ignition engines improve emissions and fuel consumption, but suffer from the same bmep reduction as compression ignition two-strokes. So, even though two-stroke engines provide a high power to weight ratio, their technology has not advanced enough to compete with the four-stroke engine.

2.4.4. A Gas Turbine Design

Gas turbines could also be used in HEV applications. They have comparable power densities to 4-stroke engines [27], and they give off very few emissions. The disadvantages of a gas turbine include high cost, poor transient response, and large volume.

One particular gas turbine has been developed for hybrid vehicle applications by NoMac Energy Systems, Inc. This turbine has a power rating of 24 kW, with a maximum power output of 30 kW. It weighs 36 kg, giving a specific power of about 0.67 kW/kg [8]. This design uses a circumferential recuperator to preheat the turbine intake air. By preheating the air, the turbine reaches an efficiency of 30%. The efficiency of an unrecuperated gas turbine is around 14% [10]. In addition to reasonable efficiency, this turbine gives off low emissions. If the NoMac turbine was put into a hybrid vehicle, it would produce much less CO, NO_x, and HC than the California standards [8]. Mackay [8] lists measurements of the emissions output from the NoMac turbine. He assumes an energy consumption rate for a typical hybrid vehicle of 0.21 kW-hr/km (0.34 kW-hr/mile) and calculates the amount of emissions per mile that a HEV would produce. The results of his calculations are shown in Table 4. The NoMac equipped HEV would have NO_x emissions 26 times lower than the California standard, CO emissions would be 333 times lower, and HC emissions would be 5 times lower [8].

Table 4. Projected emissions from a NoMac generator-set powered vehicle compared with the California emissions standards.

	NO _x	CO	HC
Estimated Emissions (g/kW-hr)	0.046	0.030	0.24
Calculated Emissions per Distance Traveled (g/km) (g/mile)	0.0098 0.0160	0.0063 0.0100	0.050 0.081
California Standard (g/km) (g/mile)	0.25 0.40	2.10 3.40	0.25 0.41
Ratio: Cal. std./NoMac	26	333	5

2.4.5. Rotary Engines

Rotary engines are the fourth type of engine considered for HEV applications and have a very high specific power output. They are compact and light-weight and have reasonable fuel consumption rates, but produce high levels of emissions. Fuel consumption is in the range of 300 to 360 g/kWh, which is comparable to many four-stroke engines. The emissions from rotary engines tend to be high [10], however, even though they can use exhaust after-treatment devices similar to SI engines [5].

2.5. Battery Information

Batteries are the most commonly used mode of energy storage for hybrid-electric vehicles. Since the battery is such a central component, its operation will have a great effect on the overall vehicle design. The following sections describe the principles of batteries that affect hybrid vehicle design. Two topics will be addressed: battery operating characteristics and battery charging.

2.5.1. Battery Operating Characteristics

Three basic principles define the performance of a battery: capacity, energy, and power. If a constant current is drawn from a battery, it will take a certain amount of time to discharge. The capacity is defined as the product of the current and the discharge time [28]. For example, a

20 Amp-hour (Ah) battery can provide 20 Amps continuously for 1 hour. The state of charge (SOC) is defined as the percent of the original Amp-hours left in the battery. If the 20 Ah battery has discharged at 10 amps for thirty minutes, the resulting SOC is calculated as follows:

$$\frac{20Ah - 10Amps \cdot \frac{1}{2}hour}{20Ah} = \frac{15Ah}{20Ah} = 0.75 \quad (1)$$

So, the SOC of the battery at this point is 75%. In actuality, the SOC depends on temperature and discharge rate, but this calculation will suffice for the applications in this thesis. Sometimes the state of charge is measured by a quantity called depth of discharge (DOD). The DOD conveys the same information as the SOC, but in the opposite manner. The SOC measures how much capacity is left in a battery, while the DOD measures the amount of capacity removed from a battery during operation. In other words, the sum of the DOD and the SOC is 1.

The second measure of performance is energy. The energy is obtained by multiplying the battery capacity by the terminal voltage. The third measure of battery performance is power. Power is defined as energy per unit time, and is equal to the product of the current and the voltage. Since the battery voltage is relatively constant, the instantaneous power is a measure of the battery's ability to discharge current [28].

Most analyses of battery operation are based on the battery state of charge. A direct correlation can be made between the battery voltage and the depth of discharge. As shown in Figure 7, the battery voltage drops rapidly when its energy nears a fully depleted state [28].

A battery's discharge rate affects its performance. Figure 7 shows that a higher discharge rate will result in a faster decrease in capacity. This can also be seen on a Peukert curve, which plots capacity against discharge rate. This curve, shown in Figure 8 [29], provides a measure of battery performance. A good battery will exhibit a horizontal line on this plot [29], which means that the battery can be discharged at any rate without diminishing the battery capacity. Another way of showing a battery's capacity as a function of discharge rate is through a discharge current

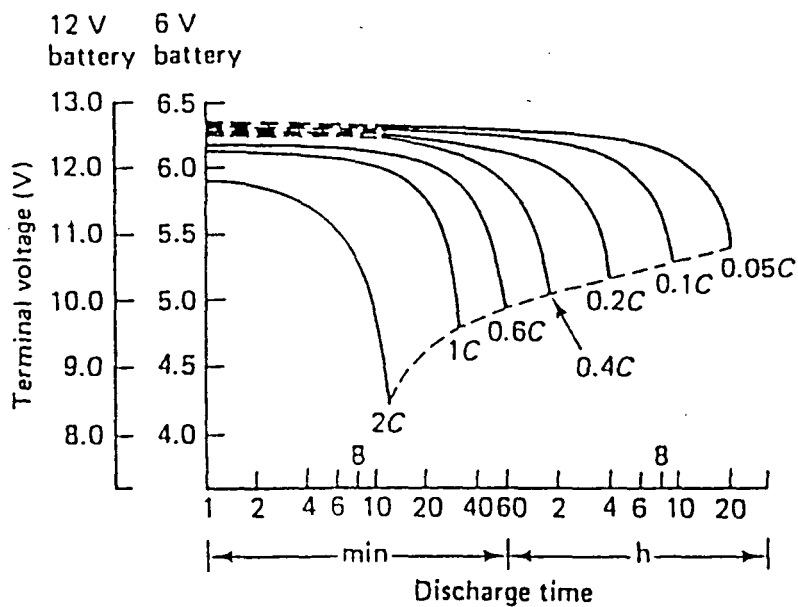


Figure 7. Discharge characteristic curves at 20°C for a Yuasa sealed lead-acid battery. C=Ah rating at 20 h discharge rate to 1.75 V/cell [28].

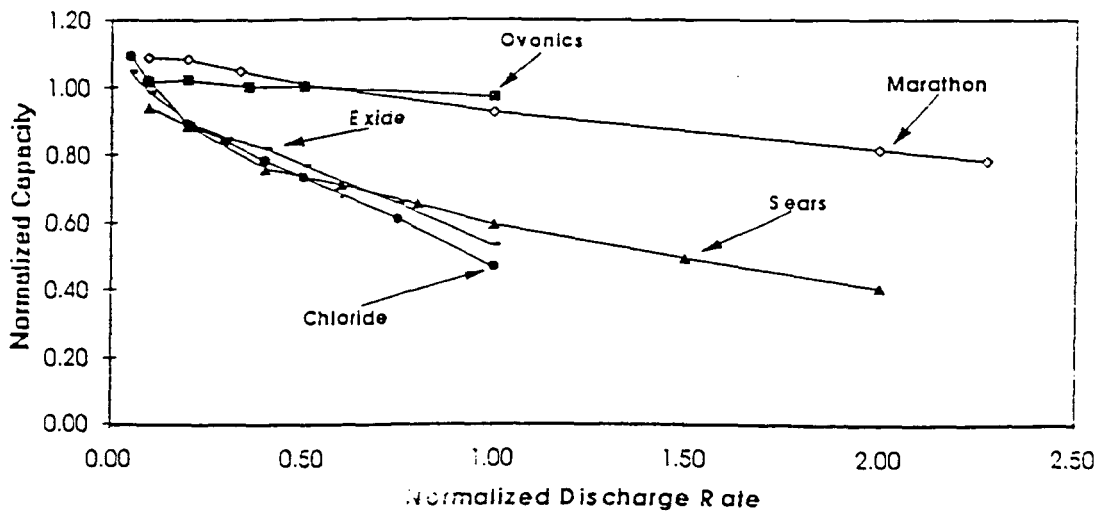


Figure 8. Peukert curves, shows effect of discharge current on the available coulombic capacity of several battery technologies tested at Texas A&M University (TAMU) [29].

versus time plot. This plot, shown in Figure 9 [30], displays the time it takes a battery to discharge at a constant current.

Another test discharges a battery at constant power. The energy that a battery produces is measured for a given power draw. The results of this test are displayed on a Ragone plot. A Ragone plot graphs the attainable energy as a function of discharge power [31]. The plot in Figure 10 [31] was made by the National Battery Test Laboratory (NBTL) at Argonne National Laboratory. It shows that the energy output decreases at higher power draws. Once again, an ideal battery would exhibit a horizontal line [29]. The Ragone Plot is useful for determining the range of an electric vehicle, provided the operating conditions are known. From rough estimates of the power drawn over a driving cycle, the plot gives an estimate of how much energy the battery can give during the cycle. The energy output of the battery is directly related to the distance the car will travel.

When not in use, a battery tends to self-discharge. If stored for a number of months, the battery's capacity can diminish significantly. Figure 11 [28] shows how well a typical lead-acid battery retains its capacity while sitting on the shelf. The figure also shows that a battery will discharge faster at higher temperatures. Self-discharge can be prevented by giving the battery a "topping-up" charge while it is in storage. If self-discharge has occurred, the battery can usually be recharged in preparation for in-vehicle use [28]. Batteries also discharge over shorter periods of time. The losses are not as significant, but a battery will still lose charge while sitting in a vehicle. Figure 12 [29] shows how some batteries lost capacity after standing for 2 to 72 hours [29].

Temperature also plays a role in a battery's operation. As mentioned above, self-discharge is temperature sensitive. Most batteries operate within a given temperature range. For lead-acid batteries, this range lies between -20°C and 50°C . Nickel-cadmium (Ni-Cd) batteries run in a similar range. The capacity of lead-acid and nickel-cadmium batteries is shown as a function of temperature in Figures 13 and 14 [28]. At low temperatures, the ability of the batteries to store

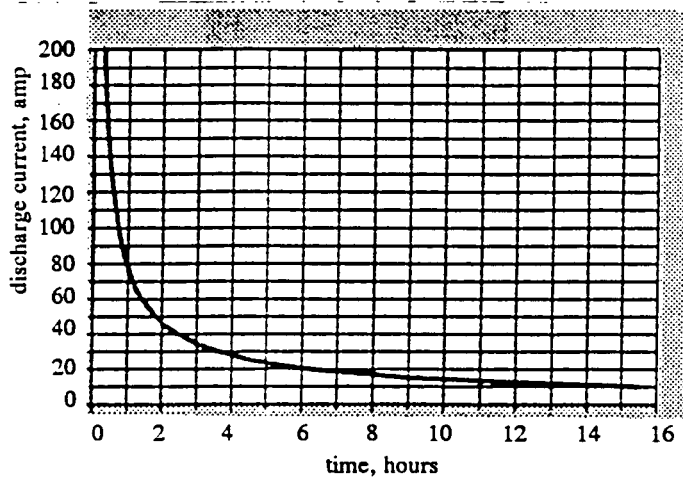


Figure 9. Battery discharge current vs. time [30].

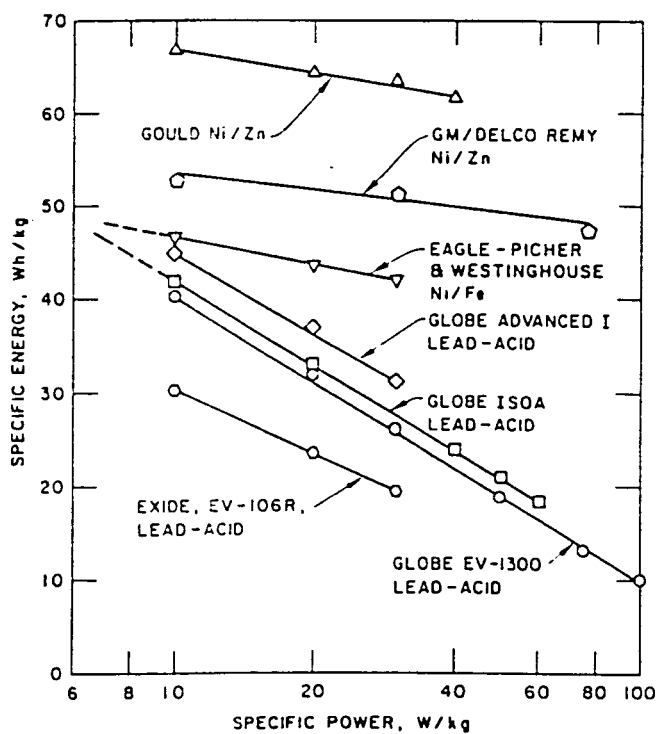


Figure 10. NBTL-derived Ragone plot showing specific energy as a function of specific power level of discharge for several types of aqueous mobile batteries [31].

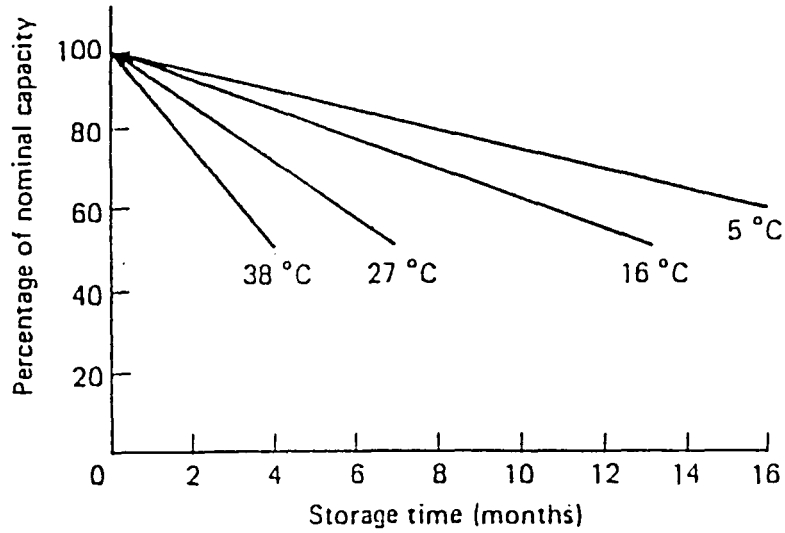


Figure 11. Typical self-discharge characteristics between 40 and 100°C of Eagle Picher Carefree rechargeable lead-acid batteries [28].

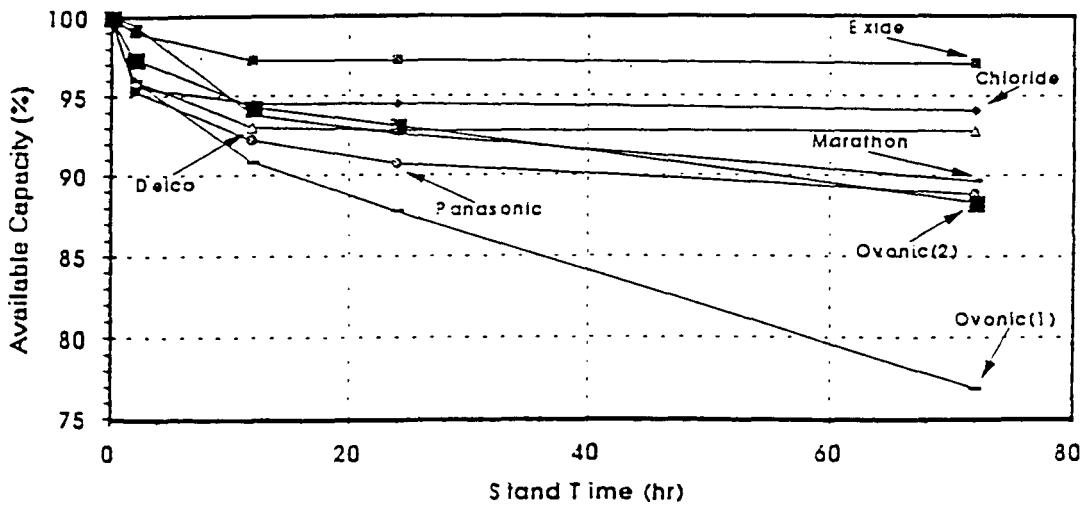


Figure 12. Self-discharge plot, shows effect of stand time on the available capacity of several advanced battery technologies. Ovanic (1): Original battery sent for testing, Ovanic (2): improved battery sent for testing [29].

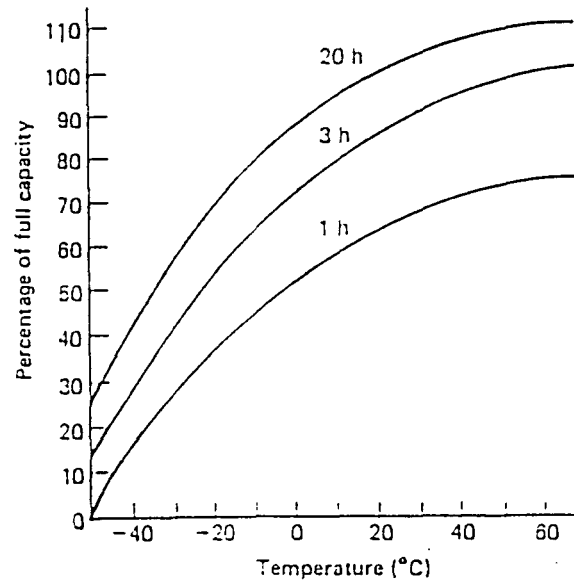


Figure 13. Capacity versus temperature at various rates of discharge. Eagle Picher Carefree rechargeable lead-acid battery [28].

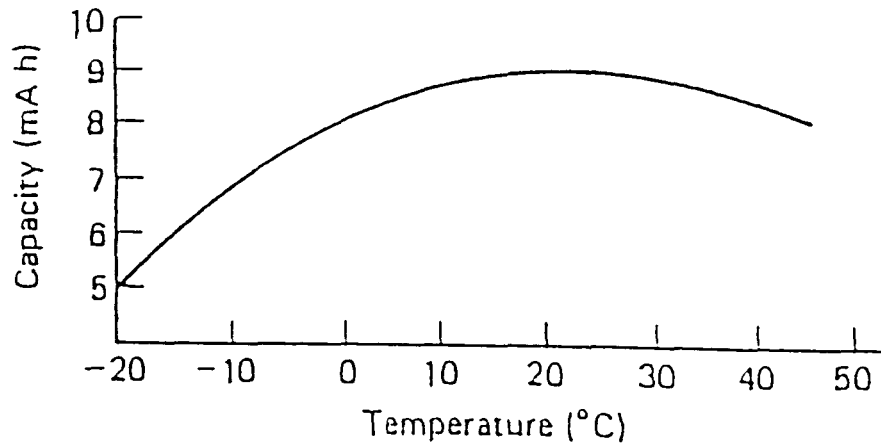


Figure 14. Sample capacity versus temperature curve for Eveready OB90 and OB90T sealed nickel-cadmium cells, 1.2V, 20 Ah capacity. Discharge current 9 mA [28].

charge is diminished. Lead-acid and Ni-Cd batteries will heat up during operation. Prolonged exposure to high temperatures can damage a battery [30], therefore, a cooling system should be used to maintain reasonable temperatures. This can be in the form of a fan [1], or simply keeping open space between the batteries to allow air to pass over them [30].

After repeated use, a battery's potential will decrease and it eventually wears out. This phenomenon, called cycle life, determines how often a battery must be replaced. As shown in Figure 15 [28], frequent deep discharging of a lead acid battery will lead to a shorter battery life. Manufacturers provide only sparse data on cycle life, and usually do not give enough information to determine the life of a battery. When given, the cycle life is typically given for specific depths of discharge.

2.5.2. Battery Charging

In order for a battery to be reused, it naturally must be recharged. There are four main ways to charge a battery: taper, constant current (cc), constant potential (cp), and pulse charging.

The most reliable method of charging an electric vehicle battery is taper charging. Used by owners of large vehicle fleets, this method reduces the current supplied to the battery during the course of charging. By varying the current input to the battery, temperature and gas production can be controlled. The temperature will rise as the battery charges, and cell reactions will release hydrogen and oxygen gas. Reducing the current minimizes both the temperature increase and gas release rate, preventing damage to the battery [28]. Figure 16 shows typical curves for voltage and current as a function of time during a taper charge.

A second method of charging a battery is constant potential charging. This method applies a constant voltage across the battery and varies the current. The current starts at a high value. It is then decreased as the charging progresses. A typical current versus time curve is shown in Figure 17 [28]. This type of charging is typically used on lead-acid batteries. The conditions for cp charging depend on the initial battery state of charge. When the depth of discharge is less than

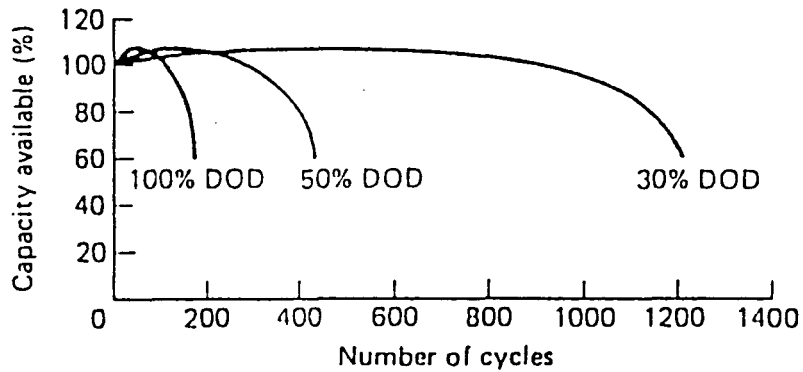


Figure 15. Cycle life versus depth of discharge (DOD) of a Yuasa sealed lead-acid battery at 20-25°C. Discharge current 0.17CA (FV 1.7V/cell), charging current 0.09CA, charging volume 125% of discharging capacity [28].

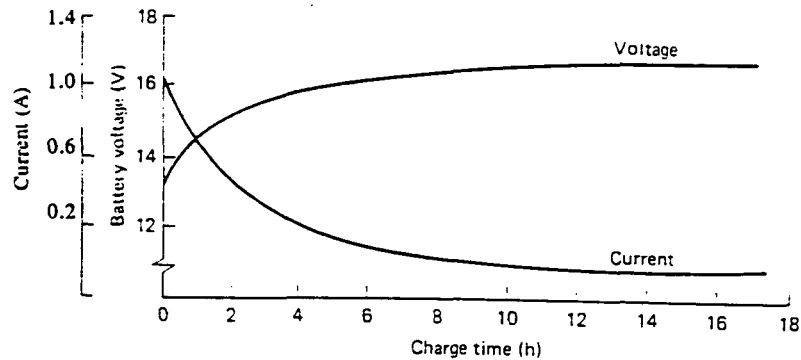


Figure 16. Voltage and current characteristics about mid-cycle life during 16h voltage-limited taper current charge of a 15V, 5Ah Eveready 561 alkaline manganese dioxide battery [28].

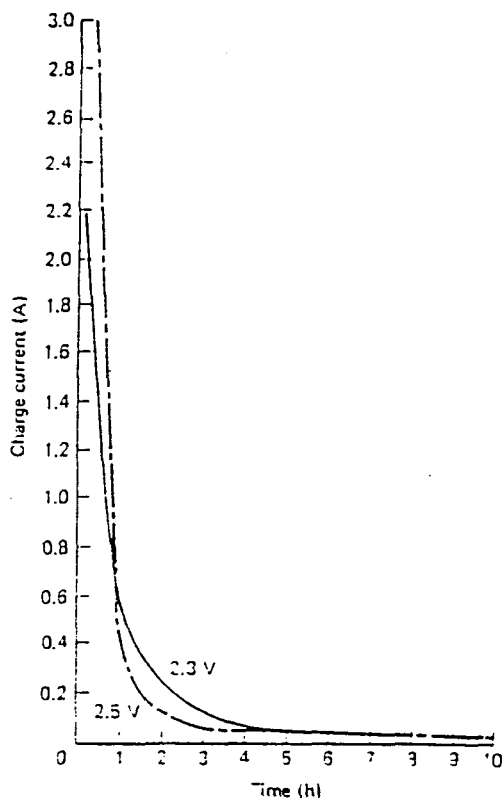


Figure 17. Constant-potential charging current versus time for a General Electric D-cell at 23°C. Actual recharge time and current are circuit dependent. Charge CP at 23°C, discharge 250 mA at 23°C to 1.4V [28].

50%, a low value of initial current should be used. When charging deep-discharged batteries, a higher current is used.

Taper and cp charging are slow, and electric vehicles require more practical charging times. Constant current (cc) charging is used to speed up the process. When using cc charging, a rough estimate of the charging time can be found if the initial DOD is known. The ampere-hours needed to restore full capacity will be equal to the current multiplied by the charging time. Higher currents shorten the charge time. However, higher currents have negative side effects. One side effect is decreased capacity, since larger currents give lower final capacities. The amount of current also affects the cell temperature [28]. The battery temperature remains low for most of the

charging process, but when nearly charged, the battery will begin to heat up due to recombination reactions. Higher currents lead to faster reaction rates in a cell, and this leads to higher heat release rates. So, the faster a battery is charged, the more the temperature will rise.

Another method of fast charging is the pulse charger. One system developed by Varta TSL gives a series of current pulses to a battery. This charger was specifically designed for sealed nickel-cadmium batteries. It charges a battery to 80% of the battery's nominal capacity and then a "trickle" charge is used to top off the battery. A trickle charge slowly charges the battery and prevents self discharge after the battery becomes fully charged. Typical trickle charge currents are around 50-80 mA [28]. The rate of charging by the Varta pulse charger depends on the final battery temperature. For temperatures up to 50°C, a $10 \times I_{10}$ current should be used, and for electrolyte temperatures up to 35°C, a $5 \times I_{10}$ current should be used [28]. The I_{10} current is the current at which a battery will fully discharge in 10 hours. A second pulse charger is made by Electronic Power Technology Inc. (EPTI) and allows a lead-acid battery to charge in 10 to 15 minutes, without appreciable heat generation. The device charges a battery by undergoing a rapid sequence of charge, discharge and rest. This cuts charge times by up to 90%, and can triple the life of a lead acid battery [1].

A number of factors can be used to determine when a battery is fully charged. For most batteries, voltage is a good measure of the state of charge. One set of researchers uses the change in voltage with time (dV/dt) as an indicator of charge [32]. When dV/dt approaches zero, the charging process is terminated. This method is not entirely accurate if an overcharge is desired, because the voltage will decrease slightly after the battery is fully charged. An overcharge is achieved by continuing to charge the battery after the rated capacity of the battery has been reached. In sealed nickel-cadmium batteries, temperature and pressure can be used as indicators. Plots of cell temperature, pressure and voltage for a typical sealed Ni-Cd battery are shown in Figure 18 [28]. The voltage increases during charging until the rated capacity is reached, and then decreases slightly. The temperature rises toward the end of the charging process. By monitoring

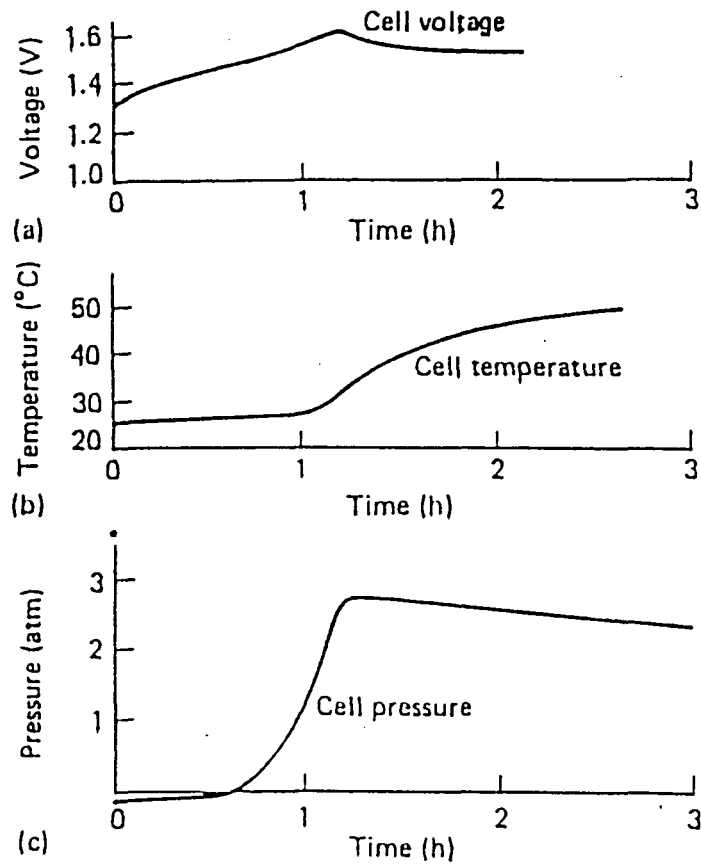


Figure 18. Related characteristics of voltage, temperature, and pressure on charging of Varta sealed nickel-cadmium cells [28].

how much the temperature has gone up, the amount of overcharge can be determined. The internal pressure will also rise in sealed units when the battery is almost charged due to the production of oxygen gas. Oxygen production will continue until an equilibrium condition is reached and the pressure will level out.

Another issue related to battery charging is hydrogen gas production. In lead-acid and nickel-cadmium batteries, the cell reactions occurring late in the charge cycle result in the decomposition of water into hydrogen and oxygen [28]. Some of the ions will recombine to form water. The rest will escape the cell in the form of a gas [28]. To allow for the release of gases, some electric vehicle designers put spacing between the batteries to allow for ventilation [30]. Sealed units prevent the gases from escaping, which aids in recombination. If the reaction rates are too high, however, pressure will build up rapidly in the battery. For this reason, a pressure relief valve is installed in a sealed battery.

2.5.3. Summary of Battery Information

Battery operation affects the design and performance of a hybrid vehicle. The cost, size, and weight associated with a battery will all affect the vehicle. Future battery developments will address four main concerns. First, batteries are expensive to maintain and replace. Designers will seek to lower these costs. Second, batteries limit a vehicle's range. By increasing the power to weight and power to volume ratios in batteries, more range could be extracted from a smaller source. Third, batteries tend to fail after a number of years of use. Increasing cycle life in batteries is an important design issue. Finally, batteries take a long time to charge to full capacity. Reducing charge time will make hybrid vehicles more attractive in today's market.

3. VEHICLE SIMULATION DESCRIPTION

A computer simulation was developed to model the operation of a series configuration hybrid vehicle over a defined driving schedule. The simulation provides a tool for determining how a HEV will perform over a driving cycle. The main reasons for developing the simulation include:

- to determine the range of engine sizes that are appropriate in a typical series HEV application,
- to examine how the APU power level affects the APU starting frequency, and
- to calculate the timing parameters to be used in the engine test.

The first two objectives directly address questions raised in section 1.3. The third objective provides information that can be used to establish a test matrix for the engine dynamometer tests. The test matrix generation is described in more detail in section 4.5.

The simulation is similar to those found in references [33] to [36]. It includes the effects of regenerative braking and incorporates component efficiencies. The specifications for each component are based on manufacturer's data. The inputs to the program include the total energy available from the battery and fuel tank, the reference states of charge, and vehicle specifications such as mass, frontal area, and drag coefficient. Using the specified information, the simulation computes the energy flow to and from the vehicle over a driving cycle.

Two different outputs can be obtained from the simulation depending on the inputs used. If the total distance traveled by the vehicle is known, the amount of battery energy dissipated and the quantity of fuel consumed over the course of the trip can be calculated. Alternatively, if the energy available from the battery and the fuel tank size are put into the program, the distance that the vehicle is able to travel can be calculated.

3.1. Model Description

The simulation first takes into account the various forces applied to the vehicle. A force balance on the vehicle is used to calculate the power required to drive the vehicle. The simulation uses the power to drive the wheels to calculate the energy flow to and from the battery.

3.1.1. Force Balance on the Simulated Vehicle

As shown in Figure 19 [33], a force balance on the vehicle yields the following relationship between the forces and the vehicle acceleration:

$$F_{dw} = F_{res} + m_{eff} a \quad (2)$$

where F_{dw} is the force to drive the wheels and a is the vehicle acceleration. m_{eff} is the effective vehicle mass, which takes into account the rotational energy of the drivetrain. The effective mass is defined by Krepec [34] as:

$$m_{eff} = m \gamma_m \quad (3)$$

where m is the actual vehicle mass and γ_m can be described using the final drive ratio (ξ_o):

$$\gamma_m = 1.04 + 0.0025 \xi_o \quad (4)$$

The forces resisting motion of the vehicle include aerodynamic, rolling, and climbing resistance. The sum of these forces is equal to the total resistance on the vehicle:

$$F_{res} = F_a + F_r + F_c \quad (5)$$

Aerodynamic resistance is defined as:

$$F_a = \frac{\rho C_d A_f}{2} (V_v + V_{wind})^2 \quad (6)$$

where ρ is the air density, C_d is the vehicle drag coefficient, A_f is the frontal area, V_v is the vehicle velocity, and V_{wind} is the wind velocity in a direction opposing the vehicle motion. Rolling resistance is defined as:

$$F_r = \mu_r mg \cos(\theta) \quad (7)$$

where mg is the vehicle weight, θ is the road incline in degrees, and μ_r is the rolling coefficient of

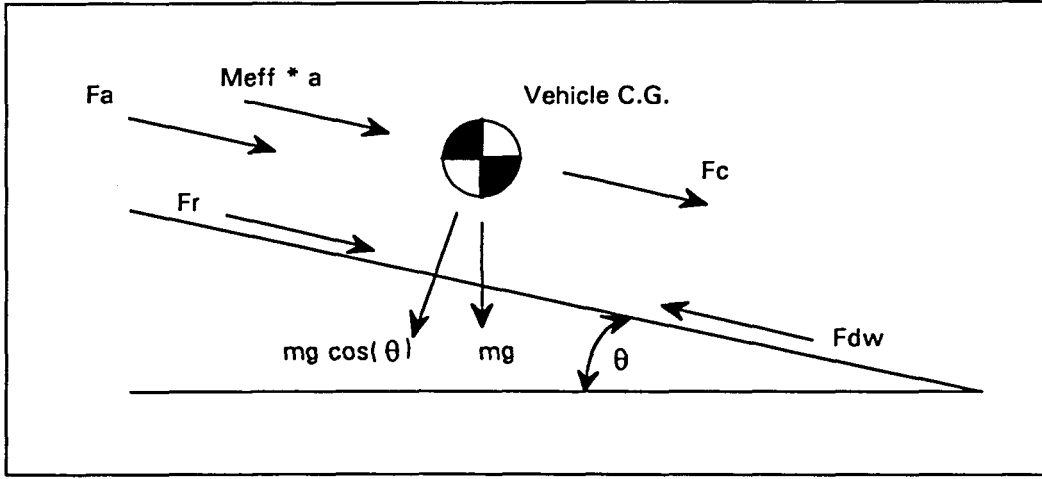


Figure 19. Diagram showing the forces applied to a typical vehicle.

friction, which follows the relationship [33]:

$$\mu_r = \mu_{const} + \left(0.0015 + \frac{V_v}{27770} \right) \quad (8)$$

where μ_{const} is equal to 0.0085 and V_v is the vehicle velocity in m/s. Climbing resistance is equal to:

$$F_c = mg \sin(\theta) \quad (9)$$

where mg and θ are defined as before.

As mentioned earlier, the program uses a specified driving schedule. The vehicle velocity is defined at each second of the schedule. The vehicle acceleration can be determined from the velocity by differentiating using a central difference technique. In equation form, the acceleration at time n is [35]:

$$a_n = \frac{V_{n+1} - V_{n-1}}{2} \quad (10)$$

From the acceleration and the velocity, the force required by the drive wheels can be determined using the force balance in equation 2. After F_{dw} has been calculated, the power consumed by the vehicle over the time interval is determined by:

$$P_{dw} = V_v F_{dw} \quad (11)$$

Power is also supplied to the vehicle by the APU. Since the APU is considered to run at constant speed and load, it gives a constant power output.

3.1.2. Battery Energy Flow Calculation

The energy flow to and from the battery can be calculated using the power output from the APU and the power required at the wheels. A schematic of the vehicle drive train is shown in Figure 20. This figure shows the path that the energy takes into and out of the battery under normal operation of the vehicle. The energy used by the battery over a given time interval is equal to:

$$\Delta E_{\text{discharge}} = (P_{\text{dw}} \Delta t) \eta_{\text{motor}} \eta_{\text{m}} \quad (12)$$

where Δt is the time step, η_{motor} is the electric motor efficiency [37], and η_{m} is the mechanical efficiency of the transaxle. The energy put into the battery during a time step is defined as:

$$\Delta E_{\text{charge}} = (P_{\text{APU}} \Delta t) \eta_{\text{gen}} \eta_{\text{batt}} \quad (13)$$

where P_{APU} is the brake power output of the APU, η_{gen} is the generator efficiency, and η_{batt} is the battery charge acceptance. The rectifier and the system controller are assumed to have 100% efficiencies. The net change in battery energy over one time step can be determined by:

$$\Delta E = \Delta E_{\text{charge}} - \Delta E_{\text{discharge}} \quad (14)$$

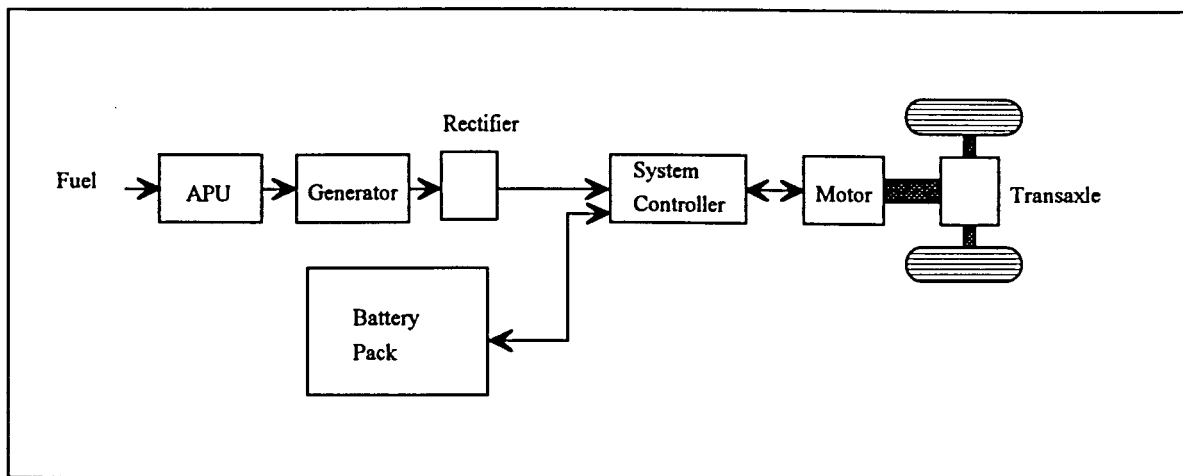


Figure 20. Drive-train schematic of a typical series hybrid vehicle.

The change in energy of the fuel can be found by using the thermal efficiency of the APU (η_{th}).

The decrease in energy of the fuel tank due to the consumption of fuel is equal to:

$$\Delta E_{fuel} = \frac{P_{APU} \Delta t}{\eta_{th}} \quad (15)$$

The volume of fuel used will then be equal to the change in energy of the fuel divided by the fuel energy per unit volume.

When regenerative braking is used, the energy flows from the wheels to the battery. The energy input to the battery during this process is equal to:

$$\Delta E_{regenerative} = (P_{dw} \Delta t) \eta_{batt} \eta_{motor} \eta_m \quad (16)$$

In the process of reaching its destination, the vehicle will consume fuel and use battery energy. The total amount of energy contained in the fuel and the fuel volume are used as reference quantities that tell the amount of fuel consumed over the course of a trip. The amount of energy contained in the battery as a function of time is measured by the state of charge (SOC), which has units of Amp-hours (Ah). For the purpose of this simulation, the battery energy level can be used interchangeably with the state of charge. This is because the battery voltage is assumed to remain constant. Since the battery energy is equal to the capacity multiplied by the voltage, the energy and capacity are related by a constant that cancels out when the SOC is calculated.

The state of charge is used to determine the starting and stopping times of the APU. Three reference SOCs are defined for this purpose. SOC_1 is the state of charge when the APU first turns on. While on, the APU charges the batteries to a higher state of charge. When the charge on the battery reaches SOC_2 , the APU turns off and ceases to charge the battery. At this point, the battery energy diminishes until it reaches SOC_1 for a second time. This process repeats until the engine is no longer used due to either fuel constraints or some external constraint, at which point the battery energy will continue to decrease until it reaches the minimum state of charge (SOC_{min}). The value of SOC_{min} is chosen to ensure long battery life. In the simulation, the battery ceases to operate when SOC_{min} is reached, thus terminating the trip.

3.2. Simulation Test Descriptions

Two types of tests were performed using the simulation: steady state and transient tests. The steady state tests were used simply to verify that the simulation worked properly. The transient tests were used to obtain results from the simulation.

3.2.1. Steady State Simulation Test

Before tests were performed in hybrid mode, the simulated vehicle was run at constant speed. Bass and Mabrito [36] describe a HEV simulation and then give constant speed test results in their paper. Using their input parameters, the results of their constant speed testing were duplicated. Table 5 shows the results from both Bass and Mabrito and the simulation described in this study. Three parameters are shown in this table: P_{roll} , P_{aero} , and P_{res} . The power level is equal to the force multiplied by the velocity, so the following set of equations applies:

$$\begin{aligned} P_{roll} &= F_r * V_v \\ P_{aero} &= F_a * V_v \\ P_{res} &= F_{res} * V_v \end{aligned} \tag{17}$$

where the forces are the same as those in equation 5, and V_v is the vehicle velocity. The correlation between the results of Bass and Mabrito and the results of the HEV simulation is very close. The largest difference is for a vehicle velocity of 80 mph, where Bass calculates a total horsepower of 35.555 hp and the simulation calculates 35.614 hp, giving a difference of 0.059 hp.

3.2.2. Transient Simulation Tests

After constant speed operation had been verified, the simulation underwent transient tests. Two cycles are used in the simulation: the EPA highway cycle and the EPA Urban Dynamometer Driving Schedule (UDDS). Each cycle defines a vehicle velocity on flat ground over time. The cycles are used by the EPA for emissions testing of vehicles.

As shown in Figure 21, the EPA highway cycle defines the vehicle velocity for 765 seconds. The highway cycle is 16.5 km (10.26 miles) long, and the peak velocity is 96.4 km/hr, which occurs at 422 seconds.

Table 5. A comparison of steady state results from the vehicle simulation and from a paper by Bass and Mabrito [36].

Velocity mph	Simulation Results			Results from Bass & Mabrito			Difference		
	Proll hp	Paero hp	Pres hp	Proll* hp	Paero** hp	Pres*** hp	Proll hp	Paero hp	Pres hp
20	2.680	0.389	3.069	2.680	0.388	3.068	0.000	0.001	0.001
25	3.350	0.760	4.110	3.349	0.758	4.107	0.001	0.002	0.003
30	4.020	1.313	5.333	4.019	1.310	5.329	0.001	0.003	0.004
35	4.690	2.085	6.775	4.689	2.080	6.769	0.001	0.005	0.006
40	5.360	3.112	8.472	5.359	3.105	8.464	0.001	0.007	0.008
45	6.030	4.431	10.461	6.029	4.420	10.449	0.001	0.011	0.012
50	6.700	6.078	12.778	6.699	6.064	12.762	0.001	0.014	0.016
55	7.370	8.089	15.459	7.369	8.071	15.439	0.001	0.018	0.020
60	8.040	10.502	18.542	8.039	10.478	18.516	0.001	0.024	0.026
65	8.710	13.353	22.063	8.708	13.322	22.030	0.002	0.031	0.033
70	9.380	16.677	26.057	9.378	16.639	26.017	0.002	0.038	0.040
75	10.050	20.512	30.562	10.048	20.465	30.513	0.002	0.047	0.049
80	10.720	24.894	35.614	10.718	24.837	35.555	0.002	0.057	0.059

*Bass calls this quantity Roll HP

**Bass calls this quantity Drag HP

***Bass calls this quantity Total HP

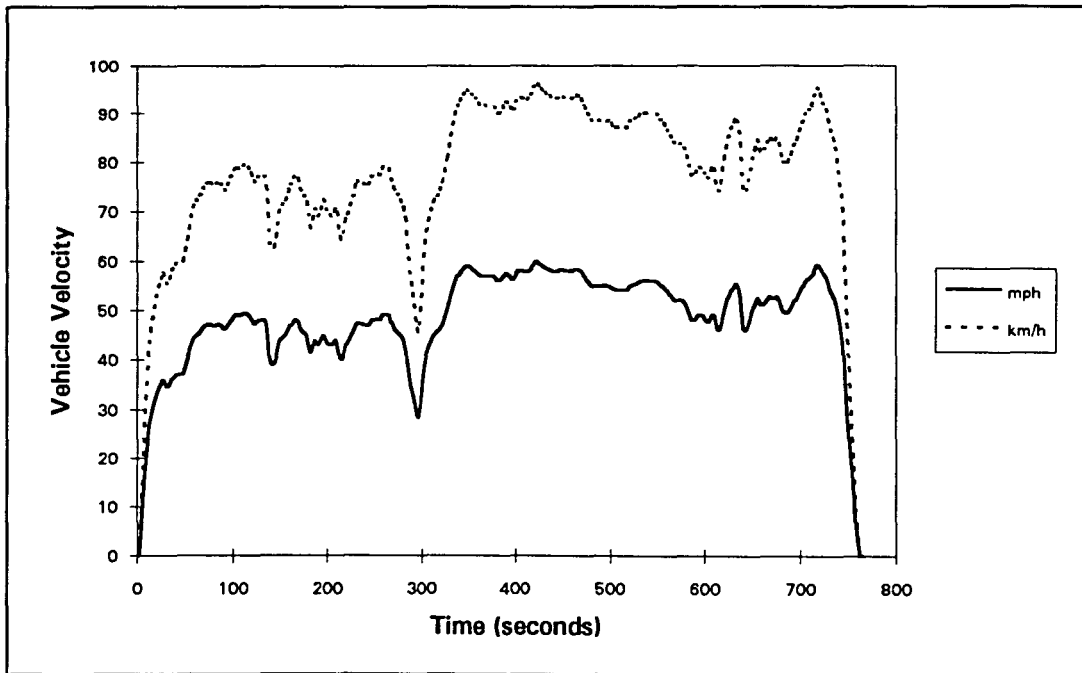


Figure 21. Velocity schedule for the EPA highway cycle.

The second driving cycle used in the simulation was the 1972 Federal Test Procedure (FTP) Schedule. This schedule is sometimes referred to as the EPA Urban Dynamometer Driving Schedule because it is used by the EPA to dynamometer test light duty vehicles for emissions over a representative urban cycle. As shown in Figure 22, it consists of a 1371 second test that has an average speed of 31.46 km/hr over the course of 11.988 km (7.451 miles).

3.3. Simulation Results

The simulation had the potential to run in four different vehicle modes. The simulated vehicle could be operated either as a hybrid vehicle or as an all electric vehicle. Regenerative braking (RB) could be used for both the hybrid and all-electric options. This results in four distinct modes: the EV with RB, the EV without RB, the HEV with RB, and the HEV without RB. The simulation was run a number of times with various combinations of vehicle parameters. Results from two sets of vehicle parameters are presented in this section. The simulated vehicles

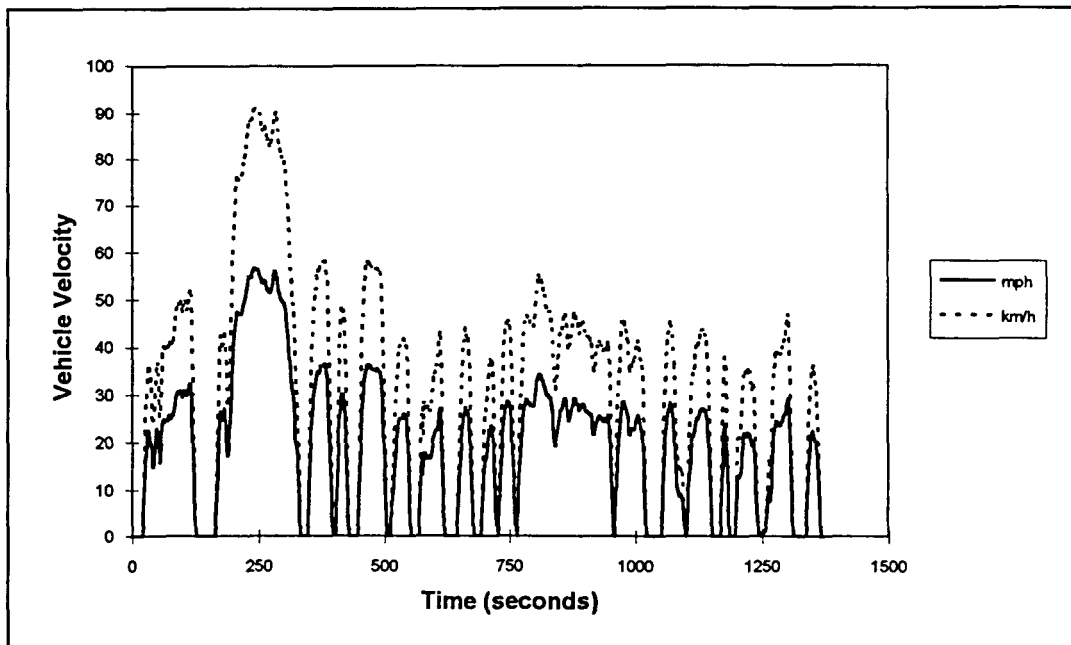


Figure 22. EPA Urban Dynamometer Driving Schedule.

were tested both with the battery energy as an input and with the vehicle range as an input. All tests were run using the EPA highway cycle.

3.3.1. Simulation Tests for Prescribed Battery Energy Cases

The first tests performed on the simulation used initial and final battery and fuel energy levels to determine the vehicle range. The vehicle parameters used in the prescribed battery energy tests are shown in Table 6. The parameters for this vehicle are taken from an electric G-van that used a 24 hp engine for range extension. Table 7 compares the vehicle range for each of the four modes of operation, with an initial battery energy of 35,100 W-hrs. The electric mode without regenerative braking has the shortest range of 43.9 km, which it traveled in 0.57 hours. When regenerative braking is included, the range extends to 45.9 km, which is a 4.6% increase. The range goes up even further with energy addition from a 100 kW APU. Without regenerative braking, the hybrid vehicle travels 91.5 km using 3 gallons of fuel. With regenerative braking, this number increases to 95.9 km.

Table 6. Vehicle parameters used in prescribed battery energy tests.

Parameter	Symbol	Value
Drag Coefficient	C_d	0.4
Frontal Area	A_f	4.2 m ²
Vehicle Mass (excluding battery)	M_v	3901 kg
Battery Mass	M_b	435 kg
Initial Battery Energy	E_0	35.1 kW-hrs
Fuel Capacity	V_{fuel}	3 gallons
Electric Motor Efficiency	η_{motor}	80%
Drive Train Mechanical Efficiency	$\eta_{mechanical}$	80%
Battery Charge Acceptance	$\eta_{battery}$	90%
Engine Thermal Efficiency	$\eta_{thermal}$	31.4%
Generator Efficiency	$\eta_{generator}$	77%
Low Reference State of Charge	SOC ₁	30%
High Reference State of Charge	SOC ₂	40%
Minimum State of Charge	SOC _{min}	20%

Table 7. Comparison of range and discharge times for each mode of operation with an initial battery energy of 35,100 Watt-hrs and 3 gallons of fuel.

Mode	Range (km)	Discharge Time (hours)
Electric without Regenerative Braking	43.9	0.57
Electric with Regenerative Braking	45.9	0.59
Hybrid without Regenerative Braking	91.5	1.18
Hybrid with Regenerative Braking	95.9	1.23

3.3.2. Program Modifications for Prescribed Vehicle Range Cases

Tests were also run specifying the vehicle range. A different vehicle was used for the fixed vehicle range tests. The vehicle parameters are shown in Table 8, and were chosen to represent a typical hybrid vehicle. Problems occurred with these tests because both the fuel volume and the battery energy were calculated by the program. This gave a number of different results for the same energy drain. The sum of the final battery energy and fuel energy was constant, but each could vary. In order to make better comparisons between driving scenarios, the program was modified to fix both the vehicle range and final battery SOC. This way, only the fuel consumption was calculated by the simulation. To implement the final battery SOC restriction, the

Table 8. Vehicle parameters used in prescribed vehicle range tests.

Parameter	Symbol	Value
Drag Coefficient	C_d	0.36
Frontal Area	A_f	1.976 m ²
Vehicle Mass (including battery)	mass	1700 kg
Initial Battery Energy	E_0	11.8 kW-hrs
Electric Motor Efficiency	η_{motor}	80%
Drive Train Mechanical Efficiency	$\eta_{\text{mechanical}}$	80%
Battery Charge Acceptance	η_{battery}	90%
Engine Thermal Efficiency	η_{thermal}	31.4%
Generator Efficiency	$\eta_{\text{generator}}$	77%
APU Starting SOC	SOC ₁	30%
APU Stopping SOC	SOC ₂	70%
Minimum State of Charge	SOC _{min}	20%

program was modified to predict the amount of APU energy needed for the vehicle to complete the prescribed course using a specified amount of battery energy. In the prediction, the following assumptions are made about the driving cycle:

- 1) The vehicle travels repeatedly over the same cycle.
- 2) The cycle it travels is the EPA highway cycle.
- 3) An integer number of cycles are completed.

Using these assumptions, the energy required from the APU is calculated as follows. For an initial cycle, the amount of energy dissipated over the cycle (E_{cycle}) is calculated. This energy is equal to the initial energy in the battery (E_{batt0}) minus the battery energy remaining after one cycle (E_{batt}).

In equation form, this reads:

$$E_{\text{cycle}} = E_{\text{batt0}} - E_{\text{batt}} \quad (18)$$

The amount of energy discharged over the entire trip (E_{dis}) is then equal to the energy discharged per cycle multiplied by the number of cycles traveled (N_{cycle}):

$$E_{\text{dis}} = E_{\text{cycle}} N_{\text{cycle}} \quad (19)$$

To find the energy required from the APU (E_{in}), the energy available from the battery was subtracted from the total energy predicted for the trip. Assuming the battery discharges to the state of charge set by SOC_{min} , the energy input from the APU is:

$$E_{in} = E_{dis} - E_{batt0}(1 - SOC_{min}) \quad (20)$$

To obtain this amount of energy from the APU at a constant power output, the engine must run for a certain length of time (τ_{on}). This reference time takes into account the generator efficiency and the battery charge acceptance:

$$\tau_{on} = \frac{E_{in}}{P_{APU} \eta_{gen} \eta_{batt}} \quad (21)$$

Another reference time is the total traveling time for the trip (τ_{cycle}). This is set equal to the number of cycles multiplied by the time required to travel a single cycle. In equation form, this reads:

$$\tau_{cycle} = N_{cycle} (time / cycle) \quad (22)$$

The time remaining during the cycle (t_{rc}) is defined as the difference between the total time for the trip (τ_{cycle}) and the instantaneous time seen by the vehicle (t_{cycle}):

$$t_{rc} = \tau_{cycle} - t_{cycle} \quad (23)$$

The time remaining for the APU to provide enough energy to complete the prescribed number of cycles with the desired final state of charge (t_{ron}) is equal to the total time that the APU must remain on (τ_{on}) minus the time that it has already run (t_{on}):

$$t_{ron} = \tau_{on} - t_{on} \quad (24)$$

The running time of the APU is equal to the sum of the times during which it has turned on. For example, if the APU has operated three times for dt_1 , dt_2 , and dt_3 seconds, the total on-time can be calculated as follows:

$$t_{on} = dt_1 + dt_2 + dt_3 \quad (25)$$

There are three different scenarios for the relationship between t_{ron} and t_{rc} . As illustrated in Figure 23, the time remaining for proper APU operation can either be greater than, equal to, or less than

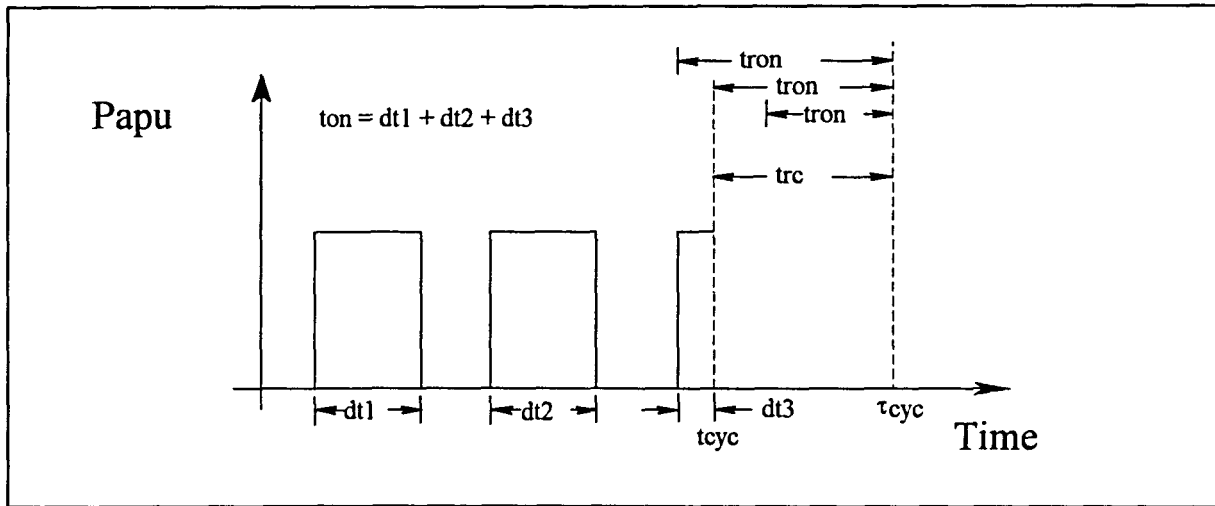


Figure 23. A possible cycle for the APU over a specified trip.

the time remaining in the cycle. If t_{ron} is greater than t_{rc} , the APU will not be able to input enough energy to charge the battery within the time remaining in the cycle. Since this condition is undesirable, the APU should be turned on before it occurs. If t_{ron} equals t_{rc} , then the time left to run the APU is equal to the time remaining in the cycle. This marks the time at which the APU should turn on. If t_{ron} is less than t_{rc} , the time remaining in the cycle exceeds the time left to run the APU, which means that the APU does not need to be turned on at this point. In summary, the APU should be turned on if either one of the following occur:

1. $t_{ron} \geq t_{rc}$
2. $SOC < SOC_1$ (SOC restriction)

and the APU should be turned off if any one of these conditions occur:

1. $t_{on} > \tau_{on}$
2. $V_{fuel} \leq 0$ (out of gas condition)
3. $SOC > SOC_2$ (provided $t_{ron} < t_{rc}$).....(SOC restriction)

Regenerative braking was not taken into account for any of the scenarios in this section (3.3.2).

Regenerative braking would decrease the energy required per cycle, thus decreasing the required APU energy production.

3.3.3. Effect of Distance Traveled

Using the above procedure, the number of cycles was varied, while keeping the power output from the APU constant. The number of driving cycles contained within a complete trip was varied from 5 to 9. Figure 24 shows the length of time that the APU must remain on to provide enough energy for the vehicle to complete the prescribed number of cycles. To complete the trip, an APU must provide an amount of energy equal to its power output multiplied by the time for which it remained on. This energy is represented by a rectangle in Figure 24. The rectangle height is equal to the power output from the APU, and the rectangle width corresponds to the APU on-time. This time can be distributed in any proportions over the trip, but for this example, the engine turns on for only the last portion of the trip. The engine could turn on at the beginning of the trip and remain on for the same amount of time, ending earlier. But in all the tests shown in Figure 24, the total engine on-time is calculated, and the starting time is determined so that all runs end at the completion of the trip. As additional cycles are added to the trip, more energy is required to complete it. This additional energy comes from the APU, which turns on earlier in the trip each time another cycle is added.

Figure 25 shows the energy discharge curve as a function of the number of cycles traveled by the vehicle. For each trip, the vehicle completes the prescribed number of cycles with a final state of charge equal to SOC_{min} . Forcing every test run to end at the same conditions allows comparisons between cases to be made on a consistent basis. At first, the vehicle discharges the battery using the electric-only mode. Then, the APU turns on at the simulation-calculated start time, which results in a change in the slope of the battery discharge curve. The slope of the second portion of the curve remains constant because the APU power output is not changed. So, as cycles are added to the trip, the start time moves higher on the electric-only dissipation curve. With the earlier starting time, the APU remains on for a longer portion of the trip, which was shown in Figure 24.

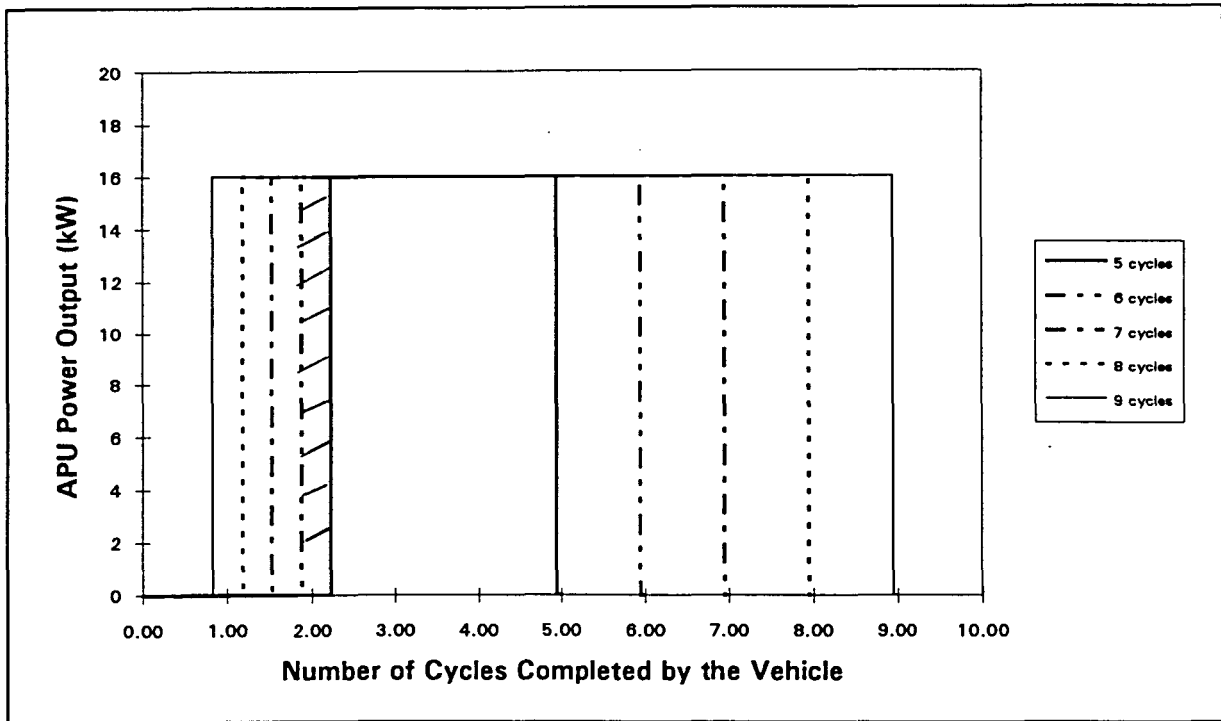


Figure 24. APU power output as a function of the number of EPA highway cycles completed by the vehicle with a fixed APU power output and a variable number of cycles traveled.

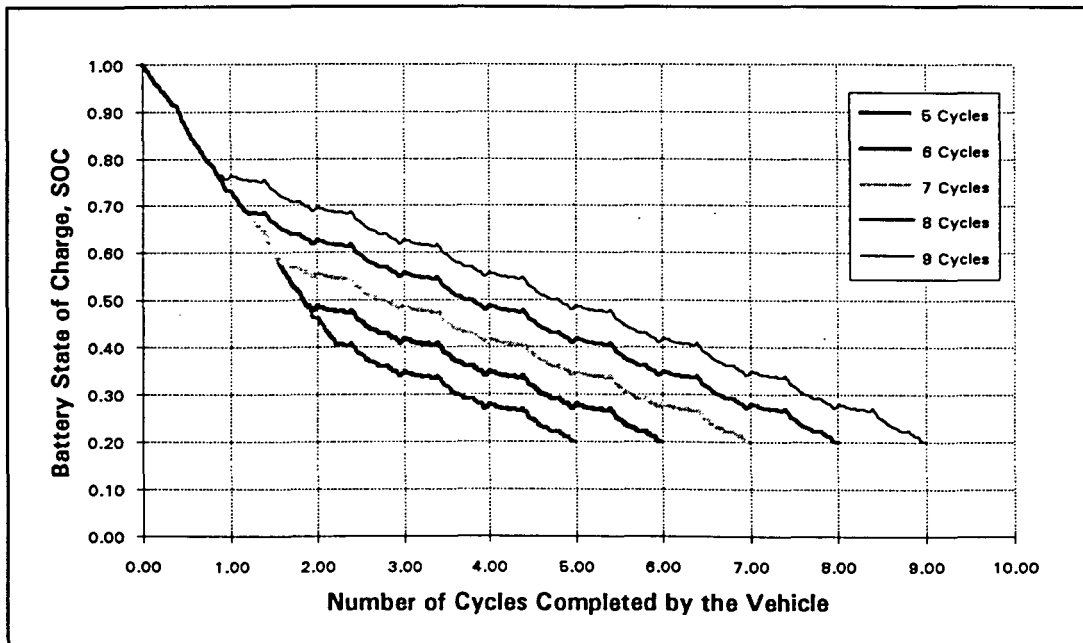


Figure 25. Battery state of charge as a function of the number of cycles completed by the vehicle, showing battery discharge curves for trips between 5 and 9 cycles long, $SOC_{\min} = 20\%$.

When the trip increases from 5 to 6 cycles, τ_{on} increases by more than one cycle. This additional time is repeated by the portion of the 6 cycle curve to the left of the 5 cycle rectangle. The time corresponding to the hash marked area in Figure 24 is the amount of time greater than 1 cycle for which the APU must remain on. When enough cycles have been added, the APU start time moves to zero. When the APU is started at the beginning of the trip, the maximum range for that size of APU will be reached. A sufficiently large APU will cause the slope of the battery discharge line to become horizontal, giving the vehicle a range dependent on the size of the gas tank. But, for smaller APUs, there will be a range limit, where the battery must be charged from some external source before the vehicle can travel any further.

3.3.4. Effect of APU Power Output

To investigate the effects of APU size, the power output of the APU was varied from 5 kW to 35 kW with SOC_1 equal to 30% and SOC_2 equal to 70%. The trip length was kept constant at 5 cycles, which fixes the amount of energy required to complete the trip. Since the energy input is proportional to the APU power output multiplied by the APU running time, the APU running time should decrease as the power output increases. This is shown by Figure 26. For lower power outputs, the running time is constrained by the time required to input the specified amount of energy. The APU must turn on early in the trip and run until the end of the cycle. As with Figure 24, this is a convention that will facilitate comparison of different power levels. In actuality, the APU can turn on and off at any time during the cycle, so long as the total running time is equal to τ_{on} . With this convention, the APU turns off at the same time for the power outputs below 19 kW. At the high end of the power outputs, 19 kW and greater, the APU turns on when the state of charge reaches SOC_1 , which in this case is 30%. In Figure 26, this can be seen by the last vertical line on the left side of the power output rectangles. All sizes of APUs 19 kW and above start at the 30% SOC line and continue until the prescribed amount of energy has been added.

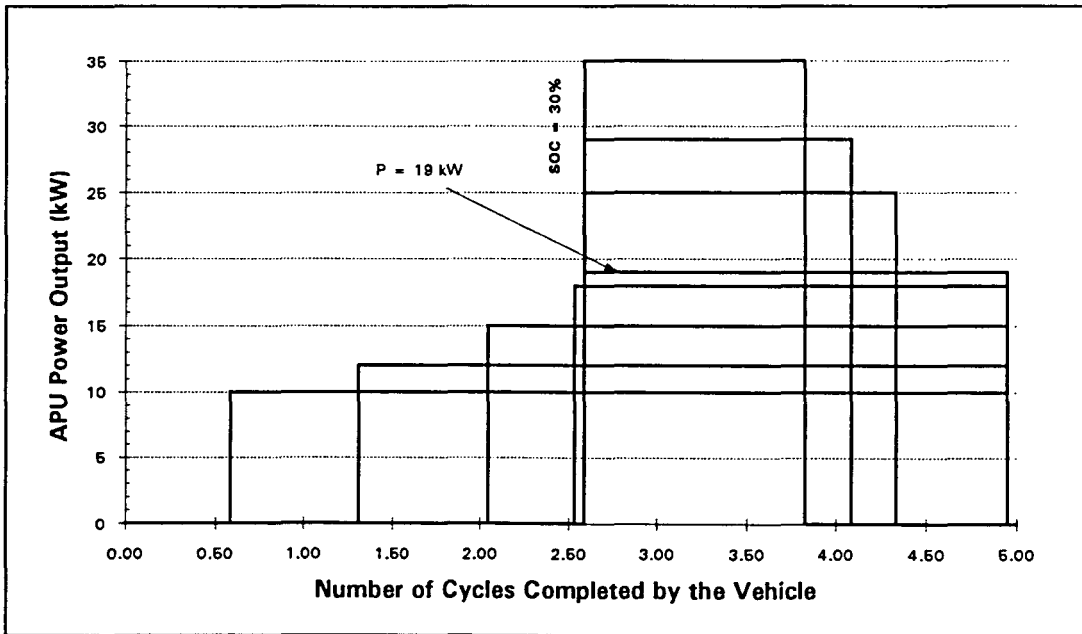


Figure 26. APU power output as a function of the number of EPA highway cycles completed by the vehicle.

Another way of looking at the APU starting and stopping times comes from an examination of Figure 27. This figure shows the dissipation of battery energy from 100% SOC to 20% SOC over 5 EPA highway cycles for various APU sizes between 10 kW and 35 kW. Although this figure looks confusing at first, a clearer picture of the discharge process can be seen by considering smaller groups of cases. Figure 28 shows the low end APU power outputs. For APU sizes below 19 kW, the auxiliary power unit must turn on early in the trip, before the SOC has reached 30%. As the power output becomes larger, the slope of the discharge curve becomes flatter and the APU is able to turn on later. When the power output level reaches 19 kW, the APU turns on at an SOC of 30%.

As shown in Figure 29, the slope increases and becomes positive when the APU power is greater than 19 kW. Consequently, the running time of the APU continues to decrease as the power output increases. For these larger sizes, the auxiliary power unit remains on for a relatively

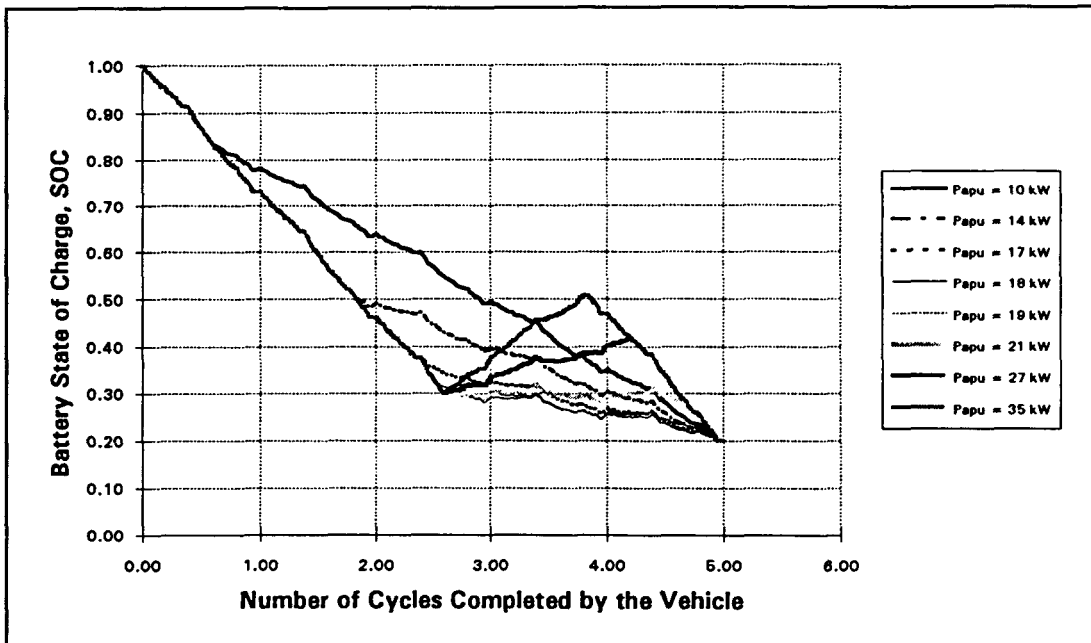


Figure 27. Battery state of charge as a function of the number of cycles completed by the vehicle, showing power outputs from 10 kW to 35 kW.

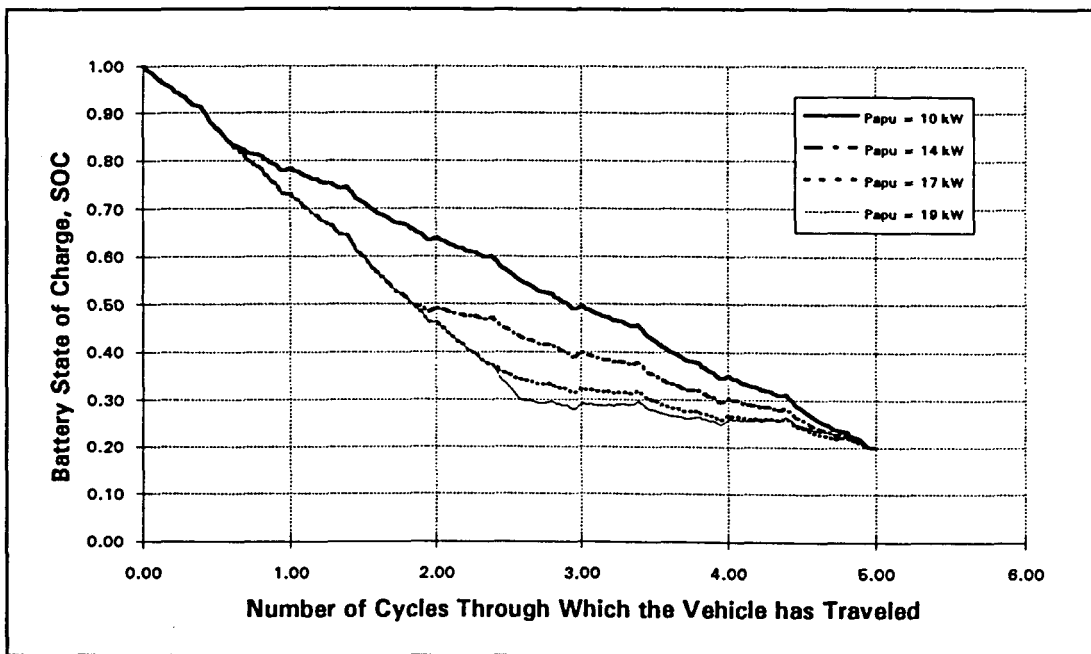


Figure 28. Battery state of charge as a function of the number of cycles completed by the vehicle, showing power outputs from 10 kW to 19 kW.

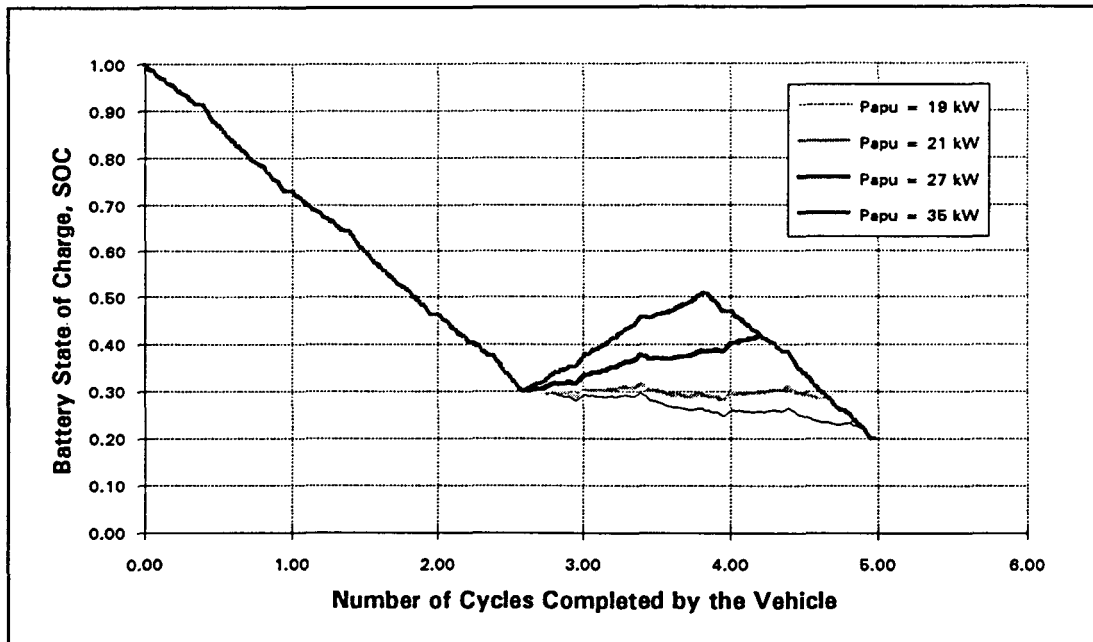


Figure 29. Battery state of charge as a function of the number of EPA highway cycles completed by the vehicle, showing power outputs from 19 kW to 35 kW.

short period of time and then discharges in electric only mode for the remainder of the trip. The electric only discharge follows the same curve for all power levels.

Figure 30 shows the transition region around a power level of 19 kW. An 18 kW APU turns on slightly before the battery reaches 30% SOC and exhibits a discharge curve similar to the 19 kW discharge. The 21 kW APU begins charging at an SOC of 30% and has a slope slightly larger than the 19 kW discharge curve. Again, the composite of Figures 28 through 30 is shown in Figure 27.

In a separate test, power outputs from 17 to 35 kW were used and SOC_2 was lowered to 40%. Figure 31 shows that by lowering SOC_2 , the APU exhibits on/off operation. The APU turns on when the battery discharges to SOC_1 and turns off when the battery recharges to SOC_2 . Figure 32 shows that an auxiliary power unit with a power level of 19 kW does not increase the battery SOC above 40%, so the APU turns on once and remains on for the remainder of the trip. When the power output increases to 27 kW, the APU charges the battery to a SOC of 40% and

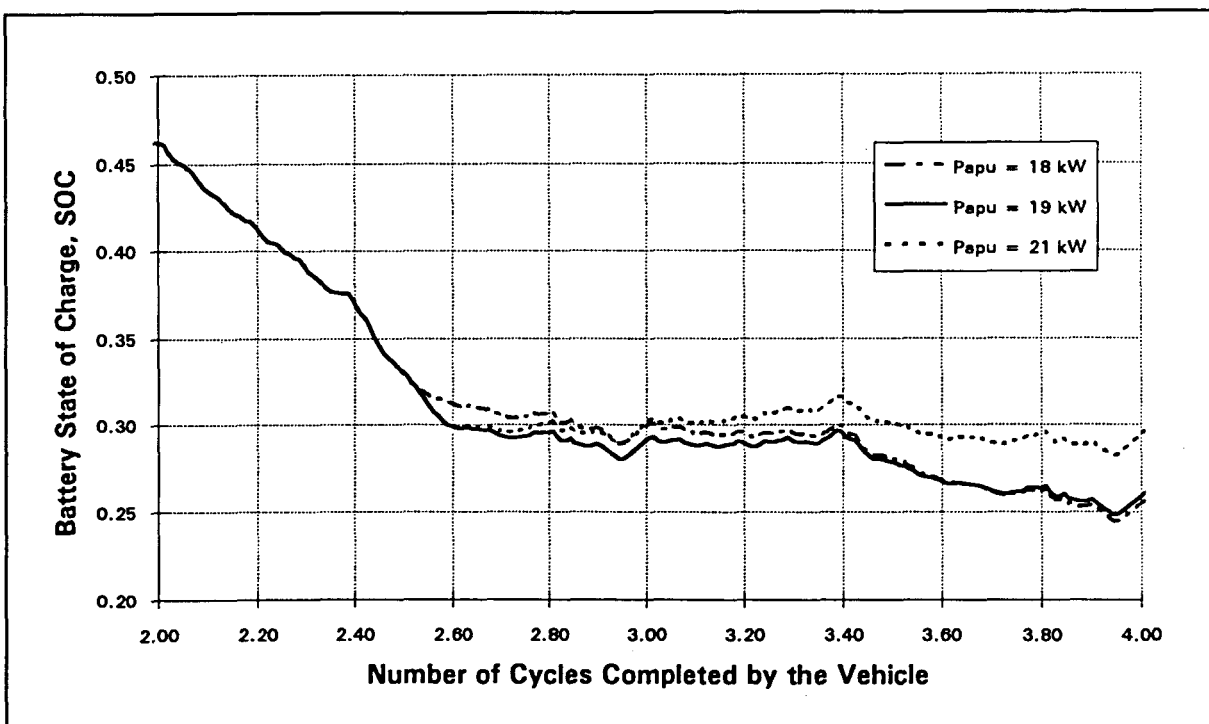


Figure 30. Battery state of charge as a function of the number of EPA highway cycles completed by the vehicle, showing power outputs from 18 kW to 21 kW.

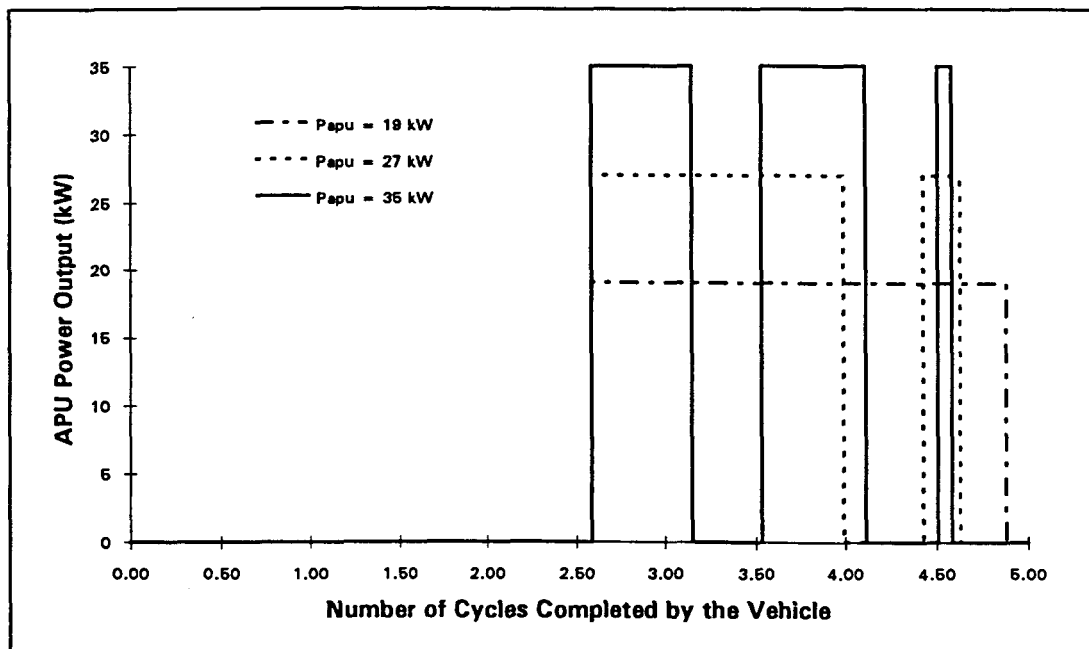


Figure 31. APU power output as a function of the number of EPA highway cycles completed by the vehicle.

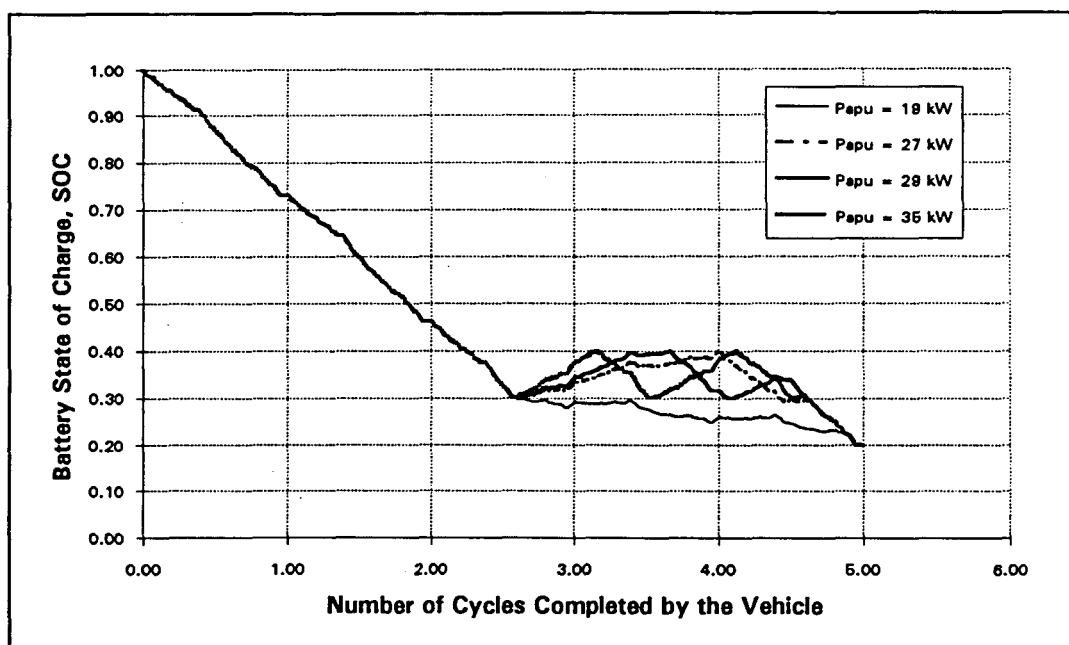


Figure 32. Battery state of charge as a function of the number of EPA highway cycles completed by the vehicle, showing power outputs from 19 kW to 35 kW.

then lets the battery dissipate in electric-only mode to 30%. Since more energy is still required, the APU turns on at this point for a second time. Both the 27 and 29 kW units will turn on twice over the course of the trip. When a power level of 35 kW is used, the APU turns on three times.

3.4. Simulation Summary

The computer simulation developed for this project models the operation of a series HEV over a specified driving cycle. The program was initially tested using a constant vehicle velocity. Then tests were performed using the EPA highway cycle.

To obtain a better comparison between simulation runs, the program was modified to fix both the battery energy discharged and the range traveled by the vehicle. Using the modified code, the number of cycles traveled by the vehicle was varied while maintaining a constant APU power output and the APU power output was varied with the number of EPA highway cycles remaining fixed. The first test showed that when the total distance traveled was increased, the APU on-time

increased more than one cycle length. The second test fulfilled the first two objectives stated at the beginning of this chapter.

The first objective was to determine an appropriate APU size for a typical HEV. The lowest APU power output possible for HEV use would run continuously over the entire cycle. For the vehicle simulated in this chapter, that power output was around 8 kW. A high power limit for the APU must be greater than the average power requirement for the cycle. Figure 30 shows that the average power requirement for this vehicle over the EPA highway cycle is around 19 kW. APUs rated above 19 kW would provide a vehicle range that is dependent on the fuel energy rather than the battery energy. The engine should be sized somewhat higher than the minimum to account for unexpected variations in the driving cycle, but at the same time the engine size should be minimized due to volume and weight considerations. For this application, an APU rated at around 35 kW would be appropriate. So, an engine larger than 8 kW would meet the minimum requirements for the HEV used in this simulation, and a 35 kW engine would provide sufficient power to run the vehicle under most circumstances.

The second objective was to examine how the APU power level affected the APU starting frequency. The simulation test that varied the APU power level demonstrated that changes in the power level sent the APU operation through three phases. For the lowest power outputs, the APU ran continuously and started when t_{ron} became greater than t_{rc} . When the power output was increased to a certain level, the starting time became determined by SOC_1 . At still higher power levels, the APU began to exhibit on/off operation, where the starting time was determined by SOC_1 and the stop time corresponded to a battery energy level equal to SOC_2 .

The third objective was to calculate timing parameters used in the engine test. This objective will be met when the simulation is repeated using inputs specified in section 4.5, where the test matrix for the engine dynamometer experiments is developed.

4. EXPERIMENTAL EQUIPMENT AND PROCEDURE

One of the main objectives of this thesis is to estimate the emissions and fuel consumption per mile of a hybrid-electric vehicle. Before this calculation can be made, the level of emissions and fuel consumption for an engine must be known. The dynamometer tests on an Onan P224 two cylinder engine provide the information needed to complete the fuel consumption and emissions calculation. The tests also show the effect that the APU power output and the number of engine starts has on fuel consumption and exhaust emissions.

As shown in Figure 33, the engine stand used in the following experiment consists of an Onan P224 gasoline engine coupled with a General Electric TH312 eddy current dynamometer. The Onan P224 is an air-cooled, opposed two-cylinder, spark-ignition four-stroke engine. A similar engine to this one was used to extend the range of an electric G-van in a hybrid vehicle application [20]. The following sections describe what measurements were made during the testing, how the measurements were taken, and what procedures were used. Section 4.1 gives an overview of what parameters were measured. Sections 4.2 through 4.4 provide a more detailed description of the data acquisition system, fuel flow meter, and emissions bench. Section 4.5 describes how the test matrix was generated, and section 4.6 gives the testing procedures.

4.1. Measured Parameters

Measurements made in this test include the engine speed and torque, the intake vacuum, the intake air flow rate, the fuel flow rate, and various engine temperatures. Speed is measured through a magnetic pick-up that gives 60 electric pulses per crankshaft revolution. Torque is measured by a load cell that reads the force applied to the dynamometer at a certain distance from the crankshaft. This force times the distance to the load cell equals the torque output from the engine. The speed and torque measurements are displayed on the front panel of the dynamometer controller, and can be accessed through analog outputs from the controller. Intake manifold vacuum is measured using a bourdon tube pressure gage and a pressure transducer. The intake air

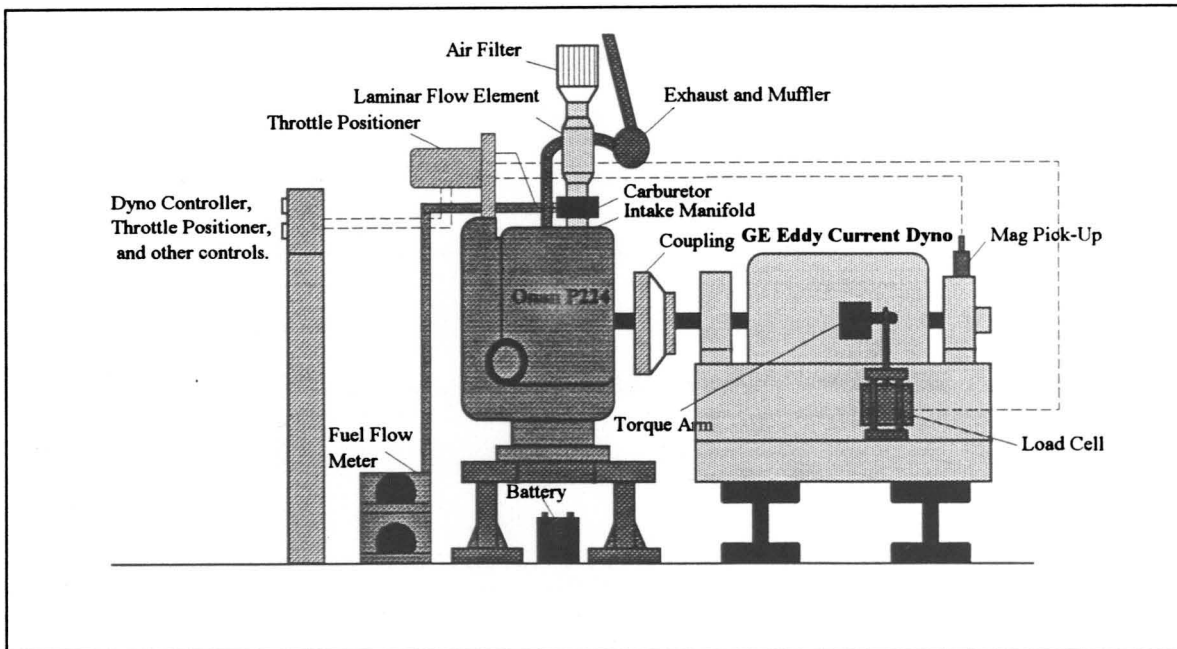


Figure 33. Schematic of the Onan P224 engine stand.

flow rate is measured using a laminar flow element (LFE). The pressure drop across the laminar flow element is read by a pressure transducer and the reading is converted into a flow rate by the following relationship:

$$\dot{m}_a = \rho Q = \left(\frac{P}{RT} \right) \left[\frac{\Delta P}{8'' H_2O} (100 \text{ scfm}) * \left(\frac{0.3048 \text{ m}}{1 \text{ ft}} \right)^3 * \frac{1 \text{ min}}{60 \text{ s}} \right] \quad (26)$$

where ΔP is the pressure drop across the LFE in inches of water, P is the ambient air pressure in kPa, R is the gas constant for air in kJ/kg-K, and T is the intake temperature in degrees Kelvin.

The mass flow rate is in kg/s. It should be noted that to accommodate the LFE onto the carburetor, the PCV line was rerouted directly to the exhaust, rather than back into the intake manifold. This may have some effect on emissions readings. Fuel flow rate is measured by a Flo-tron fuel flow meter donated by Ford Motor Company. Its operation is described in section 4.3.

Temperature measurements are made using both Type-T and Type-K thermocouples. The data acquisition system reads only Type-T. Type-K thermocouples are attached to the engine, but

must be read on a thermocouple readout. The data acquisition system reads the intake temperature, both head temperatures, the oil temperature, and the emissions sample line temperature. The fuel temperature is monitored using a thermocouple readout. The next section gives a more detailed description of the data acquisition hardware.

4.2. OPTO-22 Data Acquisition System

The engine temperatures and pressures are measured by a set of OPTO-22 data acquisition boards that were donated by Ethyl Petroleum Additives, Inc. These boards are configured in a modular system as shown in Figure 34. There are five boards in all, each containing a series of input and output modules. Four main types of modules can be placed on the boards: current output, current input, voltage output, and voltage input. There are various ranges for each type of module, and specialty modules are also available. The boards interface with an IBM compatible PC through an RS-232 communications port. This is converted into an RS-485 signal through an OPTO-22 AC7A serial port converter. The AC7A connects to the data acquisition boards, which house the input and output modules. Two types of input modules are used for data acquisition in the present setup: 0-5V input modules and Type-T thermocouple modules. All of these modules are located on one board. The 5V modules are used to read analog data from the dyno controller and pressure transducers. The thermocouple modules read temperature data from the engine and sample line.

The OPTO-22 system also allows for data averaging. The system averages a number of samples specified by the operator. The appropriate number of samples varies with the application. For transient tests, a smaller number of samples should be averaged so that the trends in the data can be distinguished. For steady state tests, a higher number of samples should be used to damp out variations. Since transient conditions are measured during startup and shutdown of the engine, the number of samples has been set at 10. The readings are taken at an interval dictated by the Visual Basic control software written for this application. The software allows the sample interval to be varied by the person controlling the system. For the on/off tests, the sample interval is set at

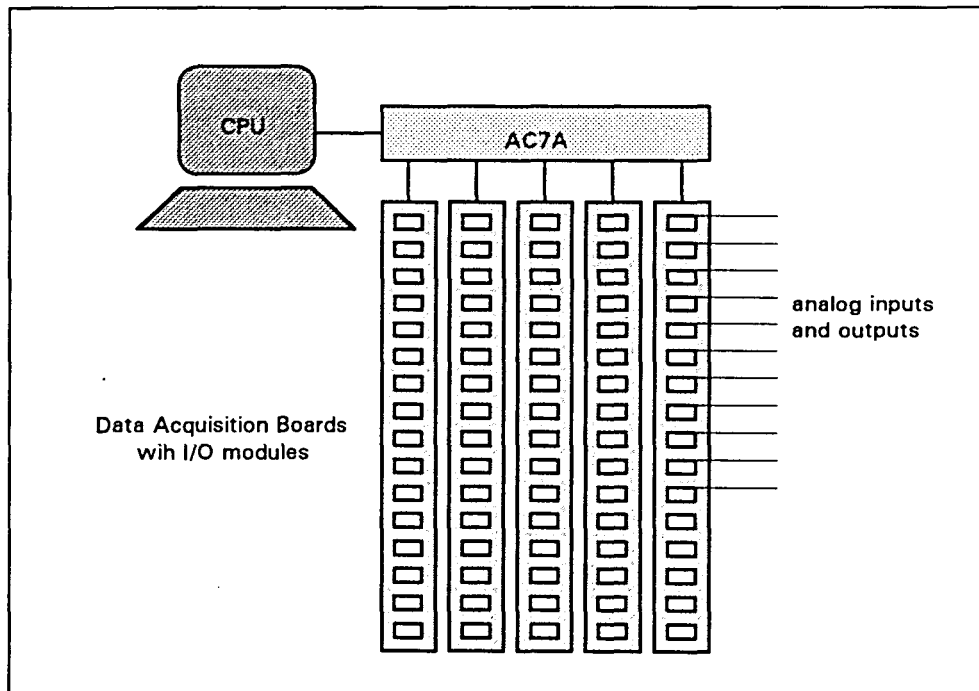


Figure 34. Configuration of OPTO-22 data acquisition system, showing the location of the microprocessor and data acquisition boards.

1 second. The actual sample interval is slightly larger than this, however. The OPTO-22 system requires a fixed amount of time to average the data, which dictates the minimum sample interval time. For 10 averaged samples, the sample interval was around 1.16 seconds. All data taken by the OPTO-22 system can be stored in a file for later use.

In addition to their input functions, the OPTO-22 boards provide the capability for an analog output. One output module is used in this test, and it has a 0-5V range. The output module is used for controlling the throttle position. A throttle controller made by Lab Equipment Corporation (LABECO) can be controlled by a potentiometer or by a 5 volt control source. For the HEV engine tests, the throttle is computer controlled. This allows the operator to set a constant torque, as will be described in section 4.6.2.

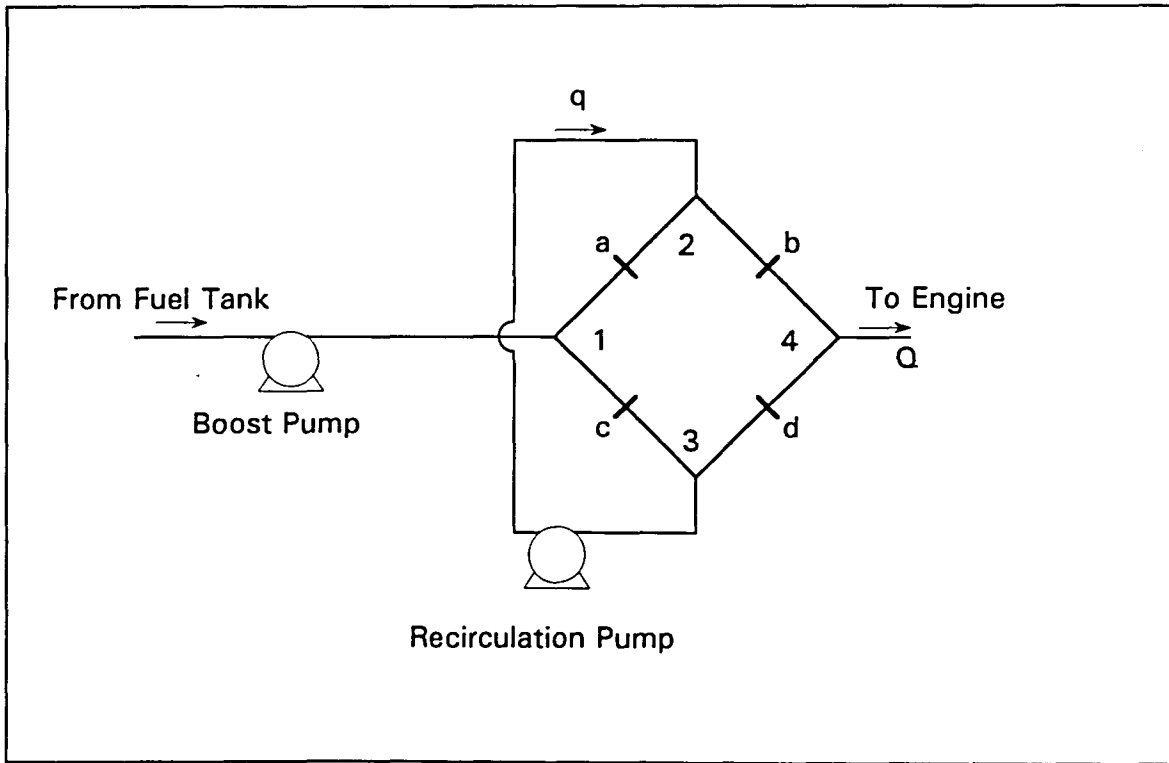


Figure 35. Schematic diagram of the Flo-tron fuel mass flow meter [38].

4.3. Fuel Mass Flow Rate Measurement

A Flo-tron fuel mass flow meter donated by Ford measures the instantaneous fuel flow rate by using a system of orifices. As shown in Figure 35, orifices **a** through **d** are in a configuration that resembles an electrical wheatstone bridge. A recirculation pump provides a flow rate q between points 2 and 3 that is superimposed on the main flow rate to the engine, Q . Depending on the relative magnitudes of q and Q , the unit has two modes of operation: Type I and Type II. Type I operation is used for high flow rates, where $Q > q$. The fuel mass flow rate can be determined in this mode by measuring the pressure drop between points 2 and 3:

$$\dot{m}_f = \frac{P_2 - P_3}{k} \quad (27)$$

where k is a constant dependent on the flow rate q and on the geometry of the orifices. When the main flow rate drops below the recirculation flow rate ($Q < q$), the meter should operate in Type

II mode. The meter must be disassembled and the orifices must be repositioned to change from Type I to Type II operation. The value for flow rate in Type II mode depends on the pressures at points 1 and 4:

$$\dot{m}_f = \frac{P_1 - P_4}{k} \quad (28)$$

where k is the same constant used in type I operation.

The value for k is determined experimentally. The pressure difference between points 1 and 4 is measured by a Model 1151 Fisher-Rosemount pressure transducer. The transducer gives a 4 to 20 mA signal. The fuel flow meter is calibrated by measuring the current output from the pressure transducer as a function of flow rate. A steady flow rate is achieved by using the boost pump to transfer gasoline between two fuel tanks. The mass of the receiving tank is measured at a specified time interval to give the mass flow rate. The measured mass flow rate is compared with the amperage output from the pressure transducer to yield the following relationship:

$$\dot{m}_f = -5.095 + 1.188 * I \quad (29)$$

where I is the current output from the meter in milliamperes (mA) and the mass flow rate of fuel is calculated in grams per second (g/s). This linear relationship is used to compute the mass flow rate of fuel during all engine tests.

Fuel is delivered to the engine through a carburetor. Normally, a vacuum pump draws fuel from a tank to supply the carburetor. The Flo-tron fuel flow meter uses a boost pump to increase the fuel pressure, making the original fuel pump unnecessary. The original fuel pump was left in the fuel line, and the engine is capable of running with the fuel flow meter shut off. Also, a system of three-way valves allows for filling of the fuel tank and periodic re-calibration of the fuel flow meter. None of these modifications seem to affect the operation of the engine or the fuel flow meter. The power and brake specific fuel consumption were essentially the same before and after the fuel flow meter was added. Before the meter was put in place, the fuel flow rate was measured by taking mass readings of the fuel tank at set time intervals. The average mass flow rate before

the fuel flow meter was installed was around 0.52 kg/kW-hr, and after installation the rate was 0.495 kg/kW-hr on average. Power output at wide-open-throttle (WOT) also remained about the same. The power was 11.43 kW prior to the addition of the meter, and was about 11.64 kW after installation².

4.4. Emissions Measurements

A Horiba emissions analyzing system was donated by Ford Motor Company with the Flo-tron fuel flow meter. The system consists of seven emissions analyzing units that are divided between two benches: engine and exhaust gas recirculation (EGR). The engine bench contains six analyzers and samples gas directly from the engine exhaust. The analyzers in this bench measure oxides of nitrogen (NO_x), oxygen (O_2), unburned hydrocarbons (HC), carbon dioxide (CO_2), and two levels of carbon monoxide, low and high (LCO and HCO). The EGR bench contains one CO_2 analyzer. It measures the carbon dioxide content of the gas recirculating from the engine exhaust manifold to the intake manifold, provided the engine is equipped with this capability.

Data acquisition from both benches is provided by means of an analog output. Each analyzer gives a voltage output proportional to the pollutant concentration in the sample gas. This output is available from a digital volt meter attached to the front of the unit, from banana jacks near the volt meter, and from wires routed internally. The analyzers operate at different ranges depending on the pollutant concentration. To switch from one range to another, knobs are provided on the front of the meter, and an external switching function allows a computer to control the analyzer range.

Flow through the system is controlled by a network of solenoid valves and stainless steel tubing. Sampling and calibration inputs are routed through this network to each of the units. All of the analyzers have five calibration inputs in addition to the sampling input. The calibration

²The fuel consumption rate data and power output data before the fuel flow meter installation are taken from one test run. The quantities after installation are taken as a numerical average of all mean results from the on/off testing.

inputs consist of a zero gas, three span gases, and another calibration gas. Zero and span knobs on the front of the meter allow the range of measurement to be established using the calibration gases.

The Horiba system also contains general functions for each of the two benches. Some functions are used for maintenance purposes and others are used during sampling or calibration. These special commands include pressure check, vacuum check, refrigeration bath bypass, bench purge, and bench back-flush.

The commands for the Horiba emissions sampling system were originally executed through a microprocessor based system. This system opened and closed solenoid valves to obtain the correct sample gas flow path. It also turned pumps on and off and remotely switched the analyzer ranges. Unfortunately, this system is no longer operational. Since attempts to repair the microprocessor proved unsuccessful, a replacement microprocessor system was installed. The installed system serves two functions: to control the gas flow through the bench and to write data from the analyzers to a file. The CPU-based microprocessor system uses a National Instruments PC-LPM-16 data acquisition card installed in an IBM compatible PC. The PC-LPM-16 writes digital outputs and reads analog inputs. The digital outputs trigger solenoid valves and other bench functions, while the analog inputs read data from the seven analyzers.

The digital outputs control the operation of the bench using as much of the original system as possible. All of the functions on the Horiba emissions bench were wired through a panel that interfaced with the old microprocessor system. The old system activated each function using a switch. When a switch was triggered, two points on the panel were connected, and the corresponding function turned on or off. The new system uses the panel to control the functions in the same way as before. The system labels each function with a digital address. When the PC-LPM-16 outputs an address, a microprocessor-based switch triggers, which activates the corresponding function. More than one function may remain active at one time. The system has not been wired to remotely change ranges, however. The system is designed for this capability,

and the hardware has been purchased, but a circuit board must be wired before the CPU can remotely change ranges.

The analog inputs on the data acquisition card provide a means of measuring the concentration of each emission. The analyzers put out a 0 to 1 volt signal, where 0 volts is an absence of that emission and 1 volt is a full scale reading. For three analyzers (O_2 , HC, and NO_x), the output is linearly proportional to concentration. For two other analyzers (HCO and CO_2), a curve fit must be used relating the percent full scale reading to concentration. The other two analyzers (LCO and EGR- CO_2) are not used for the engine tests.

Software written for the bench includes a main control program and a diagnostics program. The main control program allows the operator to warm up, zero, and span the analyzers. It also provides an on-screen feedback of emission levels. In addition, the main program writes the emission data to a file at a specified sample interval. The diagnostics program is a separate piece of software that allows the operator to activate bench functions individually. Each pump and solenoid valve can be turned on or off using this program.

Mid-way through the testing, water condensed in the stainless steel lines leading up to the analyzers. To eliminate the condensation, dirty filters were replaced and the refrigeration bath was used for the remainder of the testing. The refrigeration bath maintains a 32°F temperature over a short section of the sample line. Any liquid that condenses in the section of line submerged in the bath is drawn out of the system by a pump. Originally, the downstream side of this pump was connected to a filter that was designed to remove the water before returning the gas to the system. Since this filter was not working, water returned to the system and showed up in the rotameters before the analyzers. The problem was remedied by routing the flow around the filter and some other filters were replaced. These adjustments eliminated the condensation problem. The NO_x meter, however, must be cleaned before it can be used again. It was not used in the second half of testing.

4.5. Test Matrix Generation

One of the main objectives of the engine tests was to study the effects that the engine power level and the number of engine starts had on emission levels and fuel economy. The following sections tell how the test parameters were arrived at and what went into determining the test matrix.

4.5.1. Test Information

A 24-hp, two-cylinder Onan engine was dynamometer tested in an on/off fashion, representative of HEV operation. In the engine tests, two parameters were measured: emissions and fuel economy. These parameters were compared over a test matrix that varied the engine power at a constant speed. For each power level, the engine was started an integral number of times from 1 to 5. All tests produced the same amount of energy. In other words, the engine power output multiplied by the total operating time was constant for all combinations of power and number of starts. A more complete description of the matrix and how it was generated will be given in section 4.5.2.

In a series HEV, the engine delivers energy through a generator. So, when choosing an operating point, factors affecting both the engine and the generator should be considered. A generator typically operates at the speed where it provides the highest efficiency. Generators operate most efficiently at high speeds [9]. The genset in the hybrid-electric G-Van operated at a constant speed of 2400 rpm [20]. For this reason, all tests were performed at 2400 rpm.

4.5.2. Matrix Determination

Over a driving cycle, an engine must output a certain amount of energy. The energy level used in this engine test was determined by the HEV simulation program. The simulation modeled the operation of a HEV over a standard driving cycle. The constant input parameters were chosen based on what might be typical driving conditions for the G-van in which the 24 hp engine was used. The vehicle specifications are shown in Table 9. These specifications are the same as in section 3.3.1, except for the reference states of charge. The reference SOCs were chosen so that

Table 9. Vehicle parameters of the simulated G-van.

Parameter	Symbol	Value
Drag Coefficient	C_d	0.4
Frontal Area	A_f	4.2 m ²
Vehicle Mass (excluding battery)	M_v	3901 kg
Battery Mass	M_b	435 kg
Initial Battery Energy	E_0	35.1 kW-hrs
Electric Motor Efficiency	η_{motor}	80%
Drive Train Mechanical Efficiency	$\eta_{mechanical}$	80%
Battery Charge Acceptance	$\eta_{battery}$	90%
Engine Thermal Efficiency	$\eta_{thermal}$	31.4%
Generator Efficiency	$\eta_{generator}$	77%
Low Reference State of Charge	SOC ₁	50%
High Reference State of Charge	SOC ₂	60%
Minimum State of Charge	SOC _{min}	40%

the engine stayed on long enough to perform an adequate test. When the SOC₁ and SOC₂ from section 3.3.1 were put into the program, the vehicle ran entirely in electric mode and the APU did not turn on during the trip. By raising SOC₁ and SOC₂, to 50% and 60%, the engine remained on for a longer period of time, which allowed on/off tests to be performed.

The driving schedule used in the simulation was the EPA highway cycle. The simulated vehicle traveled over three highway cycles, giving a total range of 49.5 km (30.8 mi), and regenerative braking was included in the calculation. The variable used as an input was engine power. The output from the simulation was the time that the engine needed to stay on for the vehicle to finish the prescribed course. A test matrix was setup, dividing the simulation generated engine on-time into uniform segments. The number of segments varied from 1 to 5.

The results of the simulation are shown in Tables 10 and 11. The duration of the test was 38 minutes and 15 seconds. This was the time to complete three EPA highway cycles. The lowest power output from the engine that completes that set of cycles was 3.3 kW. This corresponded to 9.684 ft-lbs of torque at 2400 rpm. The engine needed to remain on for 0.6275 hours (37 min,

Table 10. General test information.

Test Duration	BP (kW)	τ_{on} (s)	Torque (ft-lbs)	Throttle Position (%FS)
2295 seconds	3.3	2259	9.684	36.943
38 min, 15 sec	4.9	1522	14.380	38.051
	6.5	1147	19.075	42.028
	8.1	921	23.770	46.230
Engine Speed	9.7	769	28.466	55.024
2400 rpm	11.3	660	33.161	77.296

39 sec) at this power output, which was 36 seconds short of the total test duration. The highest power output that the engine was capable of producing at 2400 rpm is 11.3 kW. This translates into 33.161 ft-lbs of torque. The engine on-time (τ_{on}) for this power level was 0.1833 hours (10 min, 59 sec). The approximate throttle position for each torque level is also shown in Table 10. This throttle setting was used when the engine was accelerating to 2400 rpm and the automatic torque control was not yet turned on. The method of controlling the torque will be described in section 4.6.2.

For each brake power (BP) level, the engine on-time was divided into an integral number of parts from 1 to 5. The number of parts was assigned the variable n . The test matrix is shown in Table 11. Two parameters were defined in the matrix: Δt and t_{off} . Δt is the time that the

Table 11. Test matrix.

BP (kW)	n = 1		n = 2		n = 3		n = 4		n = 5											
	Δt	toff																		
	min	sec																		
3.3	37	39	0	35	18	49	0	18	12	33	0	12	9	24	0	9	7	31	0	8
4.9	25	22	12	53	12	41	6	26	8	27	4	18	6	20	3	13	5	4	2	35
6.5	19	6	19	9	9	33	9	34	6	22	6	23	4	46	4	47	3	49	3	50
8.1	15	20	22	55	7	40	11	27	5	6	7	39	3	50	5	43	3	4	4	35
9.7	12	48	25	27	6	24	12	43	4	16	8	29	3	12	6	21	2	33	5	6
11.3	10	59	27	16	5	29	13	38	3	39	9	6	2	44	6	49	2	11	5	28

engine remained on, and was calculated using the following equation:

$$\Delta t = \frac{\tau_{on}}{n} \quad (30)$$

t_{off} was the interval between an engine stop and the next engine start. The engine off time was calculated assuming that the time at the beginning and end of the test sum to equal t_{off} . So, t_{off} was calculated as follows:

$$t_{off} = \frac{L}{n} - \Delta t \quad (31)$$

A graphical representation of these two parameters is shown in Figure 36 for the maximum brake torque (BP_{max}). This figure shows the engine power as a function of time for three power levels with three engine starts ($n = 3$). L in Figure 36 is the test duration defined in Table 10.

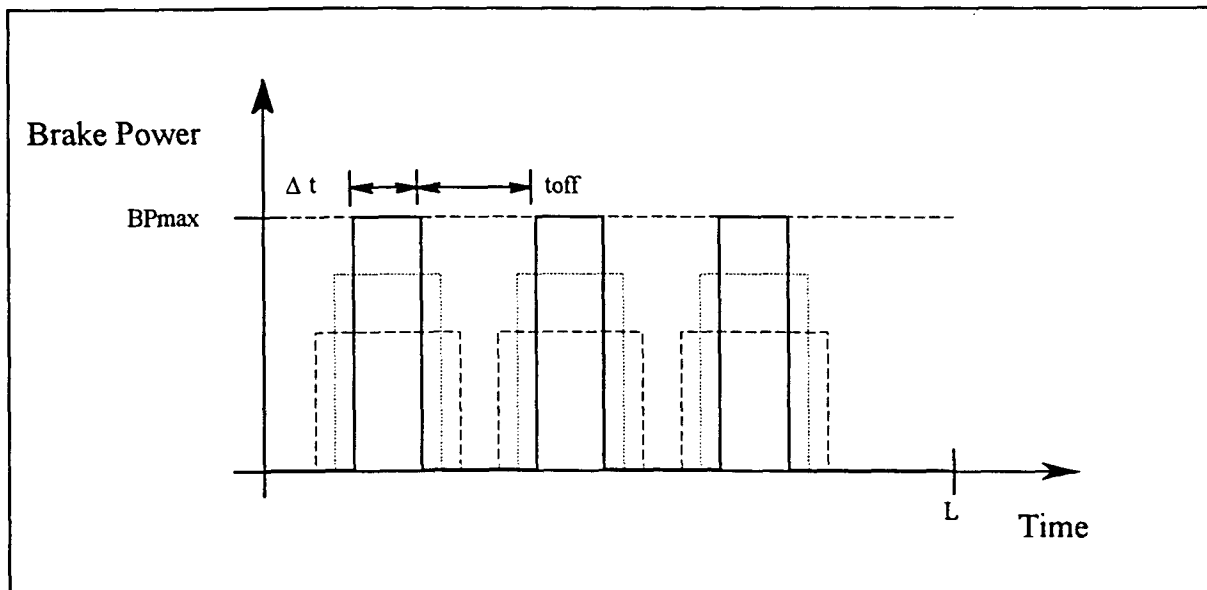


Figure 36. Sample plot of brake power as a function of time for three power levels.

4.6. Test Procedure

Tests were performed according to the matrix described in section 4.5. Each test required precise starting and stopping times, as well as consistent torque outputs. The following section describes the methods used to minimize the variability between tests.

4.6.1. Procedure to Regulate the Timing of the Engine Events

To regulate the engine events, a timer was programmed into the data acquisition and control computer. The timer took in the values for Δt , t_{off} , and n , and calculated the starting and stopping times appropriate for that test. Five seconds before a start or stop, the computer made a beeping noise. It also beeped when the engine event should occur. The operator manually turned the engine on or off when the computer beeped the second time.

Data was taken by two data acquisition systems: the OPTO-22 system for engine data and the Horiba Bench for emissions data. A time stamp was placed on the data as it was written to the files in both systems. Since two PCs were used, the CPU clocks were synchronized before the start of the test. By setting the same time on both computers, the data taken on one computer corresponded directly to the data taken on the other computer.

In between tests, the engine was allowed to cool down to a normal starting temperature. Due to "soak-back", the oil temperature and two head temperatures became nearly uniform while the engine was cooling down. "Soak-back" is by definition the process of engine temperature equilibration. It occurred when the engine was turned off, so the engine fan was not blowing air over the cooling fins on the cylinder head. Because of the lowered heat transfer through the fins, the cylinder head dissipated heat into the oil and engine block more readily. Eventually, the entire engine reached a uniform temperature. Since the temperature was still higher than ambient, heat transfer occurred to the surrounding air, slowly cooling the engine to room temperature. When the two head temperatures and the oil temperature dropped below 90°F, the engine was started for another test run. To aid in the cooling process, a window fan was put in front of the engine between tests.

4.6.2. Procedure to Maintain a Constant Torque Output

In addition to taking data, the OPTO-22 system maintained a constant torque output. The operator input a desired torque level, and the control system used the torque reading from the dynamometer controller to adjust the throttle so that the desired setting was reached. It made the adjustment based on an empirically determined equation of throttle position as a function of torque. This equation was generated by varying the throttle position from the lowest possible value to wide open throttle (WOT). An eighth order least squares regression yielded the following polynomial:

$$P = a_0 - a_1T + a_2T^2 - a_3T^3 + a_4T^4 - a_5T^5 + a_6T^6 - a_7T^7 + a_8T^8 \quad (32)$$

where P was the throttle position in percent full scale, and T was the torque output in ft-lbs. The coefficients for this polynomial are listed in Table 12. The control system used the eighth order polynomial as a first approximation of the throttle position. It then updated the throttle position as necessary using a simple proportional control method. The torque reading was compared with the reference torque, and the throttle position was adjusted as follows. The local slope of the throttle position vs. torque curve was by definition equal to the change in position divided by the change in torque:

$$m = \frac{dP}{dT} \approx \frac{\Delta P}{\Delta T} \quad (33)$$

Table 12. Coefficients for the polynomial relating throttle position to torque output.

Coefficient	Value
a0	2.2739441e+2
a1	-1.2882074e+2
a2	3.4318966e+1
a3	-4.8263830e+0
a4	3.9706600e-1
a5	-1.9738215e-2
a6	5.8332059e-4
a7	-9.4276513e-6
a8	6.4132691e-8

So, the change in throttle position was determined from the local slope and the change in torque:

$$\Delta P = m\Delta T = m(T_{act} - T_{ref}) \quad (34)$$

where T_{act} is the actual torque and T_{ref} is the reference torque. The new value for throttle position was determined by subtracting the change in throttle position from the old throttle position:

$$P^{i+1} = P^i - \alpha(\Delta P) \quad (35)$$

The change in throttle position is multiplied by a damping factor (α) that minimizes errors due to inaccuracies in the curve fit and instabilities in the engine.

4.6.3. Procedure to Start and Stop the Engine

When turning on the engine, the operator started all the equipment except the engine, including the data acquisition software. A first guess at the throttle position was put into the software for the throttle control. This opened the throttle before the engine was started to the empirically determined position. When the computer beeped, giving the engine start signal, the operator turned on the engine and activated the dynamometer. The engine accelerated to 2400 rpm, and the load settled out near the desired set point. Once the engine reached 2400 rpm, the operator activated the automatic throttle control program. The remainder of the on-time was controlled by the computer.

To turn off the engine, the operator closed the throttle by turning a switch. The switch changed the throttle control from the computer to a potentiometer. The potentiometer was set at the closed throttle position, so the throttle closed immediately. As the engine slowed to a stop, the dynamometer and the ignition key were turned off. When the engine had stopped for the last time for that test, a fan was put in front of the engine to aid the cooling process. This method of stopping the engine caused the power to drop from the set value to zero in about 5 seconds.

4.6.4. Test Procedure Summary

In summary, the tests were conducted in accordance with the test matrix shown in Table 11. This table prescribed the power levels used in testing and defined the timing of the engine events for each power level. The computer took in the timing parameters and torque level at the

beginning of the test. The control computer signaled the operator when to start and stop the engine and maintained the proper torque level when the engine was on. In between tests, the engine temperature dropped below 90°F before a test began. The main measurements taken during the test were emissions and fuel consumption. Emissions were measured by the Horiba emissions bench, and fuel consumption was measured by a Flo-tron fuel flow meter.

5. RESULTS AND DISCUSSION

As mentioned in section 1.3, the main goal of the engine tests was to study the variation of fuel consumption and emissions with the number of starts. In addition, the dynamometer test gave information that was used to estimate the fuel consumption and emissions per mile for a HEV. The tests were performed in an on/off fashion, starting the engine a specified number of times, and maintaining a constant power output while the engine was running. This test was meant to represent the operation of a series-hybrid APU.

Before on/off engine testing was done, however, two steady state baseline maps were made at 2400 rpm. The first map used pure 87 octane unleaded gasoline, and the second map used the same 89 octane ethanol blended fuel as was used for the on/off tests. An engine map characterizes an internal combustion engine when operating at steady state over a range of speeds and loads. The maps performed here only used an engine speed of 2400 rpm, mainly because of time constraints on the project. The engine load in the baseline tests was varied from idle to wide-open-throttle (WOT). Both maps provide a reference that the on/off testing can be compared with.

5.1. Data Analysis Procedure

Constant speed tests and on/off tests were both run on the engine. The constant speed tests yielded baseline information on the brake specific fuel consumption, CO emissions, and HC emissions as a function of power output. The baseline map also provided A/F ratio information at each power level. The on/off tests were performed using the same experimental setup as the baseline map. For the on/off tests, the instantaneous results were integrated or averaged over time to give the total energy output, amount of fuel consumed, and total emissions output. Even though the results from the two tests were calculated in different ways, the results will be plotted on the same graph in section 5.3, and direct comparisons can be made between the two types of tests.

5.1.1. Analysis Methods for the Steady State Tests

The steady state tests were both conducted using the same procedure. Because of the similarity between the tests, only the second is described in this section. At the beginning of the second steady state test, the engine ran at a brake power of 3.41 kW until the engine temperature reached steady state. Power was increased incrementally from 3.41 kW to 11.2 kW, where 11.2 kW was produced at wide-open-throttle (WOT). Measurements were taken at eight power levels. As shown in Figure 37, the cylinder head temperature remained relatively constant for the first level and for the last three levels. The engine temperature in the intermediate levels increased over time. Two statements can be made about Figure 37. First, the head temperature did not increase considerably for each power level. The largest temperature increase occurred for a power level of 5.93 kW. For this setting, the temperature increased by 10.69°C, which was a 6.88% change. Second, the temperature was lower than the steady state temperature reached during the on/off test

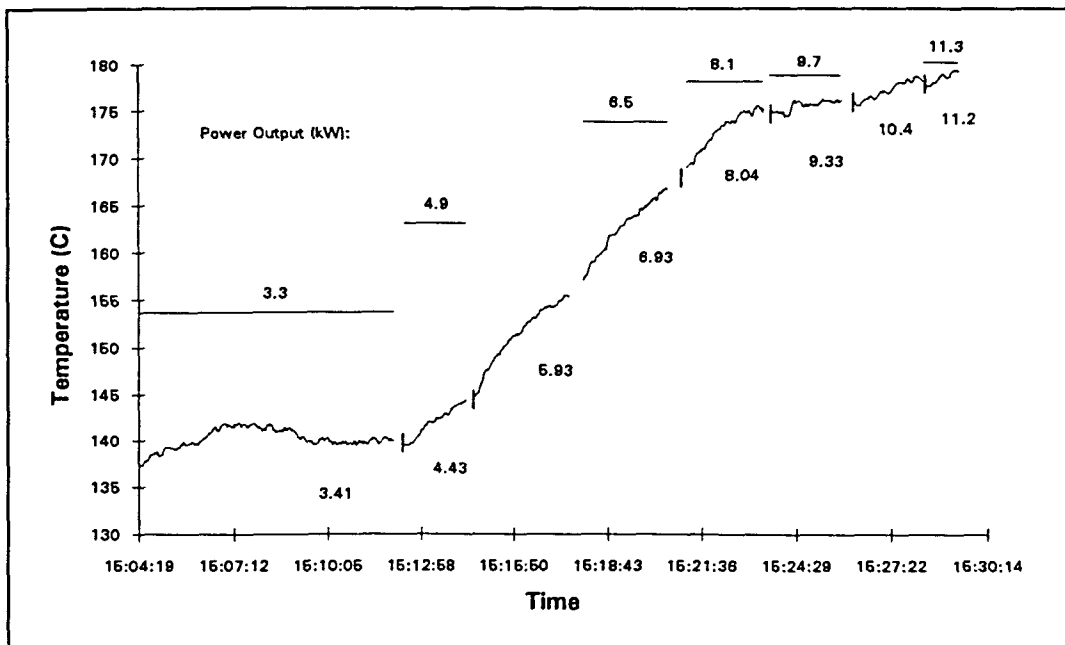


Figure 37. Average cylinder head temperature for the second steady state map at 2400 rpm. Power levels are separated by vertical lines and labeled in kW.

with one start, where the engine ran for a considerable length of time at each power level. Recalling the test matrix in Table 11, the engine ran for around 11 minutes for the highest power output and over 37 minutes for the lowest power output. For all tests, the engine reached a steady state temperature. This temperature is shown as a horizontal line above the steady-state baseline map data. The brake power levels for the on/off test with one start are labeled above the horizontal reference lines, and the brake power levels for the steady state map are labeled below the temperature data lines. The engine did not reach as high a temperature in the baseline map as it did in the on/off test with one start. The temperature difference appears to be a day-to-day variation in the engine temperature because the tests performed at 3.41 kW were allowed to run for the same length of time as the on/off tests with one start. To minimize the discrepancy in the head temperature, the data should have been taken by varying the power level in a random fashion, rather than increasing the power incrementally.

For each power level, the mass flow rates of fuel and air were measured in kg/hr, as described in chapter 4. The emissions measurements were made in molar concentrations. The carbon monoxide (CO), carbon dioxide (CO₂), and oxygen (O₂) levels were measured in percent by volume. The hydrocarbon (HC) and oxides of nitrogen (NO_x) emissions were measured in parts per million (ppm). From the molar concentrations, the mass flow rate of each emission was calculated using the following equation:

$$\dot{m}_{emission} = x_e \left(\frac{M_e}{M_{ex}} \right) \dot{m}_{ex} \quad (36)$$

where x_e is the mole fraction of the emission in $\text{kmol}_{emission}/\text{kmol}_{exhaust}$, M_e is the emission molecular weight, M_{ex} is an average exhaust molecular weight, and \dot{m}_{ex} is the exhaust mass flow rate. A value of 30.7 kg/kmol was used for the exhaust molecular weight for all calculations. This approximation was made because the engine consistently ran rich of stoichiometric, meaning that the exhaust species did not vary much between tests. The exhaust mass flow rate was calculated as the sum of the fuel and intake air mass flow rates:

$$\dot{m}_{ex} = \dot{m}_{air} + \dot{m}_{fuel} \quad (37)$$

The mass flow rates of fuel and emissions were normalized against the average brake power at each set point. This type of quantity is referred to as a "brake specific" value, and is used to calculate the mass of emissions produced if the amount of energy output from the engine is known. The three main quantities calculated in the analysis were brake specific fuel consumption (BSFC), brake specific carbon monoxide emissions (BSCO), and brake specific hydrocarbon emissions (BSHC). Oxides of nitrogen were not measured because of the equipment malfunction described in section 4.4. These parameters have units of kg/kW-hr and will be presented in section 5.3 as a function of engine power output.

The other quantity calculated in the analysis was the air/fuel (A/F) ratio. For the two engine maps, the A/F ratio was calculated by dividing the air mass flow rate by the fuel mass flow rate.

The A/F ratio was also determined from the exhaust products. By using the procedure given by Heywood [22], the air/fuel ratio was calculated from the molar concentrations of the exhaust products. The balance assumes that all species are measured with the same background moisture and that the hydrocarbons have the same hydrogen to carbon (H/C) ratio as the fuel. In the Horiba system, all analyzers sample from the same line, so all the species must have the same background moisture. The HC emissions were measured in ppm C₁, meaning the measurement was based on the number of carbon atoms present. Given these assumptions, Heywood provides the following equation:

$$\left(\frac{A}{F}\right) = 4.773 \left(\frac{M_{air}}{M_{fuel}}\right) \frac{(CO_2) + (CO)/2 + (H_2O)/2 + (NO)/2 + (NO_2) + (O_2)}{(HC) + (CO) + (CO_2)} \quad (38)$$

where M_{air} is 28.97. M_{fuel} is the fuel molecular weight normalized against the number of carbon atoms in the fuel and is equal to $12.01 + 1.008y$, where y is the H/C ratio of the fuel. A hydrogen to carbon ratio of 1.87 was assumed for these tests [22], which gives a normalized fuel molecular weight of 13.89. The true average molecular weight of gasoline is around 110. The

quantities in parentheses in equation 38 are the mole fractions of the emissions species measured by the emissions bench. The oxides of nitrogen levels do not significantly affect the A/F ratio and can be left out of the calculation. The water concentration in the exhaust was not measured by the emissions bench, but can be calculated using this relationship:

$$(H_2O) = 0.5y \frac{(CO_2) + (CO)}{(CO) / [K(CO_2)] + 1} \quad (39)$$

where y is defined above and K is the equilibrium constant for the "water-gas" reaction and is empirically determined from exhaust gas composition data [22]. The water-gas reaction dictates the equilibrium concentrations of carbon dioxide, carbon monoxide, hydrogen gas, and water concentration. It follows the form:



The value of K used in these calculations was 3.8. Equation 38 can be derived by taking a ratio of the concentrations of oxygen-containing exhaust gas species to the carbon containing species.

Equation 39 comes from a combination of the water-gas equation, an overall carbon balance, and an overall hydrogen balance.

5.1.2. Analysis Methods for On/Off Testing

The on/off testing used the same data acquisition system as the steady state tests, so the original data were in the same form. In addition, the same quantities were calculated from the data (BSFC, BSCO, BSHC, and A/F ratio), but the quantities were determined in a slightly different manner. In the on/off tests, the engine was started a specified number of times, and the number of starts was varied from 1 to 5. Data was taken from the time the engine started until it stopped for the last time. Since the data were important throughout the test, both the transient and steady state portions of the test needed to be analyzed. So, instead of using the average flow rates as the steady state test did, the instantaneous flow rates were integrated with respect to time to give a total mass for each quantity. When multiple starts were used, the mass of each parameter was calculated for

all of the on-times individually, and the total mass was calculated by summing the individual masses.

While each mass was calculated by integrating the mass flow rate, the energy production was obtained by integrating the instantaneous power. Once the mass of fuel and emissions were obtained, the three normalized quantities (BSFC, BSCO, and BSHC) were calculated by dividing the mass by the total energy produced. As before, this calculation results in parameters with units kg/kW-hr.

Simpson's 3/8th rule was used for all of the integrations. The integration started at zero engine speed, continued through the engine on-time, and finished when the engine reached zero angular velocity at the end. Since Simpson's rule requires a number of panels divisible by three, the ending point for the integration varied one or two time steps. This did not affect the integration, because the engine had stopped and was no longer producing power or emissions.

Average data was also taken during the engine on-time. The averaging was performed by taking the sum of the data when the engine was running at 2400 rpm and dividing the sum by the number of data points. A numerical average was taken rather than performing an integration because the quantities stayed relatively constant over the engine on-time, making an integration unnecessary. The average torque, air mass flow rate, and fuel mass flow rate were calculated. The torque was used to compute an average power for the test, which was the main parameter used to make comparisons between tests. The air and fuel flow rates were used to calculate an average air/fuel ratio.

Transient parameters were also analyzed. The accuracy of the on/off timing was determined by measuring the start and stop times, as well as the time it took for the engine to reach the average power level. The start time was defined as the time that the engine speed became greater than zero. The stop time was defined as the time when the engine speed dropped below 2400 rpm during the deceleration process. The other parameter was the time it took the engine to reach the average power level. This was defined as the time interval between when the engine was

at zero angular velocity and when it reached within 2% of the average power. If oscillations occurred, the starting time was measured to the point where power stayed within $\pm 2\%$ of the average power. The time to decelerate was not measured because of the method of shutting off the engine. When the dyno controller was turned off, the torque dropped to zero almost instantaneously. So, even though the engine took around 10 to 15 seconds to stop, it was producing no power for most of the interval. The transient timing variables are represented schematically in Figure 38.

5.2. Test Accuracy

The accuracy of the on/off test itself was evaluated based on the repeatability of the engine power output level and on accuracy of the engine start and stop timing. The engine control system was able to keep the engine at a relatively constant power output over the course of the test. How close the mean power level was to the reference power level, how constant the power stayed over the course of the test, and what minimum and maximum values of power were reached all go into determining the stability and accuracy of the engine power output. The magnitude of these engine power variations and what aspects of the throttle control system caused the variations will be discussed in section 5.2.1. The accuracy of the engine start and stop timing is discussed in section 5.2.2. The accuracy of the engine on/off timing will be evaluated based on how long it took the control system to bring the engine to the average power and on how close the total engine running time was to the reference on-time.

5.2.1. Engine Power Stability and Accuracy

As already mentioned, the speed setting for all the on/off tests was 2400 rpm. The dyno controller maintained this speed within ± 0.5 rpm. Because of the high precision of the dyno controller, variations in the engine power output over the course of the test were due to fluctuations in the torque. The torque was controlled by the OPTO-22 system, as described in section 4.6.2. The accuracy of the throttle control program can be described using Table 13 and Figure 39. Table 13 gives the statistics of the on/off tests, and Figure 39 shows the engine power

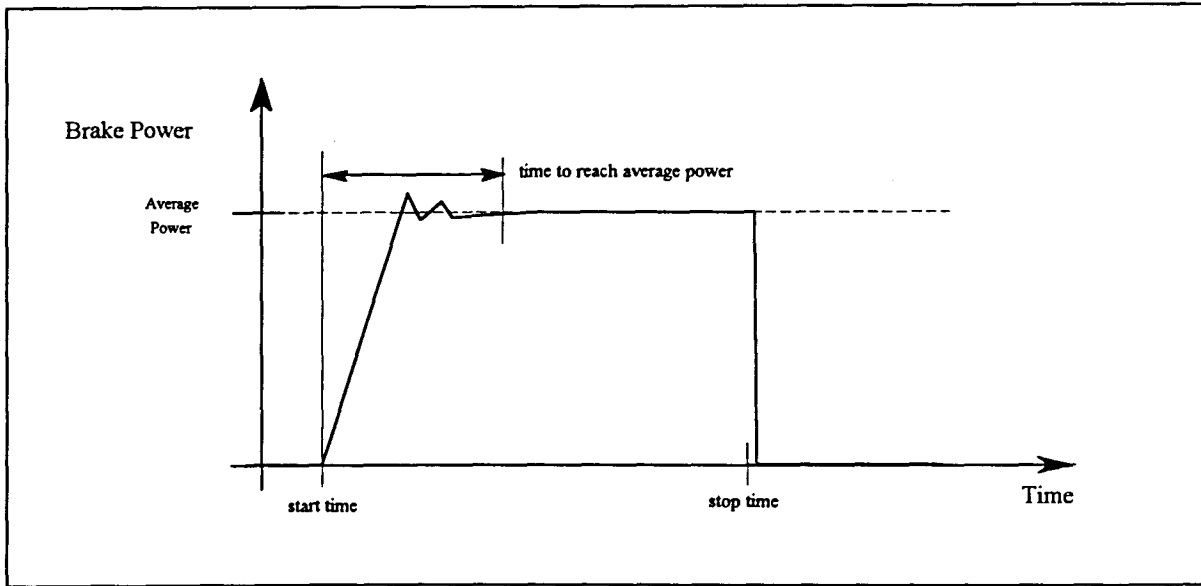


Figure 38. Schematic representation of the variables used in analyzing the engine start and stop timing.

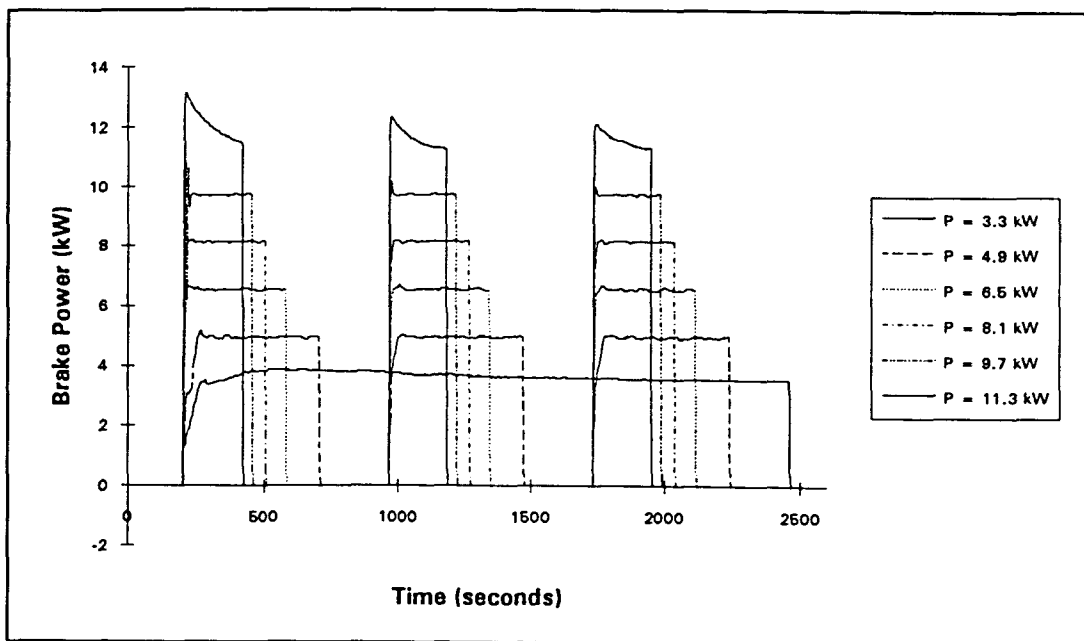
output as a function of time. Both Table 13 and Figure 39 are based on data from the on/off tests with three starts.

The first row in Table 13 shows the mean power output in kilowatts, and the second row shows the percent error with respect to the reference power output. The middle four power levels were within 0.5% of the desired setting. The two end power levels did not come as close to the reference point. The lowest power setting was 9.6% above the desired output, and the highest power level was 3.9% above the desired output. Over the course of the test, the instantaneous power deviated from the mean value. The standard deviation with respect to the mean power output is shown for each power level. Power outputs of 6.5 and 8.1 kW provided the most stable results. The other power levels gave somewhat worse results, and the highest power level showed the most variability. The last two rows in Table 13 give minimum and maximum values for power that show the limits of variability for each test. Typically, these extreme values occurred during startup.

Table 13. Power stability statistics for the on/off tests with three starts.

	P = 3.3	P = 4.9	P = 6.5	P = 8.1	P = 9.7	P = 11.3
Mean	3.6	4.9	6.5	8.1	9.7	11.7
% Error from Reference	9.59	0.50	0.42	0.08	0.06	3.89
Standard Deviation	0.22	0.30	0.08	0.15	0.27	0.46
Minimum	1.7	2.9	5.1	5.2	6.2	8.5
Maximum	3.9	5.2	6.7	8.2	10.8	13.1

The power output as a function of time is shown in Figure 39. This figure can be used to describe the inadequacies in the torque control system that caused the variations in the power output. The middle four power levels showed good stability, but the two end levels deviated from the mean power. At the low end, small changes in throttle position resulted in large torque changes. The change in throttle position calculated by the control subroutine was too small to

**Figure 39.** Engine power output as a function of time.

register on the throttle controller, so the throttle position remained fixed through most of the test. The WOT test reached a maximum output very quickly, and decreased for the remainder of the on-time. This is due to the fact that the throttle position was intentionally fixed at 77.3 percent full scale for the WOT tests. The throttle position was fixed because the torque output from the engine was higher than in the original data set used to calculate the throttle control polynomial. Because the torque reading was outside the data set, the polynomial did not apply, and a throttle position higher than the full scale value was calculated. The variability in power during the engine startup was mainly due to the initial guess at the throttle position. For the smaller outputs, the initial guess was somewhat low, and the throttle control program needed to open the throttle slightly to find the correct power setting. For a power level of 9.7 kW, the initial guess was somewhat high and the control program over compensated on the first start, causing large oscillations. The first start on the 9.7 kW level reaches the maximum and minimum values shown in Table 13 within the first 20 seconds of the test.

5.2.2. Engine On/Off Timing Accuracy

Two parameters were used to determine the start and stop timing accuracy: the time to reach an average power level and the total on-time. The first parameter was defined in section 5.1.2 as the time it takes for the engine to come within 2% of the average power. This time interval is listed in Table 14 for all power levels. The lowest power level took 169.72 seconds to reach the average power, which was the slowest time. This slow response was primarily due to the inability of the torque controller to adjust the throttle position at low levels. The fastest adjustment was the 8.1 kW level, which took 14.12 seconds. The 11.3 kW level shows a lower time interval in Table 14, but that number was the time for the engine to reach its peak power, which is a somewhat different quantity. The percentage of running time taken during the start-up is shown in the second to last row of Table 14. This is the time interval to reach the average power divided by the total on time and multiplied by 100 to get a percentage. Since the engine

Table 14. Time to reach average power and total on-time for the on/off tests with 3 starts.

	3.3 kW	4.9 kW	6.5 kW	8.1 kW	9.7 kW	11.3 kW
Time Interval to Average Power (s)	169.72	52.18	15.16	14.12	29.55	11.53
Total On-Time (s)	2259	1522	1147	918	767	665
τ_{on} (s)	2259	1522	1147	921	769	660
% of Total On-Time for Startup	7.51	3.43	1.32	1.54	3.85	1.75
Error in Running Time (s)	0.35	0.17	0.49	3.18	1.97	5.42

was on for a longer period of time at the low power outputs, the percentage of time used during startup remains relatively low. The highest percentage used is 7.51% for the 3.3 kW setting.

The second row in Table 14 lists the total engine running time, or on-time, rounded to the nearest second. This can be compared with the reference on-time (τ_{on}), which was calculated with the test matrix in section 4.5, and was listed in Table 10. The difference between the actual running time and τ_{on} is displayed in the last row of Table 14. Since the engine events were timed by the data acquisition program, the running times are very close to the reference time. The largest amount of error occurred for the 11.3 kW test. This test was 5.42 seconds higher than the reference time.

5.3. Normalized Results

The three main parameters studied in these tests were BSFC, BSCO, and BSHC. These three parameters will be analyzed in sections 5.3.2 through 5.3.4. To better understand some of the trends seen in the BSFC, BSCO, and BSHC, section 5.3.1 describes the variation of air/fuel ratio over the course of the tests.

5.3.1. Trends of the Air/Fuel Ratio Variation

All of the air/fuel ratios presented in this thesis (except for the numbers used in the following comparison) were calculated using the mass flow rates of air and fuel. An alternative method of calculating the A/F ratio from the exhaust gas composition was described in section 5.1.1. The A/F ratio was calculated using the exhaust gas composition method for the second engine baseline test and for a power level of 6.5 kW with 3 starts. A comparison between the two methods of calculating A/F ratio is shown in Table 15. For most of the tests, the two methods agreed within 2%, and the calculations done for the lowest power output of the baseline test differed by 5.21%. Typically, the two calculations should agree within 5 to 10 percent. The close correspondence of these calculations helps confirm that both systems were working properly.

Figure 40 shows the engine air/fuel ratio as a function of power output. The mixture was rich of stoichiometric throughout. Gasoline has a stoichiometric A/F ratio of around 14.6 [22]. All of the data points in Figure 40 show A/F ratios less than 14. Since the engine was running richer than expected, a third A/F ratio measurement was taken using another piece of equipment that gave ballpark values for A/F ratio. This third device showed that the A/F ratio was in the range calculated by the other two methods. For the low power outputs, the mixture was relatively lean with an A/F ratio close to stoichiometric. As load increased, the mixture richened. It became more rich quickly at first, and then leveled out at higher power levels. This is typical of the elementary carburetor that was used on the P224 engine. All tests show the same trends in A/F ratio. This would be expected because the A/F ratio is dependent on the carburetor geometry and the air flow rate, which vary little between the baseline and on/off tests. Lines are not included for the data sets in Figure 40 to emphasize the close correlation of the data.

5.3.2. Brake Specific Fuel Consumption

The first normalized quantity calculated was brake specific fuel consumption (BSFC). Figure 41 shows BSFC as a function of power output. All tests gave comparable results. For each test, the engine reached peak efficiency around 8 kW. The BSFC increased when the load was

Table 15. A comparison of the two methods of calculating A/F ratio.

	Exhaust A/F Ratio	Flow Meter A/F Ratio	% Difference
On/Off Test			
First Start	11.91	11.65	2.19
Second Start	11.75	11.57	1.55
Third Start	11.71	11.64	0.59
Baseline Test			
P = 3.4 kW	13.12	12.47	5.21
P = 4.4 kW	11.98	12.15	1.39
P = 5.9 kW	11.48	11.37	0.97
P = 6.9 kW	11.46	11.43	0.22
P = 8.0 kW	11.29	11.28	0.02
P = 9.3 kW	10.96	10.94	0.17
P = 10.4 kW	10.53	10.54	0.02
P = 11.2 kW	10.60	10.73	1.14

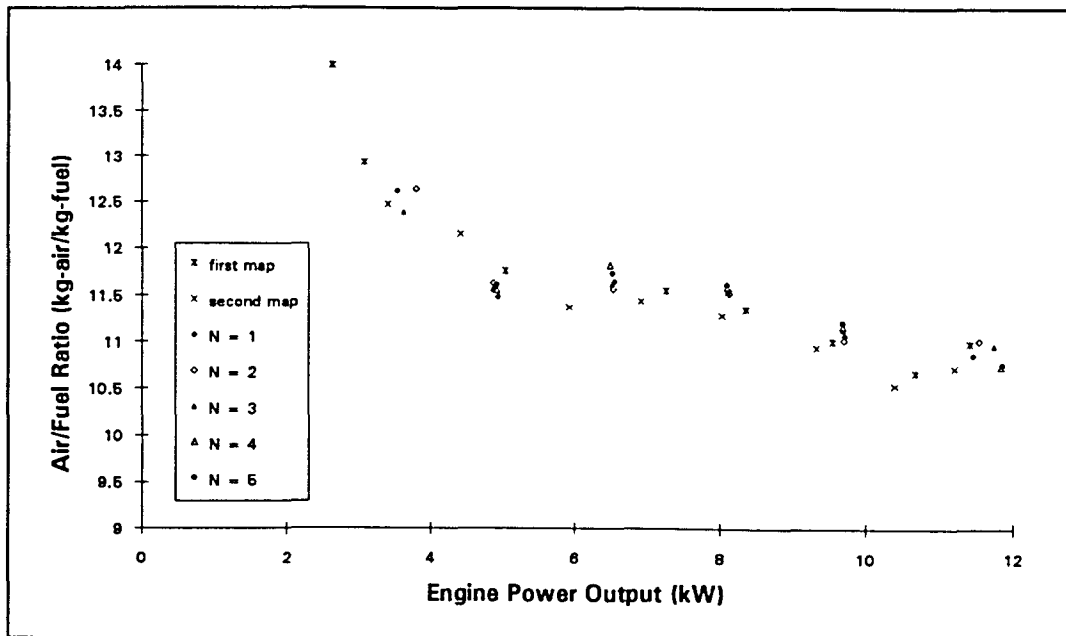


Figure 40. Air/Fuel ratio as a function of engine power output.

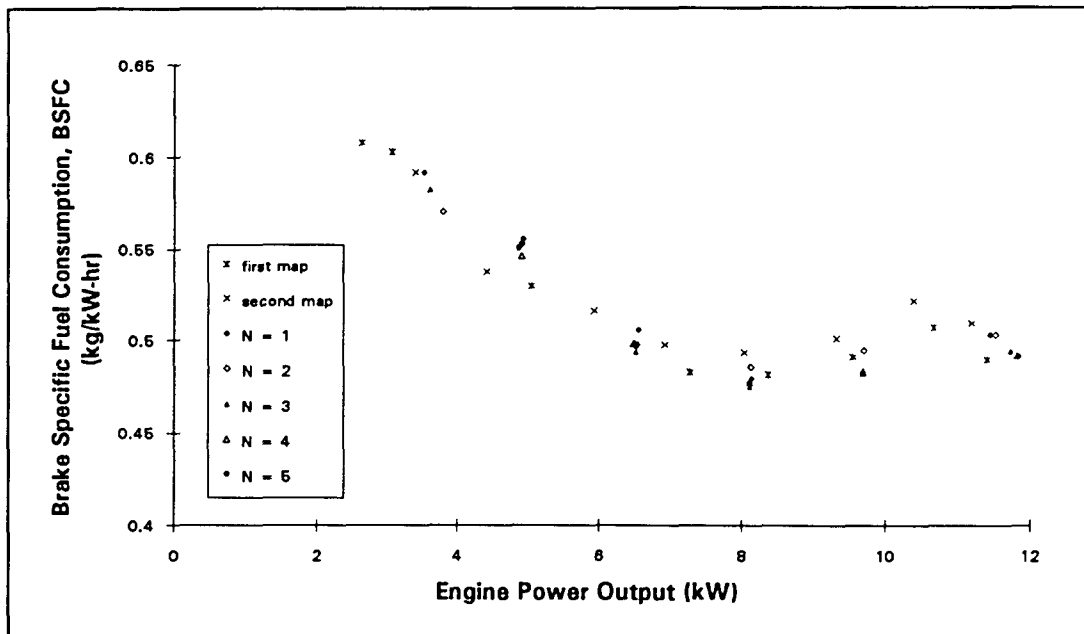


Figure 41. Brake specific fuel consumption as a function of engine power output.

either raised or lowered from the 8 kW set-point. This is typical of carbureted spark ignition engines. Heywood [22] cites three reasons for the decline in fuel economy for loads lower than the peak efficiency. The primary reason is the increased pumping work due to the lower intake manifold pressure. The other two reasons he gives are increased importance of friction, and increasing importance of heat transfer [22]. For loads higher than 8 kW, the A/F ratio decreased, which was shown in section 5.3.1. The decreased A/F ratio lowered the efficiency because the engine ran rich of stoichiometric, which translated into a higher BSFC.

For all power levels, the BSFC was not affected by the number of starts. Figure 41 shows data from all of the test runs. The trends in BSFC as a function of power output are the same for each run. In other words, a test with five starts ($N = 5$) gave the same performance as one start ($N = 1$). So, there is no fuel consumption penalty or benefit based on how often the engine starts. Lines through each data set were not included in this figure to emphasize the close correlation of all the data. The lack of variation in fuel consumption between test runs will be important in choosing an optimal operating point in the test matrix.

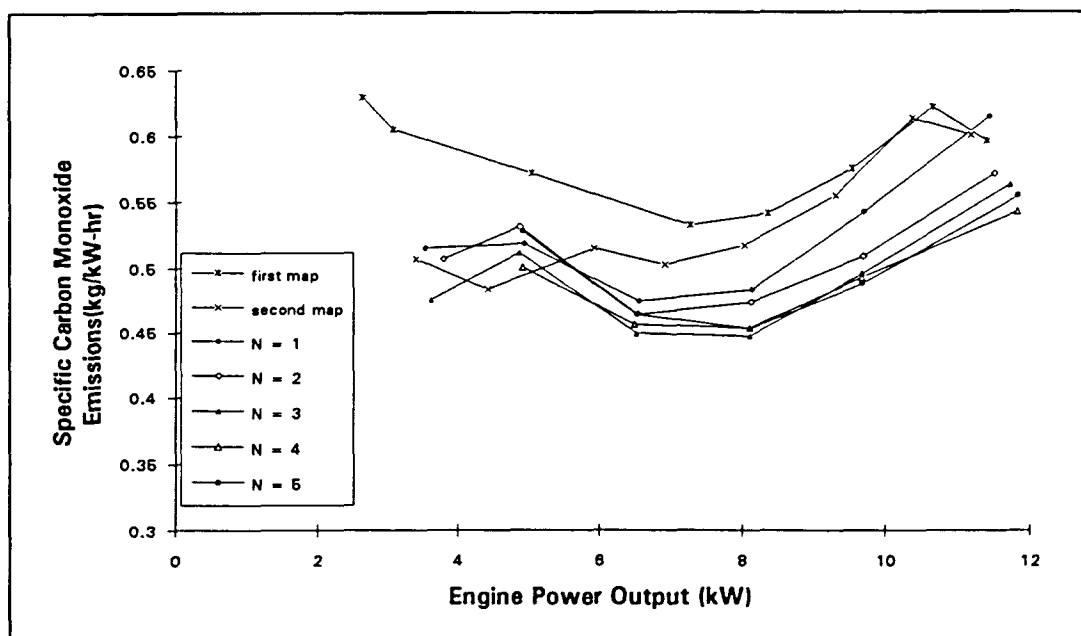


Figure 42. Specific carbon monoxide emissions as a function of engine power output.

5.3.3. Specific Carbon Monoxide Emissions

Figure 42 graphs specific carbon monoxide emissions as a function of engine power. This figure shows that the CO emissions form a U shaped curve with a minimum around 7 kW. The U-shaped curve can be attributed to the change in air/fuel ratio with engine load. It was shown in section 5.3.3 that A/F ratio decreased with increasing power output. Since it has been shown that variations in the carbon monoxide levels occur primarily with changes in A/F ratio, the percent by volume carbon monoxide output was plotted against A/F ratio for all the tests. Figure 43 shows that the CO emissions vary inversely with A/F ratio. So, as the engine load increased, the air/fuel ratio went down, causing the CO emissions on a percent by volume basis to go up. Normalizing the CO emissions against the engine power output makes the specific CO emissions higher for lower power outputs, which forms the U-shaped curve shown in Figure 42.

The level of CO emissions varied with the number of starts. Tests with 3, 4, or 5 starts showed lower levels of CO emissions for power levels above 7 kW. Below 7 kW, the data was mixed, meaning that the CO emissions showed no clear trend as the number of starts was varied.

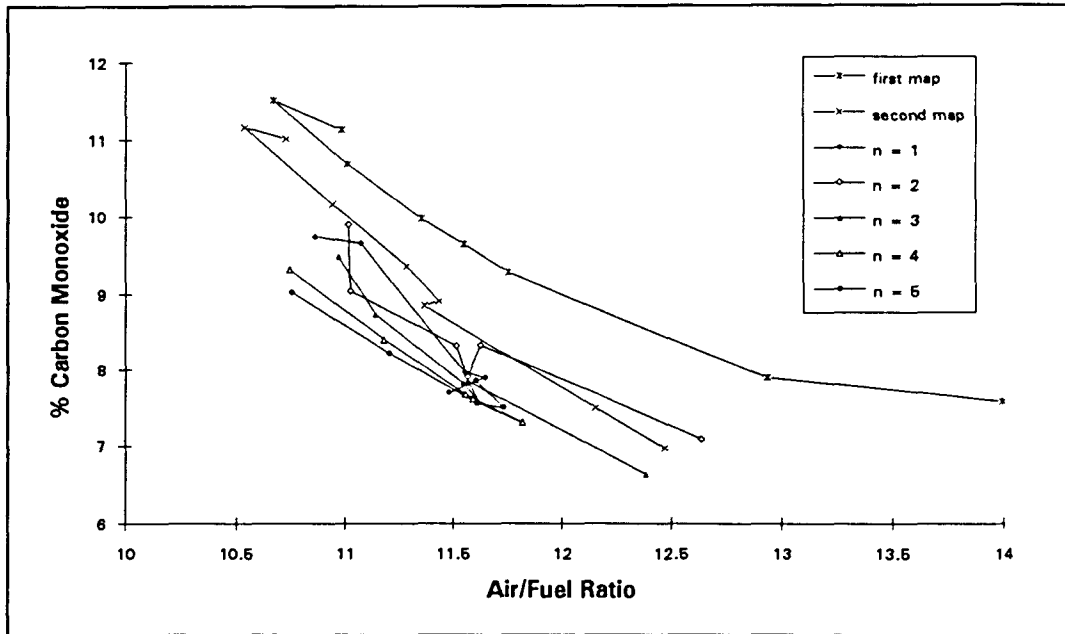


Figure 43. Percent by volume carbon monoxide emissions as a function of A/F ratio.

The improvement in CO emissions with an increased number of starts for high power levels was not expected. Usually, starting an engine increases the CO output. In passenger vehicles, the increased CO during startup is due to the absence of closed-loop A/F ratio control and to the low catalytic converter temperature. Both of these factors prevent the catalyst from working properly and increase emissions.

The pre-converted emissions should also be lower during steady-state operation than during startup. Since the intake manifold heats up as the engine runs, more fuel is vaporized in the manifold. This leads to better mixing of the charge and less variation of A/F ratio in the combustion chamber. Pockets of rich mixtures in the cylinder can lead to CO production. Better mixing would reduce CO levels, so the engine would be expected to produce less CO emissions during steady state operation because of the higher intake manifold temperature. Therefore, a reasonable prediction would say that the CO emissions should worsen as the number of starts increases.

Even though the trends in CO emissions were not expected, there are two possible explanations for the CO emissions improvement when the number of starts was increased. First, there may be some phenomenon unique to this engine that varies the local mixture strength in the engine at low loads. Variations in the mixture could be either pockets of rich mixtures in both combustion chambers, or cylinder-to-cylinder variations in air/fuel ratio. Second, the test was performed in ascending order of the number of starts. All of the tests with one start were performed first, then those with two were performed, and so on. A random order of tests may have given different results. In addition, the malfunction of the NO_x meter described in section 4.4 occurred during the on/off test with 2 starts. After the malfunction, the network of stainless steel lines in the emissions bench was modified, which could have changed the results. So, the improvement in CO emissions might have been caused by a phenomenon unique to this engine, or by the order in which the tests were performed.

5.3.4. Specific Hydrocarbon Emissions

The unburned hydrocarbon emissions level was the third parameter normalized for analysis. The specific hydrocarbon emissions are shown as a function of engine power output in Figure 44. This figure contains data from the second engine map and from all on/off tests. The first baseline test was not used because it gave results three times as high as those shown for the other tests. Since these results were the among the first readings taken by the analyzer, and since the results were not repeatable, they were not included in this discussion.

Figure 44 shows that there was very little variation in HC emissions between engine power levels. The data show that there might have been an optimal point at around 8.5 kW, but the chart could easily be interpreted to say that HC emissions were independent of load. This minimal change in HC emissions is typical of spark ignited engines. As shown in Figure 3 of section 2.3.1, HC emissions decrease only slightly as load increases.

The hydrocarbon emissions shown in Figure 44 may be lower than the actual engine emissions. The best way of measuring HC levels is to heat the sample line from the engine to the

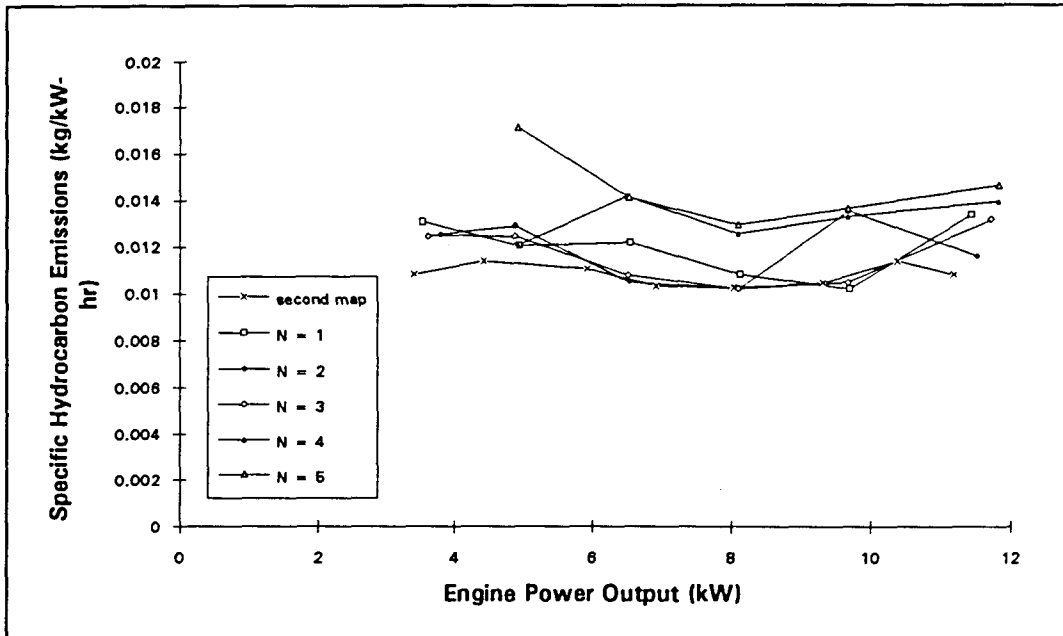


Figure 44. Specific hydrocarbon emissions level as a function of engine power output.

inlet of the analyzer. This prevents the hydrocarbons from condensing in the line. The sample line used in this experiment was heated from the engine to the Horiba emissions bench, but the lines were not heated inside the bench. To prevent the hydrocarbons from condensing in the stainless steel tubing inside the bench, the exhaust gases were routed through a refrigeration bath. In the bath, many of the higher molecular weight hydrocarbons probably condensed out. This would lower the level of HC emissions before the gases reached the analyzer.

5.4. Variation of Engine Temperature in the On/Off Testing

One parameter of interest in the on/off tests was the engine temperature. The cylinder head temperature was used as an indicator of the engine temperature. A plot of the average head temperature over the test is shown in Figure 45. The engine started at or below 90°F (32.2°C), and the temperature increased rapidly throughout the test. When the engine was turned off, the temperature decreased as the engine sat at room temperature. The temperature at the following start depended on the final temperature of the previous stop and on the length of time that the

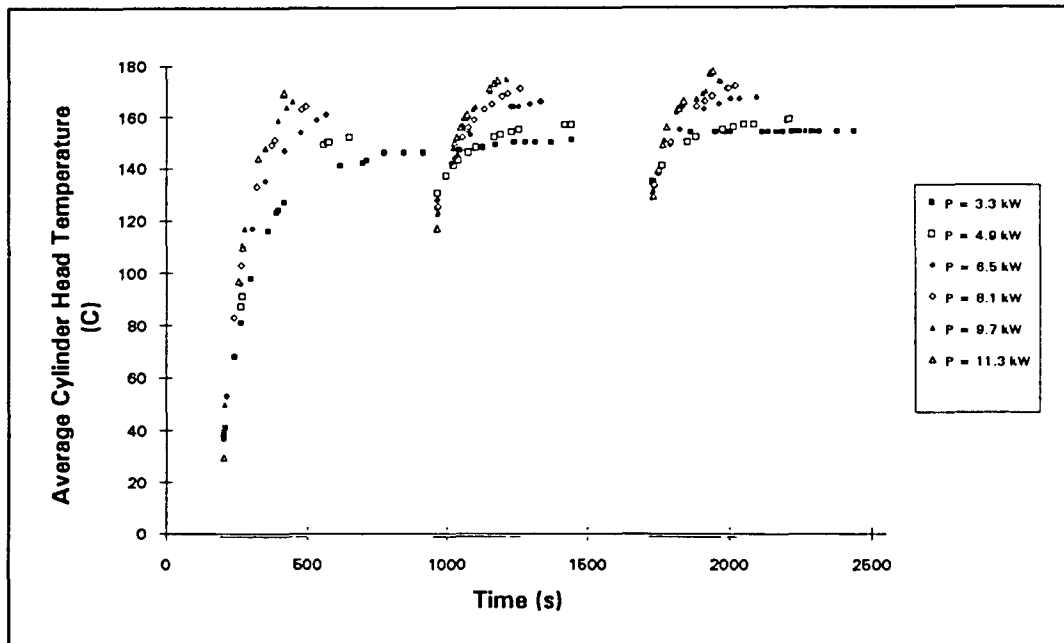


Figure 45. Average cylinder head temperature as a function of time. Data from the on/off test with three starts are shown.

engine was stopped. The second and third starting temperatures for the higher power levels were lower than for the lower power levels because the engine remained off for a longer period of time.

5.5. Application of Engine Test Results to the Operation of a HEV

Aspects of on/off tests have been compared for a range of engine power outputs and for various numbers of starts. The air/fuel ratio, fuel consumption, carbon monoxide emissions, and hydrocarbon emissions were all examined. So far, only relative comparisons have been made with respect to fuel economy and emissions. The absolute amount of emissions per mile that a HEV would produce is also important. Section 5.5.1 below describes a calculation that estimates the fuel consumption and emissions per mile of the range-extended G-van modeled in the simulation. The calculation done in section 5.5.1 will show that the engine may not be suited for in-vehicle use. Section 5.5.2 will suggest some modifications that could be made to the engine and how those changes would affect on/off testing. Specifically, the section will cover changing the air/fuel ratio and adding exhaust after-treatment.

5.5.1. Calculation of Fuel Economy and Emissions for a Simulated HEV

A calculation was performed that combined information gathered from the simulation with data from the engine. Throughout section 5.3, the rates of fuel consumption and emissions output were expressed in units of kg/kW-hr. By multiplying these quantities by the APU energy consumption per mile of vehicle travel, the mass of emissions and fuel consumption per mile were calculated. The APU energy output per mile was determined in section 4.5. The total energy required from the APU was equal to 2.07 kW-hrs. The total distance traveled by the simulated vehicle was 30.78 miles, which is three EPA highway cycles. Combining these two simulation-calculated parameters gives an APU energy consumption of 0.0673 kW-hrs/mile. This number was multiplied by each of the fuel consumption and emission output rates to obtain a gas mileage and a total emission output per mile for each data point.

The results of this calculation are shown in Table 16. Table 16 shows the minimum estimated CO and HC emissions of all the on/off tests and the 1994 federal exhaust emissions standards. Exhaust emissions are typically measured over the Urban Dynamometer Driving Schedule (UDDS), but the simulation used the EPA highway cycle. Since a different driving schedule was used, the simulation cannot be directly compared to the 1994 standards. The standards simply provide a reference level for the simulation results. The estimated emissions were much higher than the 1994 standards. The calculated emission levels were 30.07 g/mile of carbon monoxide and 0.69 g/mile hydrocarbons, compared with the standards, which were 3.4 and 0.41 g/mile [39].

The calculated emission levels were somewhat overestimated because the reference states of charge in the simulation were set so a reasonable engine test could be performed. As described in section 4.5, SOC_{min} was set at 40%. Had this reference state of charge been set lower, the battery would have composed a greater percentage of the energy provided to the vehicle, and the engine would have operated less frequently. If the engine operated less, it would have produced

Table 16. Estimation of the fuel consumption and emissions output from a typical HEV.

Parameter	Value
Energy Calculation	
Number of EPA Highway Cycles	3
Distance per Cycle	10.26 miles
Total Distance Traveled	30.78 miles
Total Vehicle Energy Requirement	23.13 kW-hrs
Initial Battery Energy	35.10 kW-hrs
Minimum SOC	40 %
Final Battery Energy	21.06 kW-hrs
APU Energy Requirement	2.07 kW-hrs
Energy Requirement per Distance Traveled	0.0673 kW-hrs/mile
Computed Results	
Fuel Efficiency (best)	88.8 mpg
(worst)	71.3 mpg
CO Emissions (best)	30.07 g/mile
HC Emissions (best)	0.69 g/mile
1994 Federal Standards	
CO Emissions	3.4 g/mile
HC Emissions	0.41 g/mile

less emissions per vehicle mile. However, the emission levels calculated in this section show that the emissions from a HEV can be higher than for a conventional vehicle.

In addition to showing the emission levels, Table 16 shows that the vehicle displayed excellent gas mileage. The good fuel economy was due to the small amount of energy required from the APU. For this application, the APU provided less than 9% of the energy required to complete the trip. The rest of the energy came from the battery. This allowed the engine to be less fuel efficient than other engines, and still consume small amounts of fuel per mile. So, if the Onan P224 engine was placed in an electric G-van, it could be expected to produce large amounts of emissions but good fuel economy.

5.5.2. Engine Modifications Needed for Hybrid Vehicle Use

Due to the high levels of emissions, the Onan P224 could not be used in a passenger car unless some modifications were made. The high emissions were primarily due to the engine

operating at a rich air/fuel ratio. Some attempt was made to lean out the mixture, with limited success. Engines of this size are typically set rich to minimize cycle-to-cycle variations and to aid in cold starting. Cycle-to-cycle variations are caused by nonuniformities in the mixture composition. Variations in gas motion and in the amounts of fuel, air, and residual gas supplied to each cylinder on a given cycle will affect the combustion process [22]. Since the air flow distribution of a small engine can be non-uniform, large cycle-to-cycle variations may result. If the mixture strength becomes more lean than the partial burn limit or the ignition limit, the engine may not run smoothly. The partial burn limit is the A/F ratio where complete combustion does not occur. Ignition still occurs at the partial burn limit, but the flame does not propagate through the entire chamber. The ignition limit is the A/F ratio where ignition fails to occur for an arbitrary number of cycles. Both affect the drivability of the engine. To compensate for excessive leaning due to variations, designers set the engine to run rich. The air/fuel ratio is also set rich so it can start easily in cold temperatures. During cold weather, the fuel does not vaporize as readily, which inhibits starting. Putting more fuel in the engine allows enough to vaporize so the engine will start [22]. The engine is also equipped with a choke plate to enrich the mixture during startups.

Since the engine ran at such a low A/F ratio, the engine started without the aid of the choke. This made testing simple, but produced high levels of carbon monoxide. If this engine were to run in a vehicular application such as a hybrid vehicle, some way of improving the emissions must be found. Two changes might be made. First, the mixture should be leaned out somewhat. This could be accomplished by replacing or rebuilding the carburetor. Second, some form of exhaust after-treatment should be used. For the air/fuel ratios of this engine, an oxidizing catalyst with an air pump would be appropriate.

Leaning out the mixture and adding a catalytic converter to the engine would both affect the on/off tests. If the A/F ratio was made leaner, it might be necessary to use the choke when starting the engine. This would affect the testing in two ways. First, the engine may take longer

to start, introducing some variability into the timing of the engine starts. Second, the startup effects would be more significant. If the engine ran leaner, less CO emissions would be produced during the tests. When started, however, the A/F ratio would richen due to the use of a choke, which would increase the amount of CO emissions during a start. Since the CO emissions would be greater during startup than for the steady state operation, each engine start would add more CO emissions to the total level. So, leaning out the mixture strength would necessitate the use of a choke, which may introduce variability into the testing process and may cause the CO emissions to increase with the number of engine starts.

Exhaust after-treatment would also affect the on/off test results. During steady-state operation, the catalyst would reduce the overall emission levels. In the transient portions of the test, the catalyst must warm up to its light-off temperature before becoming effective. This phenomenon was discussed in section 2.3. The conversion efficiency for a typical oxidizing catalytic converter was shown in Figure 4. Due to the low conversion rates when the catalyst is cold, current catalytic converter research is in the areas of electrically heated catalysts [40, 41] and warm-up catalysts [27]. Electrically heated catalysts use resistive heating to increase the catalyst temperature, and warm-up catalysts are placed directly downstream of the exhaust manifold, which exposes them to higher exhaust temperatures. These two catalytic converter designs increase the catalyst temperature more quickly than conventional catalytic converters.

5.6. On/Off Test Results Summary

The on/off engine tests studied the effects of the engine power output and the number of engine starts on emissions and fuel economy. When the levels of fuel consumption and emissions were compared as a function of engine power output, it was determined that the engine reached a peak efficiency at around 8 kW. This power setting gave the best fuel economy. The least CO emissions were produced at about 7 kW. Hydrocarbon emissions did not vary significantly with changes in the power level. Therefore, the engine should be set at 8 kW for best fuel economy or 7 kW for least CO emissions. Had NO_x been measured, the results may have been slightly

different. For the rich side of stoichiometric, NO_x emission decrease as the A/F ratio goes down. So, the power output that gave least NO_x emissions may have been higher than the power level that gave best CO emissions.

When the normalized quantities (BSFC, BSCO, and BSHC) were compared as a function of the number of starts, only one quantity showed variation. BSFC and BSHC were virtually independent of the number of starts. The carbon monoxide emissions, however, showed improvement when the number of starts was increased at engine power levels above 7 kW. The CO emissions did not improve when the number of starts was increased beyond 3. Since starting an engine causes increased wear, the number of starts should be minimized. Therefore, the optimal number of starts for this engine under the conditions of the on/off tests described in this thesis was 3. So, if this engine were used in a hybrid vehicle traveling the simulated trip described in section 4.5, it should run at 7 or 8 kW and start 3 times over the trip. This is consistent with the actual operation of the Onan gen-set installed in the electric G-van, since the gen-set was rated at 7 kW. The researchers only started the engine once for each of the tests performed on the G-van, but they were not attempting to optimize the number of starts [20].

6. CONCLUSIONS

As mentioned in section 2.1, electric vehicles are being introduced into California because of smog problems. Hybrid vehicles are being developed to compensate for the range limitations of EVs, while retaining low levels of pollution. The primary objective of this thesis was to determine whether HEVs actually reduce tailpipe emissions with respect to the average automobile.

This thesis described a numerical vehicle simulation and engine dynamometer tests. The numerical simulation determined the energy consumption of a hybrid-electric vehicle over a defined driving cycle. The vehicle used in the simulation was an electric G-van that utilized a 24 hp 2-cylinder engine for range extension. Dynamometer tests were performed on a 2-cylinder spark-ignition engine like the one placed in the G-van. The dynamometer tests varied the engine power output and number of engine starts, while maintaining a total engine running time specified by the simulation. Fuel economy and emissions were measured during the test. Combining the energy information from the simulation with the fuel consumption information from the dynamometer tests, an estimated gas mileage and emission output rate were calculated for the G-van. In the process of estimating the vehicle gas mileage and fuel economy, the following results were determined:

- A HEV could be expected to give off high levels of emissions and to provide good fuel economy. The calculations done in this thesis show that CO emissions would be around 30.1 g/mile and that the vehicle would have a gas mileage of over 71 mpg.
- The Onan P224 engine used in the testing has an intermittent rating at 3600 rpm of 24 hp (17.9 kW). This rating is somewhat low for a series-hybrid APU. The computer simulation described in chapter 3 showed that engine sizes between 19 and 35 kW are reasonable for HEV applications.
- The optimal setting for the Onan engine is at 8 kW for best fuel economy and 7 kW for least emissions.

- CO emissions from the engine improve with an increased number of starts at high power levels. No significant improvement is gained by starting the vehicle more than 3 times, so the optimal number of engine starts is 3. The reason for the decrease in CO emissions with more starts is unknown, but the improvement could have been due to the order in which the tests were performed, or to a phenomenon in this engine which varied the local A/F ratio as the number of starts increased.
- For this engine, emissions levels could be improved by increasing the air/fuel ratio or by adding an exhaust after-treatment device.
- If the engine were run more lean, the choke would be used during startup, which would increase the CO emissions each time the engine was started. Using the choke to start the engine would also increase the variability of the engine on-time.
- There was no exhaust gas after-treatment equipped with the Onan P224 engine. A catalytic converter would decrease emissions during steady state engine operation. A conventional catalyst would not be effective during startup, however. Future HEV research would include an investigation of catalysts that would be effective during transient engine testing.
- The methodology used in this thesis could be applied to future HEV research. A computer simulation was developed to determine the approximate size of the APU that should be used in a HEV application. The simulation also estimated a running time for the engine. The running time was used in dynamometer engine tests to obtain information on the rates of fuel consumption and emissions outputs. The results of the simulation and engine tests were compiled to give an estimated fuel consumption and emission output per mile for a typical hybrid-electric vehicle. Testing engines in the manner described in this thesis could enable engineers to modify or design APUs to aptly suit the requirements of HEV operation.

REFERENCES

1. Woodruff, D., "Electric Cars: Will They Work? And Who Will Buy Them?" Business Week. May 30, 1994, p. 104-114.
2. McCarty, L.H., "Hybrid Auto Runs on Electricity, Gasoline, or Both." Design News. April 20, 1987. p. 94-95.
3. Frere, D., "Audi's Hybrid Duo." Road & Track. v.41, May 1990, p.174-5.
4. Kalberlah, A., "Electric Hybrid Drive Systems for Passenger Cars and Taxis." SAE Technical Paper Series, no. 910247, Warrendale, PA: Society of Automotive Engineers, 1991.
5. Gelman, D.J. and Perrot, T.L., "Advanced Heat Engines for Range Extender Hybrid Vehicles." SAE Technical Paper Series, no. 930041, Warrendale, PA: Society of Automotive Engineers, 1993.
6. Cogan, R., "Volvo ECC." Motor Trend. April 1993, p. 62-63.
7. Beard, J., "Green Hybrid takes to the track at Le Mans." New Scientist. March 26, 1994, p. 18-19.
8. Mackay, R., "Gas Turbine Generator Sets for Hybrid Vehicles." SAE Technical Paper Series, no. 920441, Warrendale, PA: Society of Automotive Engineers, 1992.
9. Burke, A. F., "Hybrid/Electric Vehicle Design Options and Evaluations." SAE Technical Paper Series, no. 920447, Warrendale, PA: Society of Automotive Engineers, 1992.
10. Burke, A.F., "On-Off Engine Operation for Hybrid/Electric Vehicles." SAE Technical Paper Series, no. 930042, Warrendale, PA: Society of Automotive Engineers, 1993.
11. Cogan, R., "Electric Vehicles: Powerplay on the Auto Circuit." Motor Trend. v.45. October 1993, p. 99-105.
12. McCosh, D., "We Drive the World's Best Electric Car." Popular Science. v. 244. January 1994, p. 52-8.
13. Wyczalek, F.A., "Automotive Propulsion Technology for the 1990's." SAE Technical Paper Series, no. 920573, Warrendale, PA: Society of Automotive Engineers, 1992.
14. Organization for Economic Cooperation and Development, Electric Vehicles. Paris: OECD, 1993.
15. World Health Organization and United Nations Environment Programme, Urban Air Pollution in Megacities of the World. Cambridge, Massachusetts, 1992.

16. Personal communication with David Dooley, Midwest Power Systems, Inc. September, 1994.
17. Forster, B.A., The Acid Rain Debate: Science and Special Interests in Policy Formation. Ames: Iowa State University Press. 1993.
18. Myers, P.S., Uyehara, O.A., and Newhall, H.K., "The ABC's of Engine Exhaust Emissions." SAE Technical Paper Series, no. 710481, Warrendale, PA: Society of Automotive Engineers, 1971.
19. Institute of Transportation Engineers Educational Foundation, "The Transportation Engineer and the 1977 Clean Air Act Amendments." Arlington, VA, 1979.
20. Keller, A.S. and Whitehead, G.D., "Performance Testing of the Extended-Range (Hybrid) Electric G Van." SAE Technical Paper Series, no. 920439, Warrendale, PA: Society of Automotive Engineers, 1992.
21. Reuyl, John S., "XA-100 Hybrid Electric Vehicle." SAE Technical Paper Series, no. 920440, Warrendale, PA: Society of Automotive Engineers, 1992.
22. Heywood, J.B., Internal Combustion Engine Fundamentals. New York: McGraw-Hill, Inc. 1988.
23. Jost, K., "Chrysler's hybrid concept." Automotive Engineering, vol 104, no. 5, May, 1996.
24. Yasuda, M. and Maruyama, H., "A New 1.6-Liter Twin-Cam 16-Valve Nissan Engine." SAE Technical Paper Series, no. 910677, Warrendale, PA: Society of Automotive Engineers, 1991.
25. Larsson, T., Bergstrom, K., Bengtsson, A., Petersson, J., and Denbratt, I., "The Volvo 5-cylinder Engine with 4-valve Technology-A New Member of Volvo's Modular Engine Family." SAE Technical Paper Series, no. 911906, Warrendale, PA: Society of Automotive Engineers, 1991.
26. Graham, C.R., Graves, M.C., Pedigo, R.G., and Tenkel, F.G., "General Motors High Performance 4.3L V6 Engine." SAE Technical Paper Series, no. 920676, Warrendale, PA: Society of Automotive Engineers, 1992.
27. Nakamura, H., Motoyama, H., and Kiyota, Y., "Passenger Car Engines for the 21st Century." SAE Technical Paper Series, no. 911908, Warrendale, PA: Society of Automotive Engineers, 1991.
28. Crompton, T.R., Battery Reference Book. London: Butterworth & Co. Ltd., 1990.
29. Dickinson, B.E., Swan, D.H., and Lalk, T.R., "Comparison of Advanced Battery Technologies for Electric Vehicles." SAE Technical Paper Series, no. 931789. SAE special publication SP-984, 1993, p. 1-11.

30. Madeka, F.C., Davis, G.W., and Hodges, G.L., "The Selection of Lead-Acid Batteries for Use in Hybrid Electric Vehicles." SAE Technical Paper Series, no. 940338. SAE special publication SP-1023, 1994, p. 63-68.
31. Gay, E.C. and Webster, C.E., "Testing and Evaluation of EV-1300 Lead-Acid Modules for the Hybrid Vehicle Application." SAE Technical Paper Series, no. 840474, 1984. Published in "Electric Vehicles: A Decade of Transition. PT-40", p.21-26.
32. Whitehead, M. L., "A High Energy Tabular Battery for a 1800 kg Payload Electric Delivery Van." SAE Technical Paper Series, no. 790162, Warrendale, PA: Society of Automotive Engineers, 1979.
33. Frantzeskakis, P., Krepec, T., and Sankar, S., "Specific Analysis on Electric Vehicle Performance Characteristics with the Aid of Optimization Techniques." SAE Technical Paper Series, no. 940336, Warrendale, PA: Society of Automotive Engineers, 1994.
34. Krepec, T. and Dionatos, D., "The Concordia University Hybrid Electric Conversion Vehicle." 1993 Ford Hybrid Electric Vehicle Challenge. SAE SP-980.
35. Baer, J.T. and Frank, A.A., "Vehicle Design Optimization for Minimizing Operating Costs of Electric Vehicles." SAE Technical Paper Series, no. 931792, Warrendale, PA: Society of Automotive Engineers, 1993.
36. Bass, E., Mabrito, B., Kong, H., and McAlwee, G., "A Competition Hybrid Electric Vehicle." SAE Technical Paper Series, no. 921544, Warrendale, PA: Society of Automotive Engineers, 1992.
37. Luecke, G., Van Gerpen, J., and Merriman, C., "A State of the Art Review of Hybrid-Electric Vehicle Technology." Iowa State University, 1995.
38. Warren, C.C. and Leone, T.G., "Fuel Flow Measurement Experience using the Flo-tron Fuel Measurement System." Ford Technical Memorandum No. PME-91-05, 1991.
39. Gushee, D.E., "Alternative Fuels for Cars: Are They Cleaner than Gasoline?" Chemtech. July, 1992, pp, 406-411.
40. Whittenberger, W.A. and Kubsh, J.E. "Recent Developments in Electrically Heated Metal Monoliths." SAE Technical Paper Series, no. 900503, Warrendale, PA: Society of Automotive Engineers, 1990.
41. Gottberg, I., Rydquist, J.E., Backlund, O., Wallman, S., Maus, W., Bruck, R., and Swars, H. "New Potential Exhaust Gas Aftertreatment Technologies for 'Clean Car' Legislation." SAE Technical Paper Series, no. 910840, Warrendale, PA: Society of Automotive Engineers, 1991.